DISS. ETH NO. 29821

Transcriptional regulation and chromatin reorganization in mechanically induced cellular reprogramming and rejuvenation

A thesis submitted to attain the degree of
DOCTOR OF SCIENCES
(Dr.sc. ETH Zurich)

Presented by

Luezhen Yuan

Master of Science in Mechanobiology
University of Singapore, Singapore
Born October 13th, 1994 Citizen of China

Accepted on the recommendation of
Prof. Dr. G.V. Shivashankar, thesis supervisor
Prof. Dr. Marcy Zenobi-Wong, co-examiner

2023

ACKNOWLEDGEMENTS

First and foremost, I would like to express my sincere gratitude to my supervisor Prof. G.V. Shivashankar, who kindly opened the door to the realm of science and mechanobiology for me six years ago, and have constantly supported me in my pursuit of the master and PhD degree. I learnt many aspects of being a good scientist from him. Under his guidance, I learned the intricacies of being a good scientist, from delivering impactful presentations to formulating relevant scientific inquiries, and from designing strategic experiments to managing time and efforts effectively. Shiva's tireless efforts and unwavering support have presented me with unparalleled opportunities, such as the PhD position in Switzerland and various opportunities for conference presentations, collaborative projects, and exposure to industry positions. His motivation at crucial stages has been instrumental in keeping me on track, fueling my enthusiasm for science, and encouraging me to strive for academic excellence.

I extend my gratitude to those who played pivotal roles in the success of my PhD journey. Prof. Ohad Medalia, my co-supervisor, Prof. Viola Vogel, the chair of my PhD defense, and Prof. Marcy Zenobi-Wong, my co-examiner, provided critical questions and unwavering support during my defense. Special thanks to Prof. Caroline Uhler for her valuable suggestions and scientific insights. I am also grateful to Ms. Farida D'Addario and Ms. Sarah Amstutz for their support during my PhD program.

A heartfelt thank you to my collaborator, Dr. Bibhas Roy. Our collaboration resulted in numerous fruitful projects and valuable experiences, including navigating the paper publishing process, conducting innovative experiments, and engaging in industry work. Dr. Trinadh Rao Sornapudi's mastery of challenging experiments significantly contributed to my thesis, and I appreciate his collaborative efforts. I also express my gratitude to Rajshikhar Gupta, who travelled with me to Spain several times for experiments.

I thank my lab members and collaborators that helped me on ordering, experiments and academic discussions including but not limited to: Paulina Schärer, Saradha Venkatachalapathy, Rajshikhar Gupta, Hui Liu, Daniel Paysan, Kiran Challa, Anita Goyala, Maryam Moazeni Afarani, Anne Rosati Shim, Yagyik Goswami, Yawen Liao, Zeynep Karavelioglu, Kapil Jain, Jana Braunger, Louis Cammarata.

I extend my appreciation to the Focal Biosciences team for their support during my one-year research project on high throughput screening and drug discovery. Working with data scientist Mr. Suliman Bouizaguen remains a good memory.

Finally, I express my deepest gratitude to my family and friends who have shared in the joys and memories of this journey. A heartfelt and special thank you goes to my dear friend Yawen Liao, whose companionship has filled our personal moments with happiness, warmth, care, and support.

TABLE OF CONTENTS

Abstract

This doctoral thesis explores the remarkable domain of mechanobiology, transcriptional regulation, and its relevance in regenerative medicine. Cells are known to be plastic, capable of transitioning between different states based on their microenvironment. Mechanical cues, in particular, have emerged as a potent trigger for cell-state transitions, such as reprogramming and differentiation, offering exciting prospects for regenerative medicine. However, the molecular mechanisms underlying these mechanically induced transitions remained poorly understood.

The first chapter discusses recent work on exploring the role of mechanical environment and nucleus mechanisms in transcriptional regulation in various cell state transitions. The second chapter unveils the power of laterally confined growth of fibroblasts in inducing dedifferentiation programs. The molecular mechanisms underlying mechanically induced cell-state transitions are illuminated, with a focus on the critical role of the somatic transcription factor, Lef1. Lef1 has been implicated in various cellular contexts, but its central role in mechanically induced fibroblast dedifferentiation emerges as a key finding. Network optimization methods applied to time-lapse RNA-seq data identify Lef1-dependent signaling as potential regulators of these transitions, shedding light on Lef1's interaction with downstream reprogramming factors. Moreover, it identifies Smad4 and Atf2 as potential critical activators of Lef1, establishing an important mechanotransduction pathway for fibroblast dedifferentiation.

Building on this foundation, the thesis dives into the rejuvenation of fibroblasts - a key focus for functional tissue regeneration. Traditional methods of cellular rejuvenation can be limited, often necessitating complete reprogramming and carrying risks like genomic mutations and low efficiency. However, the mechanically induced partially reprogrammed spheroids offer an innovative solution. When embedded in 3D collagen matrices with optimized stiffness, these spheroids regain fibroblastic properties and transform into 3D connective tissue networks. These redifferentiated fibroblasts exhibit reduced DNA damage, enhanced cytoskeletal gene expression, and acto-myosin contractility. Besides, increased deposition of matrix protein and enhanced collagen

remodeling indicate that these redifferentiated fibroblasts are rejuvenation. This work highlights efficient fibroblast rejuvenation through mechanical reprogramming, promising novel approaches in regenerative medicine.

We next investigate mechanical reprogramming and redifferentiation with the goal of presenting a cellular rejuvenation approach for aged dermal fibroblasts. Aging is characterized by cellular functional decline and epigenetic changes, necessitating innovative rejuvenation strategies. Mechanically rejuvenated aged fibroblasts reset their global transcription profile, upregulating genes related to cell proliferation and extracellular matrix secretion. Innovative Hi-C analysis reveals genes associated with aging and rejuvenation within reorganized interchromatin contact regions. Imaging experiments unveil chromatin compaction changes, and novel measurements based on Lamina-associated domains (LAD) interactions offer insights into 3D chromatin organization. The findings introduce a multi-omics analysis approach and contribute to the understanding of chromatin-mediated cellular rejuvenation, with potential therapeutic implications.

Finally, we consider the context of tissue regeneration and wound healing, where cell-based therapies play a pivotal role. Traditional autologous transplantation is hampered by cellular senescence and reduced remodeling capabilities. The thesis presents an alternative approach, implanting partially reprogrammed aged human dermal fibroblasts into in vitro aged skin models for tissue regeneration and wound healing. The implanted cells exhibit enhanced extracellular matrix protein expression and synthesis, leading to improved tissue regeneration at wound sites. Transcriptome analysis and chromatin biomarkers unveil the upregulation of tissue regeneration and wound healing pathways, offering a novel, non-genetic approach for cell-based therapies in regenerative medicine.

Zusammenfassung

Diese Doktorarbeit erforscht das bemerkenswerte Gebiet der Mechanobiologie, der transkriptionellen Regulation und deren Bedeutung in der regenerativen Medizin. Zellen sind bekanntermaßen plastisch und in der Lage, basierend auf ihrer Mikroumgebung zwischen verschiedenen Zuständen zu wechseln. Mechanische Signale, insbesondere, haben sich als starker Auslöser für Zellzustandsübergänge, wie Reprogrammierung und Differenzierung, erwiesen und bieten aufregende Perspektiven für die regenerative Medizin. Dennoch sind die molekularen Mechanismen, die diesen durch mechanische Einflüsse ausgelösten Übergängen zugrunde liegen, noch wenig verstanden.

Das erste Kapitel befasst sich mit aktuellen Arbeiten zur Erforschung der Rolle der mechanischen Umgebung und der Mechanismen des Zellkerns in der transkriptionellen Regulation in verschiedenen Zellzustandsübergängen. Im zweiten Kapitel wird die Wirkung des lateralen, begrenzten Wachstums von Fibroblasten auf die Induktion von Dedifferenzierungsprogrammen aufgedeckt. Die Mechanismen, die den durch mechanische Einflüsse verursachten Übergängen der Zellzustände zugrunde liegen, werden beleuchtet, wobei ein Schwerpunkt auf der entscheidenden Rolle des somatischen Transkriptionsfaktors Lef1 liegt. Lef1 wurde in verschiedenen zellulären Kontexten impliziert, aber seine zentrale Rolle bei der durch mechanische Einflüsse verursachten Dedifferenzierung von Fibroblasten ergibt sich als eine Schlüsselerkenntnis. Die Anwendung von Netzwerkoptimierungsmethoden auf Zeitraffer-RNA-Seq-Daten identifiziert Lef1-abhängige Signale als potenzielle Regulatoren dieser Übergänge und wirft Licht auf die Wechselwirkung von Lef1 mit nachgelagerten Reprogrammierungsfaktoren. Darüber hinaus werden Smad4 und Atf2 als potenzielle wichtige Aktivatoren von Lef1 identifiziert und eine wichtige Mechanotransduktionspathway für die Dedifferenzierung von Fibroblasten etabliert.

Auf dieser Grundlage taucht die Arbeit in die Wiederbelebung von Fibroblasten ein - ein Schwerpunkt für die funktionelle Geweberegeneration. Traditionelle Methoden der zellulären Wiederbelebung können begrenzt sein und erfordern oft eine vollständige Reprogrammierung, was Risiken wie genomische Mutationen und geringe Effizienz

mit sich bringt. Die mechanisch induzierten teilweise reprogrammierten Sphäroide bieten jedoch eine innovative Lösung. Wenn sie in 3D-Kollagenmatrizen mit optimierter Steifigkeit eingebettet werden, nehmen diese Sphäroide ihre fibroblastischen Eigenschaften wieder an und entwickeln sich zu 3D-Bindegewebsnetzen. Diese verjüngten Fibroblasten weisen eine geringere DNA-Schädigung, eine erhöhte Expression von Genen des Zytoskeletts und eine Aktin-Myosin-Kontraktionsfähigkeit auf. Die vermehrte Ablagerung von Matrixproteinen und die Remodelierung von Kollagen deuten auf ihre Verjüngung hin. Diese Arbeit hebt die effiziente Wiederbelebung von Fibroblasten durch mechanische Reprogrammierung hervor und verspricht neue Ansätze in der regenerativen Medizin.

Im nächsten Schritt untersuchen wir die mechanische Reprogrammierung und die Redifferenzierung mit dem Ziel, einen zellulären Verjüngungsansatz für gealterte Dermalfibroblasten vorzustellen. Das Altern ist durch den funktionalen Abbau der Zellen und epigenetische Veränderungen gekennzeichnet, die innovative Verjüngungsstrategien erfordern. Mechanisch verjüngte gealterte Fibroblasten setzen ihr globales Transkriptionsprofil zurück und erhöhen die Expression von Genen, die mit der Zellproliferation und der Sekretion der extrazellulären Matrix in Verbindung stehen. Innovative Hi-C-Analysen zeigen, dass Gene, die mit dem Altern und der Verjüngung in Zusammenhang stehen, sich innerhalb neu organisierten Interchromatin-Kontaktregionen befinden. Bildexperimente enthüllen Veränderungen in der Chromatinverdichtung, und neue Messungen basierend auf der Interaktion von Lamina-assoziierten Domänen (LAD) bieten Einblicke in die 3D-Chromatinorganisation. Die Ergebnisse stellen einen Multi-Omics-Ansatz vor und tragen zum Verständnis der chromatinvermittelten zellulären Verjüngungsprogramme bei, mit möglichen therapeutischen Implikationen.

Schließlich betrachten wir den Kontext der Geweberegeneration und der Wundheilung, in dem zellbasierte Therapien eine entscheidende Rolle spielen. Die traditionelle autologe Transplantation wird durch zelluläre Seneszenz und reduzierte Remodeling-Fähigkeiten behindert. Die Arbeit präsentiert einen alternativen Ansatz, bei dem teilweise verjüngte, gealterte menschliche Dermalfibroblasten in in vitro gealterte Hautmodelle für die Geweberegeneration und Wundheilung implantiert werden. Die implantierten Zellen zeigen eine erhöhte Expression und Synthese von extrazellulären

Matrixproteinen, was zu einer verbesserten Geweberegeneration an den Wundstellen führt. Die Transkriptomanalyse und Chromatin-Biomarker enthüllen die Aktivierung von Signalwegen zur Geweberegeneration und Wundheilung und bieten einen neuartigen, nicht-genetischen Ansatz für zellbasierte Therapien in der regenerativen Medizin.

List of abbreviations

cDNA - Complementary DNA
DamID-seq - DNA adenine methyltransferase identification assay and sequencing
DE - Differential Expression
ChIP - Chromatin Immunoprecipitation
DIC - Differential Interference Contrast
DMEM - Dulbecco's Modified Eagle Medium
DMSO - Dimethyl Sulfoxide
DNA - Deoxyribonucleic Acid
ECM - Extracellular Matrix
ES - Embryonic Stem
FBS - Fetal Bovine Serum
FISH - Fluorescence In Situ Hybridization
FN - Fibronectin
GO - Gene Ontology
HiC-seq - High-throughput chromosome conformation capture technique and sequencing
iPSCs - Induced Pluripotent Stem Cells
LAD - Lamina-Associated Domain
LDA - Linear Discriminant Analysis
LINC - Linker of Nucleoskeleton and Cytoskeleton
mRNA - Messenger RNA
PBS - Phosphate-Buffered Saline
PCR - Polymerase Chain Reaction
PC – Principal Component
PCA - Principal Component Analysis
PCC - Pearson correlation coefficient
PDMS - Polydimethylsiloxane
PPI - Protein-Protein Interaction
qRT-PCR - Quantitative Reverse Transcription Polymerase Chain Reaction
RNA - Ribonucleic Acid
RNA-seq - RNA sequencing

SD - Standard Deviation

siRNA - Small Interfering RNA

SUN - Sad1 and UNC-84

TF - Transcription Factor

Chapter 1: Introduction

Multicellular organisms, such as animals, plants, and most fungi, consist of various cell types that work in coordination to maintain tissue integrity and functionality. Cells that belong to the same cell type share morphological or phenotypical features. Distinct cell types arise from the selective activation of specific genes, resulting in the production of different proteins that contribute to the diverse functions and shapes of these cells. The regulation of gene expression is a highly complex process that can be influenced by environmental signals, operating at various levels, including gene transcription, pre-messenger RNA processing, RNA translation, and posttranslational protein modification. In this introduction chapter, we introduced several topics ranging from microenvironmental signals, transcriptional regulation to healthcare application, with the particular focus on the mechanical aspect of the gene expression regulation.

The role of mechanical environment in transcriptional regulation

Within the intricate microenvironment of tissues, cells sense chemical and physical signals. Chemical signals encompass signaling proteins like FGFs, Hedgehog, Wnts, and BMPs, which elicit changes in gene expression depending on their concentration (Y. Xie et al. 2020; Jing et al. 2023; Liu et al. 2022; Salazar, Gamer, and Rosen 2016). Simultaneously, physical signals, such as shear and tensile forces originating from blood flow, the extracellular matrix (ECM), or cell-cell adhesion, play crucial roles in maintaining cellular and tissue homeostasis. For example, endothelial cells are exposed to both shear and tensional forces and to a combination of growth factors from the blood flow (Dewey et al. 1981; Gordon, Schimmel, and Frye 2020). Smooth muscle cells are found in the walls of blood vessels, the digestive tract, and other organs. They contract and relax to control the movement of fluids and other materials, and they are constantly under tension (Meiss 2000). Skeletal muscle cells contract and relax in response to signals, e.g. acetylcholine (ACh) at the neuromuscular junction, from the nervous system (Lemke and Schnorrer 2017; Rodríguez Cruz et al. 2020). Mesenchymal cells are found in connective tissues throughout the body. They experience high tensional forces during wound healing, tissue repair, and development (Brown et al. 1998; Harn et al. 2019). Neurons in the nervous system

are constantly under tension as they extend and retract their axons and dendrites (Bueno and Shah 2008). Many cell types can sense compressive forces. Chondrocytes are the cells that make up cartilage and osteocytes are the cells that make up bone (Akkiraju and Nohe 2015). They are constantly under compression as they support the weight of the body and absorb impact.

Numerous mechanisms confer the remarkable capacity of cells to sense both chemical and physical cues. Membrane-bound receptor complexes form key components in these mechanisms. For example, integrins within focal adhesion complexes can sense the rigidity and geometry of the ECM (Z. Sun, Guo, and Fässler 2016). Stretch-activated ion channels assemblies perceive microenvironmental conditions and adapt the permeability of cell membranes to extracellular ions (Sukharev and Sachs 2012). Additionally, cadherin adhesion complexes respond to mechanical signals at cell-cell junctions, mechanically coupling neighboring cells (Yap, Duszyc, and Viasnoff 2018). Furthermore, G protein-coupled receptors and Notch receptors are known to respond to both mechanical and biochemical cues in the microenvironment (Wilde et al. 2022; Hardman, Goldman, and Pliotas 2023; Sprinzak and Blacklow 2021).

The physical signals cells encounter are embedded within the ECM, an insoluble network comprising macromolecules secreted by cells. These macromolecules include collagen, proteoglycans, and specialized glycoproteins such as fibronectin and Laminin (Frantz, Stewart, and Weaver 2010). The ECM provides critical structural support and signaling cues for cells. The ECM provides a scaffold for cells to attach to and grow on. It also helps to transmit forces throughout a tissue, which is important for functions such as muscle contraction (Csapo, Gumpenberger, and Wessner 2020). The ECM can influence cell proliferation and differentiation (Dolega et al. 2021; Senoo and Hata 1994). It facilitates cell adhesion, migration and gene expression (Walma and Yamada 2020).

One exemplary mechanism illustrating a cell's ability to sense its local mechanical environment is through the formation of focal adhesion complexes. These complexes serve as sensory hubs, relaying mechanical information from the extracellular environment to the intracellular machinery (Bershadsky, Balaban, and Geiger 2003).

Once mechanical properties of the environment are detected through these complexes, various cellular responses are initiated, including post-translational modifications of proteins bound within focal adhesions and remodeling of the cytoskeleton. Beyond sensing the mechanical properties of the extracellular matrix, cell-cell communication also involves mechanical aspects, alongside biochemical signaling pathways (Yap, Duszyc, and Viasnoff 2018). These intertwined processes collectively influence cellular gene expression and mechanical properties, allowing cells to adapt to their surroundings.

Alterations in gene expression and in cellular mechanical properties are pivotal outcomes of the response to mechanical signals. The shape of cells, a defining feature of different cell types, significantly influences cellular functions (Prasad and Alizadeh 2019). For instance, neurons have distinctive shapes conducive to their function, while muscle cells possess elongated structures that aid in contractility. Epithelial and fibroblast cells experience tensional forces and exhibit distinct shapes associated with their specialized roles.

The cell's shape also impacts cytoskeleton organization and regulates gene expression (Hall 1998; Schakenraad et al. 2020). The polymerization state of actin affects the cytoplasmic-to-nuclear shuttling of various transcription factors. MRTF is a transcription factor that is normally bound to globular actin (G-actin) in the cytoplasm (Hill, Wynne, and Treisman 1995; Miralles et al. 2003; Morita and Hayashi 2013). When actin polymerizes, MRTF is released and translocates to the nucleus, activating MRTF-SRF signaling and transcription of genes involved in cell migration and proliferation. NF-κB is a transcription factor that is normally sequestered in the cytoplasm by its inhibitor, IκB. When actin polymerizes, IκB is degraded, allowing NF-κB to translocate to the nucleus and activate transcription of genes involved in inflammation and immunity (Németh et al. 2004; Mitra et al. 2017). Furthermore, mechanotransduction pathways involving transcription factors like YAP and TAZ are regulated by the actomyosin cytoskeleton (Dasgupta and McCollum 2019).

The perception of mechanical signals from the microenvironment has profound functional implications in tissue homeostasis and cell fate determination. For example, mesenchymal stem cells sense the rigidity of the ECM as part of their differentiation

process (Engler et al. 2006). Hematopoietic stem cells respond to shear forces generated by blood flow to differentiate into various blood cell lineages (Honghu Li et al. 2021). Epithelial cells can undergo an epithelial-mesenchymal transition in response to local mechanical cues, which is crucial in establishing early developmental expression programs (Schiffhauer and Robinson 2017; Gracia et al. 2019). Notably, defects in cellular mechanosensory processes have been linked to diseases such as fibrosis, compromised immune responses, cardiomyopathies, and various types of cancer (Jaalouk and Lammerding 2009; Di et al. 2023).

Unraveling the genetic, molecular, and cellular mechanisms underlying mechanical signal-induced cellular changes necessitates a combination of generic and specific experimental tools and computational approaches. Generic techniques include quantitative reverse transcription polymerase chain reaction (qRT-PCR), next-generation sequencing technologies, Western blotting, immunocytochemistry, high-resolution imaging, and live cell imaging. Specific experimental tools encompass surface patterning, 3D cell culture, local force measurement techniques (e.g., traction force microscopy and micropillar arrays), microscopy techniques (e.g., particle tracking, fluorescence recovery after photobleaching [FRAP], and Förster resonance energy transfer [FRET]), and RNA interference techniques for gene function analysis.

The role of nuclear morphology and chromatin organization in transcriptional regulation

Cells, whether in tissues or in culture, experience continuous mechanical stresses that profoundly affect their growth, differentiation, and migration. Understanding the mechanical properties of living cells is essential for investigating how extracellular biochemical or physical signals are processed and transduced. Different cell types exhibit distinct subcellular mechanical properties, influencing their response to mechanical stresses. Neurons are relatively soft cells, with a stiffness of around 1-10 kPa. Cancer cells are often less stiff than normal cells, with a stiffness of around 1-10 kPa. Stem cells are also relatively soft cells, with a stiffness of around 1-10 kPa. Fibroblasts are much stiffer cells, with a stiffness of around 10-100 kPa. There can be a great deal of variation in stiffness within a given cell type. For example, neurons that

have been injured or stressed may become stiffer, while cancer cells that are actively migrating may become less stiff (Franze, Janmey, and Guck 2013; W. Xu et al. 2012). The stiffness of a cell can have a significant impact on its behavior. For example, stiffer cells are more likely to spread out and adhere to surfaces, while softer cells are more likely to remain rounded and mobile (W. Xu et al. 2012; Daniel et al. 2023). Stiffer cells are also more resistant to deformation, while softer cells are more easily deformed. The stiffness of a cell is also thought to play a role in cell differentiation and gene expression. For example, stem cells that are cultured on stiff substrates are more likely to differentiate into bone cells, while stem cells that are cultured on soft substrates are more likely to differentiate into neuronal cells (Even-Ram, Artym, and Yamada 2006; Engler et al. 2006).

The mechanical properties of the nucleus and its regulation play a pivotal role in transcriptional regulation and genome integrity. These properties are determined by the interplay between the cytoskeleton-nucleus linkage, the integrity and composition of the nuclear Lamina, and the degree of DNA packaging into chromatin (D.-H. Kim and Wirtz 2015; Lombardi and Lammerding 2010; Rowat, Lammerding, and Ipsen 2006; X. Wang et al. 2018; Shivashankar 2011). Studies on the intranuclear regions revealed that the intranuclear region is much stiffer, more elastic, and more solid-like than the cytoplasm (Tseng et al. 2004)

Mechanical stresses are transmitted to the nucleus through cytoskeletal structures, and the cytoskeleton significantly influences nuclear mechanics. The cytoskeleton is made up of three main types of filaments: actin filaments, microtubules, and intermediate filaments. All three types of cytoskeletal filaments can affect nucleus mechanisms in different ways. Actin cytoskeleton link to the nucleus and regulate the nucleus positioning and shape (Davidson and Cadot 2021). Microtubules exert cytoplasmic forces on the nucleus by establishing transient or stable connections with nuclear envelope elements and are involved in nuclear positioning and division (Shokrollahi and Mekhail 2021). Microtubules and Intermediate filaments help to maintain the integrity of the nuclear envelope (Patteson et al. 2019; Almeida et al. 2015). They also play a role in nuclear size and shape. The regulation of nucleus shape and positioning by these three type of cytoskeleton is important for protecting the nucleus from damage during cell movement and division.

When a cell experiences a mechanical force, such as stretching or compression, the cytoskeleton is deformed. This deformation is transmitted to the nucleus through the linker of nucleoskeleton and cytoskeleton (LINC) complex, which allows for direct mechanical signal transmission (Tzur, Wilson, and Gruenbaum 2006; Worman and Gundersen 2006). The LINC complex is made up of two main types of proteins SUN protein and Nesprin protein. SUN proteins are located on the inner nuclear membrane. Nesprin proteins are located on the outer nuclear membrane. SUN and nesprin proteins interact with each other through a specialized domain called the KASH domain (Crisp et al. 2006). The LINC complex plays a vital role in mechanical signal transmission between the nucleus and the cytoplasm. For example, when a muscle cell is stretched, the LINC complex transmits the mechanical signal to the nucleus, which triggers changes in gene expression that lead to muscle growth (Van Ingen and Kirby 2021). The LINC complex is also essential for the embryogenesis and function of many tissues and organs (X. Zhang et al. 2009; Mroß et al. 2018; Lüke et al. 2008). Mutations in LINC complex proteins can lead to a variety of diseases, including muscular dystrophy, Hutchinson-Gilford progeria syndrome, and Laminopathies (C.-Y. Chen et al. 2012; Meinke et al. 2014; Puckelwartz et al. 2010).

The transmission of mechanical stress from the local environment, through the cytoskeleton and LINC complex, to the nucleus results in various consequences, including alterations in nucleus size, shape, and dynamics (Crisp and Burke 2008; Vahabikashi et al. 2022). Different cell types exhibit distinct nuclear sizes and shapes, influencing their capacity for nuclear deformation, which, in turn, depends on nuclear stiffness, levels of nuclear Lamins (Lamin A/C and Lamin B), and the structural role of Lamin A/C proteins in binding to inner nuclear membrane proteins. For example, stem cells feature lower levels of Lamin A/C and softer nuclei, while somatic cells possess higher levels of Lamin A/C, resulting in tissue-specific nuclear stiffness (Constantinescu et al. 2006; Eckersley-Maslin et al. 2013).

The nucleus of a fibroblast is a dynamic structure that can change its shape and orientation in response to changes in the cell's microenvironment. This is thought to be important for allowing fibroblasts to adapt to different mechanical forces and to communicate with other cells in the tissue (Langevin et al. 2010; Maninová et al. 2013;

Brasch et al. 2019). One example of how fibroblasts adapt their nucleus shape and orientation to facilitate long-range mechanical coupling is during wound healing (X. Li et al. 2017). When a wound occurs, the fibroblasts at the edge of the wound become aligned with each other and parallel to the wound and their nuclei become more elongated (X. Li et al. 2017; Laufer et al. 1974). This allows the fibroblasts to generate and transmit forces more effectively and drive collagen orientation, which helps to close the wound (Richardson and Holmes 2016). In addition, nuclei exhibit dynamic behaviors, including translational motility and rotation and are important in neuronal migration, muscle cell development, etc. (Nakazawa and Kengaku 2020; Hickey and Pelling 2017; Wilson and Holzbaur 2012).

In recent years, it has become increasingly evident that the spatial organization of genetic material within the nucleus profoundly influences transcriptional regulation. From stem cells to somatic cells, the compaction state of chromatin correlates closely with nucleus shape, dynamics, and transcriptional profiles. For example, stem cells have nuclei with relaxed chromatin, which makes their nuclei more mobile and allows them to differentiate into different types of cells (Delgado-Olguin and Recillas-Targa 2011; Schlesinger and Meshorer 2019; Talwar, Jain, and Shivashankar 2014). Somatic cells, on the other hand, have nuclei with condensed chromatin, which makes their nuclei less mobile and allows them to stabilize in specific cell types. Besides, chromatin organization involves different regions of the nucleus, including heterochromatin and euchromatin, as well as Lamina-associated domains (LADs). Regulation mechanisms encompass post-translational modifications of histones and chromatin structural changes (Bannister and Kouzarides 2011; Valencia and Kadoch 2019).

A significant gap in our understanding lies in the mechanotransduction pathways that link nuclear mechanical properties to gene expression programs, within the context of the spatial and temporal organization of the genome (Uhler and Shivashankar 2017). A comprehensive understanding of this coupling necessitates detailed observations of processes occurring at different regions of the nucleus. Advanced techniques, including high-resolution imaging and quantitative image analysis, as well as various sequencing methods such as Hi-C-seq and ATAC-seq, along with labeling techniques

like FISH and perturbation methods such as laser ablation and magnetic tweezer techniques, are indispensable for elucidating these complex interactions.

Cell state transition in vivo and in vitro

Every somatic cell nucleus harbors the entire genome, and even inactive genes retain the potential for expression. A small subset of genes is specific to each cell type, and cells within tissues undergo dynamic processes of differentiation, transdifferentiation, and dedifferentiation during development and disease (D. H. Kim et al. 2017; Przybyla, Muncie, and Weaver 2016; Thiery et al. 2009). Understanding the plasticity of cellular transcriptional states during these transitions is fundamental to comprehending healthy and pathological cell behaviors (Shen and Clairambault 2020; Huyghe, Trajkova, and Lavial 2023).

A pivotal discovery illuminating the plasticity of cellular states is the identification of four transcription factors (Oct4, Sox2, Klf4 and cMyc) capable of reprogramming somatic cells into stem-like cells, with profound implications for regenerative medicine (Takahashi and Yamanaka 2006). Cellular reprogramming has significant applications, including the generation of induced pluripotent stem cells (iPSCs) and potential therapies for various diseases. Beyond the exogenous expression of transcription factors, alternative routes of cellular reprogramming have also been demonstrated. For example, small compounds have been shown to induce reprogramming processes, expanding the toolkit for manipulating cellular states (Hou et al. 2013).

Mechanical signals, such as the topology and stiffness of the matrix, can also induce cell state switches. Placing stem cells on matrices with varying stiffness can direct their differentiation into distinct lineages, underscoring the profound impact of mechanical cues on cell behavior (Even-Ram, Artym, and Yamada 2006; Engler et al. 2006). Extreme mechanical deformations, such as strong shear, strain, or compression, can sometimes prompt cells to alter their gene expression profiles as a countermeasure (Nava et al. 2020). In extreme cases, this can lead to changes in cell type and initiate transdifferentiation processes, with potential implications for diseases like cancer (Jiang et al. 2023). However, it remains uncertain whether it is possible to

reprogram somatic cells solely by leveraging mechanical signals without the need for exogenous biochemical factors. Moreover, the transcriptional regulation and the intricacies of cellular and nuclear mechanisms under prolonged exposure to mechanical stimuli remain areas that warrant investigation.

Aging is associated with functional decline, characterized by various cellular changes, including extracellular matrix (ECM) degradation, transcriptional and epigenetic modifications, cytoplasmic stiffening, and decreased nuclear stiffness (Phillip et al. 2015; Schulze et al. 2010). Reversing age-associated cell states requires addressing deficiencies in mechanosensing and mechanotransduction, as well as adapting to the mechanical signals from the aged ECM environment. For example, the use of F-actin-depolymerizing drugs like cytochalasin B has demonstrated the restoration of cellular mechanical properties (Sokolov, Iyer, and Woodworth 2006). Recent studies have shown that the transient expression of reprogramming factors (Oct4, Sox2, Klf4, and c-Myc) in mouse models can improve recovery from age-associated phenotypes (Ocampo et al. 2016). However, the mechanisms underlying the restoration of spatial chromatin organization and the cellular and nuclear changes associated with cellular rejuvenation remain insufficiently understood.

In summary, the intricate interplay between the mechanical environment, transcriptional regulation, and cellular state transitions is multifaceted. Investigating cellular processes such as mechanosensing, chromatin organization, and cellular reprogramming is crucial for comprehending how cells respond to their mechanical surroundings and adapt to various contexts, both in health and disease. This research seeks to unravel the complex mechanisms governing these processes through a combination of experimental and computational approaches. By doing so, it aims to illuminate fundamental aspects of cell biology and explore potential applications in regenerative medicine and disease therapy.

Aims of the present work

The primary objective of this Ph.D. thesis research is to explore and elucidate the intricate relationships between mechanical cues, cellular reprogramming and

rejuvenation, transcriptional regulation, and chromatin organization. The study is driven by the following key research purposes:

1. **Understanding Mechanotransduction in Cellular State Transitions:** Investigate how cells sense and respond to sustained mechanical signals within their microenvironment to regulate transitions between different cellular states. Specifically, the research aims to identify the transcriptional regulatory mechanisms underlying mechanically induced reprogramming, with a focus on the role of transcription factor Lef1 and its upstream and downstream signaling pathways.
2. **Transcriptional and Chromatin Organization Changes in Cellular Rejuvenation:** Explore the epigenetic mechanisms underlying cellular rejuvenation, with a specific focus on transcriptional changes and genome-wide chromatin organization. Investigate how mechanically rejuvenated cells reset their transcriptional profiles and how this correlates with changes in chromatin organization, including chromosome radial positioning and Lamina-associated domains.
3. **Rejuvenating Somatic Cells in Skin Model:** This involves investigating how mechanical confinement and micro-patterned substrates can induce stem-cell-like properties and rejuvenation of aged fibroblasts, with a particular emphasis on their cellular and nuclear morphological changes and the implications for tissue engineering and regenerative medicine.

Thesis outline

Chapter 1: Introduction

This chapter provides the foundation for this thesis, highlighting the current understanding on mechanotransduction. Specifically, it will discuss how cells respond to mechanical cues in their microenvironment and adjust transcriptional regulation and lead to cell state transition. This chapter also discuss the importance of cellular reprogramming in regenerative medicine.

Chapter 2: Lef1 dependent transcriptional regulation mechanical induced reprogramming

This chapter will delve into the molecular mechanisms behind mechanically induced cell-state transitions, focusing on Lef1 and its signaling pathways. It will also explore the upstream activation pathways of Lef1 and their contributions to fibroblast dedifferentiation.

Chapter 3: Cytoskeleton pathways and chromatin reorganization in mechanical induced reprogramming and rejuvenation

This chapter aims to investigate the rejuvenation of fibroblasts through mechanical means, focusing on the epigenetic mechanisms involved in cellular aging and rejuvenation. This chapter will detail the experiments involving the growth of fibroblasts on micro-patterned substrates, their response to 3D collagen matrices, and the resulting changes in gene expression, contractility, matrix deposition, and collagen remodelling. Additionally, it will discuss the implications of open chromatin states in partially reprogrammed cells for their redifferentiation potential. This chapter further studies the transcriptional and genome-wide chromatin organization changes observed in young, aged, and mechanically rejuvenated fibroblasts.

Chapter 4: Rejuvenation of aged fibroblasts in human skin model

This chapter explores the potential applications of the research findings in cell-based therapies for tissue regeneration and wound healing during aging. This chapter will discuss the implantation of partially reprogrammed aged fibroblasts into an in vitro aged skin model and the resulting enhancements in extracellular matrix protein expression, synthesis, and alignment. It will also detail the transcriptome analysis and chromatin biomarkers that reveal the upregulation of tissue regeneration and wound healing pathways, showcasing the novel non-genetic avenue for regenerative medicine.

Chapter 5: Conclusion

In the concluding chapter, the thesis will summarize the key findings, their implications, and potential future research directions in the field of mechanotransduction, cellular reprogramming, and chromatin organization, ultimately highlighting the significance of

this work in advancing our understanding of cellular rejuvenation and its applications in regenerative medicine.

Chapter2: Lef1 dependent transcriptional regulation mechanically induced reprogramming

This part of the result section is adapted from paper:
Luezhen Yuan, Bibhas Roy, Prasuna Ratna, Carolin Uhler, G.V. Shivashankar, Lateral confined growth of cells activates Lef1 dependent pathways to regulate cell-state transitions, Scientific Reports 2022.
DOI: 10.1038/s41598-022-21596-4

I contributed to this publication by planning and conducting experiments, data analysis and writing the manuscript. In particular, I was involved in cell culture on micro patterned substrate, immunostaining, fluorescent imaging, image analysis, RNAi, qPCR and RNAseq analysis.

Introduction

Cells within in vivo systems continually undergo various cellular state transitions, including differentiation, trans-differentiation, and dedifferentiation, which are vital in processes such as embryonic development, tissue repair, and disease progression, including cancer (D. H. Kim et al. 2017; Przybyla, Muncie, and Weaver 2016; Thiery et al. 2009). These transitions are orchestrated by complex signaling pathways and transcription factors that guide cell fate determination and lineage commitment during development and tissue homeostasis. Moreover, these processes can be disrupted, contributing to pathological conditions.

Embryonic development relies on precise differentiation programs that give rise to diverse tissues and organs. Similarly, tissue repair involves trans-differentiation events that allow cells to adapt to injury-induced changes, such as the transformation of keratinocytes into fibroblasts or myofibroblasts during skin wound healing. Dedifferentiation, conversely, refers to mature cells reverting to a more stem cell-like state, facilitating tissue regeneration and repair. However, when dysregulated, dedifferentiation can promote cancer progression by conferring stem cell-like properties to cancer cells, which may lead to therapeutic relapse (Walcher et al. 2020).

Therefore, understanding and controlling these cellular transitions are pivotal for both physiological and pathological processes.

In 2006, Shinya Yamanaka's ground-breaking discovery revolutionized stem cell research by demonstrating that the constitutive expression of four transcription factors - Oct4, Sox2, Klf4, and cMyc - could reprogram somatic cells into induced pluripotent stem cells (iPSCs) in vitro (Takahashi and Yamanaka 2006). iPSCs are similar to embryonic stem cells (ESCs) in their ability to differentiate into any cell type in the body, but they are generated from adult cells rather than embryos, circumventing the ethical issues associated with the use of embryos. Since this discovery, researchers have made significant progress in understanding the molecular mechanisms underlying reprogramming, and have developed new methods to improve the efficiency and safety of iPSC generation. For example, researchers have identified additional transcription factors and small molecules that can enhance reprogramming efficiency or replace the need for some of the original factors, and have developed new delivery methods, such as non-integrating viral vectors or modified mRNA, to reduce the risk of genomic integration and tumorigenesis (Hou et al. 2013; Deng et al. 2015). Additionally, iPSCs have been used for a wide range of applications, including disease modelling, drug screening, and cell therapy. iPSCs can be generated from patients with genetic diseases or disorders, allowing researchers to study disease mechanisms and test potential therapies in vitro. iPSCs can also be differentiated into specific cell types, such as neurons or cardiomyocytes, for drug screening or cell replacement therapies. Overall, the discovery of iPSCs has opened up new avenues for stem cell research and has the potential to revolutionize regenerative medicine.

While the discovery of induced pluripotent stem cells (iPSCs) has revolutionized the field of stem cell research, it is important to note that in vivo, various types of cell-state transitions occur in the absence of exogenous Yamanaka factors. Recent studies have shown that the local mechanical microenvironment can play a crucial role in the modulation of cell-state transitions (Shivashankar 2019). The stiffness of the extracellular matrix can affect gene expression and cellular response, leading to changes in cell state. Studies have shown that increased matrix stiffness can activate the Yes-associated protein (YAP)/transcriptional coactivator with PDZ-binding motif (TAZ) pathway, which promotes cell proliferation and differentiation (Cai, Wang, and

Meng 2021; Dupont et al. 2011). Epithelial cells can undergo a transition to a mesenchymal state in response to mechanical cues such as substrate stiffness, tension, or compression, a process known as epithelial-mesenchymal transition (EMT) (Rice et al. 2017). During EMT, cells lose their polarity and cell-cell contacts, and acquire migratory and invasive properties. The reverse process, mesenchymal-epithelial transition (MET), can occur in development, allowing cells to regain epithelial characteristics (D. Pei et al. 2019). Overall, the local mechanical microenvironment plays a critical role in the modulation of cell-state transitions in vivo, highlighting the importance of considering the physical cues in the design of regenerative therapies and tissue engineering strategies.

A recent study from our lab demonstrated that fibroblasts cultured in laterally confined microenvironments may acquire stemness-like properties after multiple cell divisions (Roy et al. 2018). In that study, we used microfabrication techniques to create laterally confined rectangular patterns on a 2D substrate, which restricted the growth of individual cells in XY direction. After several divisions, the confined fibroblasts showed changes in gene expression and nuclear reprogramming, leading to the acquisition of stemness-like properties. Importantly, this reprogramming occurred in the absence of exogenous biochemical factors, suggesting that mechanical cues alone were sufficient to drive the cell-state transition. However, the underlying nuclear mechanotransduction pathways driving such cell-state transitions are unclear.

Recent single-cell experiments have revealed how cells undergo dedifferentiation in three steps upon constitutive expression of Yamanaka factors (Schiebinger et al. 2019). In the initiation phase, cells gradually repress somatic cell genes and undergo mesenchymal-to-epithelial transition via complex biochemical regulatory pathways. In the maturation phase, cells rapidly acquire an iPSC gene expression profile, coupled with the sequential activation of Oct4, Nanog, and Sox2 (Stadhouders et al. 2018). Finally, in the stabilization phase, cells gain an endogenous pluripotency network (Theunissen and Jaenisch 2014). Given the important role of reprogramming factors in rewiring the genome and establishing the stem cell gene expression profile, we speculated that in fibroblasts grown under lateral confinement, somatic transcription factors would be required to activate the endogenous factors to induce cell-state transitions. Supporting this hypothesis, previous studies have shown that altering cell

geometry can mechanically induce epigenetic modifications in somatic cells and activate downstream transcription factors such as YAP, mRTFA, and p65 (Downing et al. 2013; Dupont et al. 2011; Jain et al. 2013). Since the fibroblast cell-state transitions, using lateral confinement, is controlled by cell geometry changes, we hypothesized that matrix dependent mechanotransduction pathways must exist to ensure the regulation of genome programs.

In this study, we utilized time-lapse RNA-seq analysis and a network optimization method based on Prize-Collecting Steiner Trees to investigate the mechanisms underlying lateral confinement induced fibroblast cell-state transition. Specifically, we identified Lef1-dependent pathways as critical regulators of this transition. To further investigate this pathway, we used ChIP-qPCR to show that Lef1 directly interacts with its target promoter during cell-state alterations. Additionally, we analyzed the upstream activation pathways of Lef1 and identified Smad4 and Atf2 as potential upstream regulators. These findings have important implications for understanding the coupling between nuclear mechanotransduction and cell-state transitions, and suggest a potential role for Lef1-dependent pathways in regulating these transitions. Furthermore, this research provides insight into the molecular mechanisms that drive cellular reprogramming and could inform the development of new approaches for regenerative medicine.

Material and Methods

Microcontact printing

To create micro-patterned substrates, we fabricated polydimethylsiloxane (PDMS) stamps following a previously described protocol (Jain et al. 2013). Subsequently, we used these stamps to pattern fibronectin (0.1 mg/ml working solution, Sigma F1141) onto uncoated hydrophobic polymer dishes (Ibidi 81151), generating rectangular fibronectin islands measuring approximately 19 x 95 μm (approximately 1800 μm^2). To prevent cell adhesion outside of these islands, we passivated the dish with 0.2% Pluronic acid for 5 minutes and washed it three times with PBS.

Lateral confinement growth of NIH 3T3 cells

Fibroblast growth was performed as per the protocol described previously (Roy et al. 2018). NIH 3T3 cells were obtained from ATCC and maintained in standard NIH 3T3 cell culture medium, consisting of DMEM high glucose (Gibco, Thermo Fisher Scientific 11965092) supplemented with 10% (vol/vol) FBS (Gibco; Thermo Fisher Scientific 16000044) and 1% (vol/vol) penicillin-streptomycin (Gibco; Thermo Fisher Scientific 15140122). For this study, cells between passages 10 and 20 were used and cultured at 37°C in a humidified atmosphere with 5% CO2. Individual NIH 3T3 fibroblast cells (at a concentration of 7000 cells per mL) were seeded onto the fibronectin-patterned islands. Unattached cells were washed off after approximately 30 minutes. Standard NIH 3T3 cell culture medium was used for the initial 6 days, followed by a switch to mouse ES medium (Merck Millipore, ES-101-B). Medium changes occurred every 48 hours. To block the interaction between Beta-catenin and TCF family transcription factors, we employed 25 μM iCRT3, using an equivalent volume of DMSO as a control.

Quantitative real-time PCR (qRT-PCR)

We utilized qRT-PCR to quantify the mRNA levels of genes of interest. After removing the cell culture medium, we lysed the cells and isolated total RNA using the RNeasy Plus Mini Kit (Qiagen 74134). Reverse transcription was carried out with an iScript cDNA synthesis kit (Bio-rad, 1708891) on a thermal cycler (Bio-rad C1000). Subsequently, quantitative PCR was performed on a real-time PCR system (Bio-rad CFX96) for 40 cycles, using Evagreen supermix (Bio-rad 1725200). To determine the fold changes in mRNA levels compared to the control sample, we employed the ΔΔCt method, normalizing to Polr2a levels. The primer sequences used are listed below (Table 2-1).

Genes	Forward	Reverse
Lef1	GTAGCTGAGTGCACGCTAAA	TAATTGTCTCGCGCTGACC
Oct4	AGACCACCATCTGTCGCT	CAATGCTAGTTCGCTTTCTC
Nanog Promoter	CAAACCAAAAAGAGCCATTCAAGCTT	GTCGGCTTCTGTGTATAAGCAGA

Oct4 Promoter	CTTTGAGGAGAGGTGGAGAGCT	GCCTTGGCTGGACAATCCT

Table 2-1. Primers used for qRT-PCR and ChIP-qPCR.

RNA interference

Lef1 siRNA and control siRNA (Dicer-Substrate siRNA) were designed by Integrated DNA Technologies. The sequences of the siRNAs used are listed in Table 2-2. Transfection was carried out using Lipofectamine 3000 (Thermo Fisher L3000015) along with reduced serum medium (Opti-MEM, Thermo Fisher 31985070). Cells, initially seeded in Ibidi dishes with 1 mL of cell culture medium for 3 hours, were treated with 1.5 µL Lipofectamine and 10 pmol siRNA. The same medium-changing schedule as described under "Lateral Confinement Growth of NIH 3T3 Cells" was followed.

Dicer substrate siRNA	Sequence	Target exon (for NM_010703)
Lef1 siRNA 1	GUGCGUCAAUGCUCAUUUUAACAACUG	12
	GUUGUUAAAAUGAGCAUUGACGCAC	
Lef1 siRNA 2	CAUGAAAGCAUUCAGAGGCUUCUUAAU	8
	UAAGAAGCCUCUGAAUGCUUUCATG	
Lef1 siRNA 3	GGCAUCAUUAUGUAGCCAGAGUAACUG	3
	GUUACUCUGGCUACAUAAUGAUGCC	

Table 2-2. Sequences of the Dicer substrate siRNA and target exons.

Immunostaining

For immunostaining, cells were cultured in polymer dishes as described previously (Roy et al. 2018). Cells were fixed for 20 minutes using a 4% (by weight) formaldehyde solution (Sigma-Aldrich 252549). Subsequently, cells were permeabilized with 0.5% (by volume) Tween 20 (Sigma-Aldrich P1379) in PBS for 20 minutes and then blocked with 1% (by weight) bovine serum albumin (BSA, Sigma-Aldrich A7906) and 22.5 mg/mL glycine in PBST (0.1% by volume Tween 20 in PBS) for 30 minutes. Cells were

incubated with primary antibodies diluted in 1% BSA in PBST at 4°C overnight, followed by incubation with secondary antibodies in 1% BSA at room temperature for 1 hour. Finally, nuclei were stained with DAPI or Hoechst (Thermo Fisher Scientific R37606 or R37605) fluorescent dyes. The primary antibodies used included Atf2 (Abcam ab32019), Beta-Catenin (Abcam ab19381), GEF-H1 (Abcam ab155785), Lef1 (Abcam ab137872 and ab52017), Oct4 (Abcam ab19857), RNA pol II (Abcam ab5408), and Smad4 (CST 46535).

Live cell imaging setup

We conducted imaging using a Nikon A1 confocal laser scanning microscope equipped with a 40X water immersion objective. Samples were imaged every 8 minutes for approximately 7 hours. Within each 8-minute time window, we selected 17 colonies for imaging. We captured 31 z-stack images covering 30 μm with a step size of 1 μm to fully encompass each colony. The incubator covered the entire microscope body, maintaining a 5% CO2 and 37°C temperature. Nuclei stained with DAPI are shown in blue, and colony shape was imaged using a 640 nm laser in Differential Interference Contrast (DIC) mode.

To assess cell death under the lateral confinement cell culture conditions, we stained all the nuclei with Hoechst and the dead nuclei with DRAQ7. DRAQ7 is non-permeant to live cells and is then used for the staining of dead cells. After incubating the samples with both Hoechst and DRAQ7 dyes for 30 minutes, we imaged them in live condition to determine the number of dead cells.

Imaging for quantifying size of the colonies

Green fluorescence images stained by actin were acquired using a Nikon A1 confocal microscope with a pinhole size of 8 Airy units (AU). To quantify spheroid size, individual spheroids were segmented from the background using the Otsu thresholding method in Fiji, and their projected areas were measured.

Fix cell imaging setup

Samples were imaged using Nikon A1R or Nikon A1 confocal laser scanning microscopes. Confocal images were acquired using a 20X 0.75 NA objective, a 60X 1.4 NA oil objective, or a 100X 1.4 NA oil objective. Confocal z-stack images were

captured with 1 or 2 micron z-steps, with the z-depth no more than 60 microns from the bottom of the dish. DIC images were also acquired using the Nikon A1 confocal microscope.

To measure nuclear fluorescence intensity for proteins of interest, each DAPI-stained nucleus was segmented in 3D from the background and separated from other nuclei. Rough 3D segmentations were obtained by combining local and global Otsu thresholding in 2D for all z-planes. For each segment in each z-plane, watershed segmentation was used to separate spatially overlapping nuclei (due to imaging resolution limitation), using a rough nuclear diameter of 10 microns. An in-house software was used to link the segmented 2D nucleus planes in the z-axis by finding the segments with the closest centroid distance. From the distribution of the closest center distance, a threshold of 1 micron was selected to determine whether two 2D segments belonged to the same or different nuclei in neighboring z-planes. A second threshold of 100 cubic microns was used to filter out 3D segments derived from the previous steps with volumes that were too small. Fluorescence intensity within the nucleus was normalized to the volume of the segmented 3D nucleus. We also used Imaris software to obtain nuclear fluorescence intensities for proteins of interest.

ChIP-qPCR and Epitect assay

ChIP-qPCR was performed as described previously (Roy et al. 2018). Cells were crosslinked with formaldehyde and quenched with glycine. After cell lysis, chromatin was digested using HindIII restriction enzyme (Thermo Fisher FD0505). A ChIP-grade anti-Lef1 mouse antibody (Merck 17-604) was coupled with Dynabeads coated with sheep anti-mouse antibody (ThermoFisher 11201D). Beads were added to the chromatin to isolate DNA associated with Lef1. Following immunoprecipitation (IP), precipitated chromatin was treated with Proteinase K (Thermo Fisher 4333793), and DNA was isolated using the sodium acetate method. PCR primers were either obtained from the Epitect array (Qiagen 334211) or reported in Table 2-1.

RNA-seq analysis

RNA-seq data were generated in a previous study in our lab (Roy et al. 2018). The study included four conditions: 3 hours, 3 days, 6 days, and 10 days after cell seeding, each with three biological replicates and four technical replicates. We used the tophat

(v2.1.1) sequence alignment software to map sequencing reads to the mouse genome (GenBank Assembly ID GCA_000001635.8), downloaded from Ensembl, with default parameters (D. Kim et al. 2013; Zerbino et al. 2018). Genome annotation files were also obtained from Ensembl. The four technical replicates were combined after sequence alignment. The cufflinks (v2.2.1) software was used to calculate the number of reads for each RNA isoform (Trapnell et al. 2010). To obtain the count number for each gene, we combined the number of reads for RNA isoforms from the same gene, deriving reads per million (RPM) values. These values were used in the differential gene expression analysis tool DESeq2 (v1.20.0) (Love, Huber, and Anders 2014). Genes showing significant differential expressions had adjusted p values (Benjamini–Hochberg) below 0.01. Additional RNA-seq datasets for analysis were downloaded from the NCBI-SRA database, with accession IDs listed in Figure 2-5A.

Prize-Collecting Steiner Tree analysis

Prize-Collecting Steiner Tree analysis is a network analysis method used to identify critical functional contexts for specific genes of interest within the global interaction network (S. -s. C. Huang and Fraenkel 2009). It takes input in the form of an interaction network with assigned values to nodes (prizes) and edges (costs). To represent transcriptional regulatory pathways in mice (Mus Musculus), we utilized protein-protein interaction (PPI) data from the STRING database, containing 15,564 proteins and 975,722 interactions. Additionally, we incorporated transcription factor (TF)-target gene relationships from 13 sources, including the TRANSFAC and JASPAR databases, comprising 387 TFs and 19,790 protein-coding gene targets collected from the Harmonizome and Enrichr database (Rouillard et al. 2016; E. Y. Chen et al. 2013). Proteins from the PPI datasets and TFs from the TF-target gene relationships were represented as protein nodes, while target genes in TF-target gene relationships were represented as RNA nodes. Prizes for protein nodes were defined as log2 fold change in gene expression level comparing 3 days to 3 hours, while prizes for RNA nodes were defined as log2 fold change in gene expression level comparing day 3 to day 6. Edge costs represented the reliability of the relationships as defined in the PPI dataset. The Prize-Collecting Steiner Tree method determined a tree that maximized the prizes of the nodes in the tree minus the costs of the edges in the tree, enabling the prediction of the underlying transcriptional regulatory network.

Statistics and Reproducibility

All boxplots are presented as mean ± SD, with the box indicating the 25-75 percentile range and whiskers representing 1.5 times the interquartile range. Each experiment was conducted in at least three replicates. Statistical significance in mean differences was evaluated using Student's unpaired two-tailed t-test between the sample of interest and the corresponding control, with significance levels denoted as follows: *P < 0.05; **P < 0.01; ***P < 0.001.

Results

Morphological changes during the 10 days culture

To explore the mechanisms underlying mechanically-induced changes in fibroblasts, we cultivated mouse embryonic fibroblasts (NIH 3T3 cell line) within lateral confinement, without introducing any exogenous biochemical factors. This model system involves microcontact printing, cell culture and seeding, and a strategy for changing the cell culture media during lateral confinement. Detailed methods are presented in the Method section.

The cells were cultivated and allowed to divide under lateral confinement conditions for a span of 10 days (Figure 2-1). By the 2nd day, the cells were predominantly located at the surface of the dish bottom. By the Day 4 time point, elongated colonies had formed as a result of continued cell division. At this time point, cells start to grow into a multi-layered colony and the rectangular bottom surface is still covered by the cells. After Day 4 time points, the circularity of the colonies start to change. During a live cell imaging experiment on the 5th day, we observed a transition in colony shape from elongated to more rounded (Figure 2-1). This change was accompanied by cells at the bottom surface losing attachment to parts of the rectangular island. These observations hinted at alterations in cell contractility within the colonies at the bottom surface.

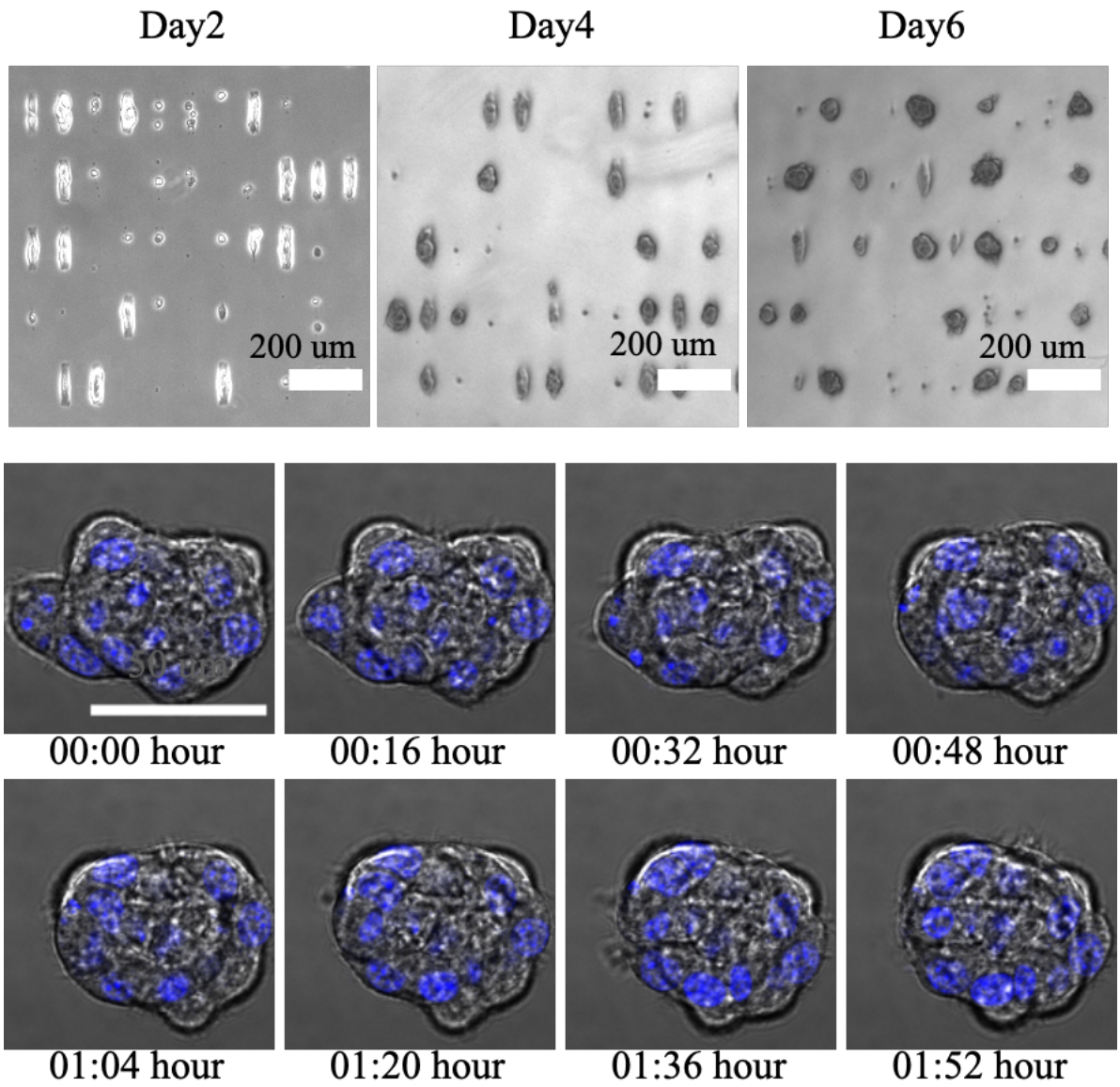

Figure 2-1. Cell and colony morphological changes during lateral confinement induced reprogramming. Top row: Bright Field image showing the cells growing on the rectangular pattern at Day2, Day4 and Day6 time points. Rectangular pattern is 19*95 um size. Scale bar is 200 um. Bottom two rows: 2 hours live cell imaging of one colonies at Day5 time points.

On the 6th day, the majority of colonies had taken on a rounded spheroid shape, indicating that cells continued to proliferate and adapt to their environment. Over the course of the 10-day confinement, spheroid size steadily increased. We quantified spheroid size by measuring the projected area of individual spheroids, which we segmented from the background using bright field images obtained with an EVOS microscope. By Day 10, these fully grown spheroids had an average projected area of

about 12,000 μm² and contained approximately 200 cells (Figure 2-2 B). In summary, this experiment tracked the behavior of cells grown under lateral confinement for 10 days.

We observed that by Day 10, the spheroid cells had acquired stem cell-like properties, consistent with previous studies (Figure 2-2A). We characterized this change by assessing the expression of the stem cell transcription factor Oct4, widely used as a marker for fibroblast de-differentiation. Our experiment revealed an increase in Oct4 protein expression in Day 10 spheroid cells, confirming their de-differentiation. However, the intensity of Oct4 expression varied among nuclei, as seen in Z-plane imaging (Figure 2-2C). These low Oct4 level nucleus tend to locate at the inner part of the spheroid, which suggest that the location of cells in the spheroid may affect the dedifferentiation process.

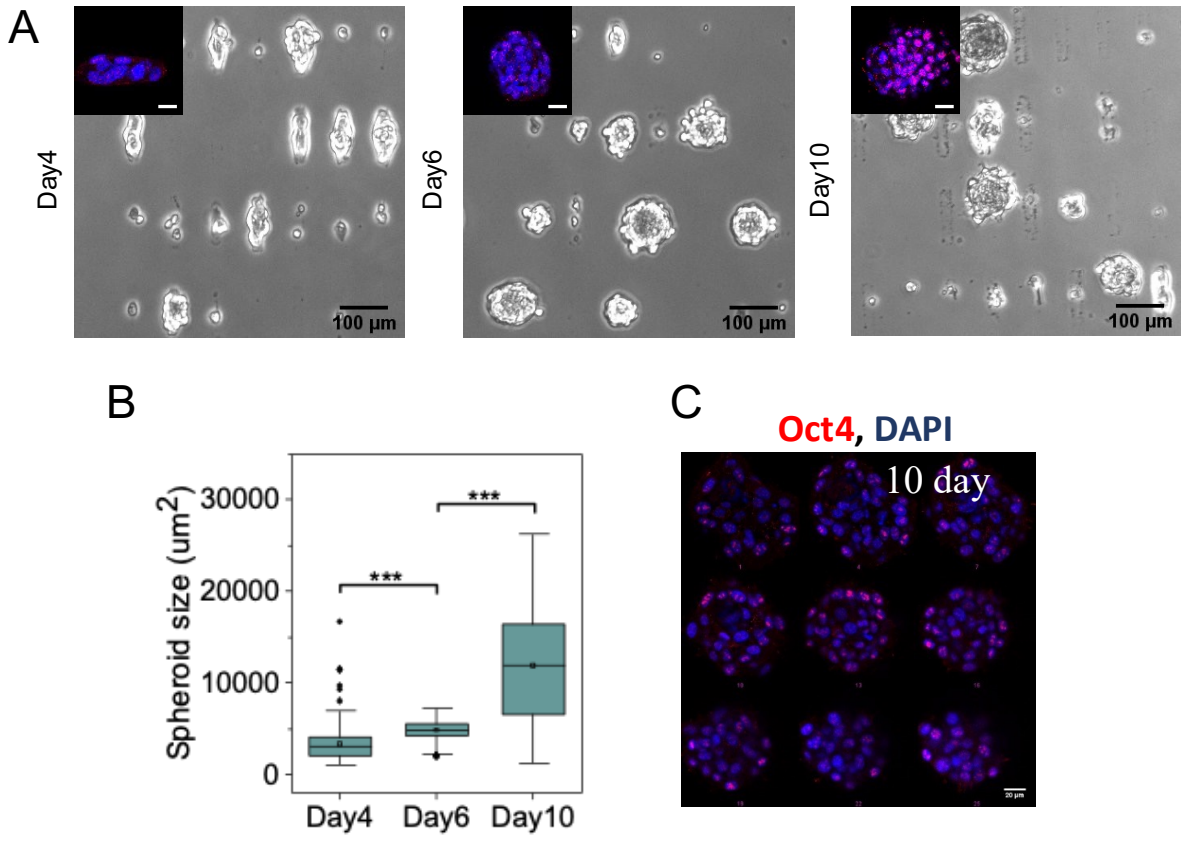

Figure 2-2. Immunostaining of stem cell marker Oct4 showed cells progression to the dedifferentiated state. (A) Differential interference contrast images of cells grown under lateral confinement for 4, 6, or 10 days. The insets show fluorescence images

of Oct4 staining (in red) and nuclei (in blue). Inset scale bar is 20 um. (B) The box plot of spheroid sizes on days 4, 6, and 10 reveals that cells organize into a spheroid on the micropattern, which progressively increases in size. *** $P < 0.001$; n= 499, 440, 153 for day4, 6, and 10 respectively; two-sided Student's t-test was used. (C) Confocal z-stack images of one day10 spheroid showing heterogeneity in Oct4 nuclear staining; scale bar is 20 um.

The growing of the spheroid may create a hypoxic environment for inner located cells, which has been reported in different spheroid culture system (Schmitz et al. 2021). This hypoxia might contribute to cell death, potentially explaining the heterogeneous Oct4 staining. To assess cell death under lateral confinement conditions, we stained all the nuclei with Hoechst and the dead nuclei with DRAQ7, a dye that selectively labels dead cells (Figure 2-3A). We observed very few dead cells in Day 2 colonies, suggesting that lateral confinement conditions did not induce significant cell death at this early stage. However, as colonies grew denser, the number of dead cells increased. Around Day 4, approximately 10% of the cells within the colonies were dead (Figure 2-3B). By Day 10, this number had risen to approximately 30%, with most dead cells located in the inner part of the spheroid. This pattern of cell death suggests that cells in the central region of the spheroid might be more susceptible to cell death due to factors such as nutrient deprivation or the accumulation of waste products.

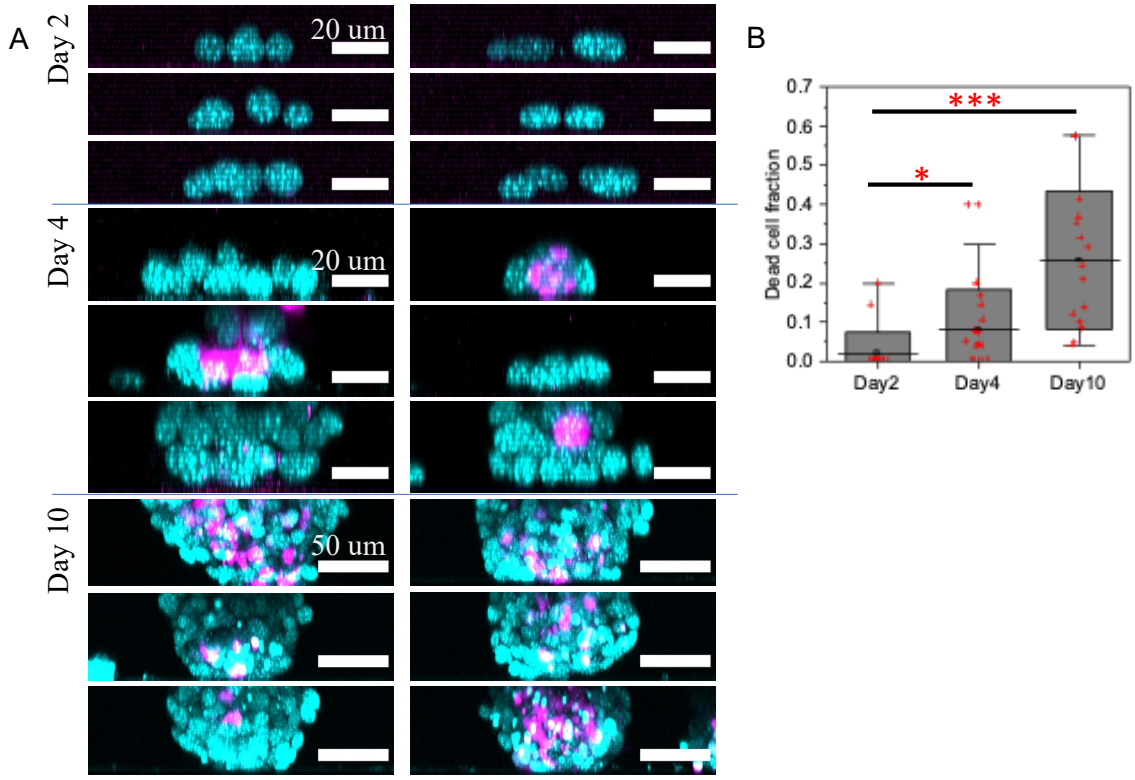

Figure 2-3. Live and dead cells during the lateral confinement induced de-differentiation process. (A) X-Z projection of colonies at Day2/4/10 time point. Hoechst 33342 (DNA) in cyan, DRAQ7 (dead cell) in magenta. (B) Boxplot showing increase of dead cell fraction in colonies during laterally confined growth. * $P < 0.05$, *** $P < 0.001$.

Global gene expression analysis of fibroblast cells grown under lateral confinement reveals their de-differentiation

We conducted time-lapse RNA-seq analysis during lateral confinement-induced growth of fibroblasts at four time points: 3 hours, 3 days, 6 days, and 10 days. We use the transcriptome at 3 hours when cells were elongated on the micropattern as the starting point of the reprogramming process. The transcriptome began to change on Day 3 as cells started forming spheroids on the fibronectin micropattern. The most substantial shift in the transcriptome occurred between Day 3 and Day 6, with approximately 4,000 genes identified as up-regulated with a fold change exceeding 4 (FDR < 0.01) during this period. This suggests that cells experienced a significant change in their gene expression profile during this timeframe. From Day 6 to Day 10,

fewer than 100 differentially expressed genes were detected, even though cells had transitioned into mouse ES medium. This indicates that the process of cell state transition had already begun by Day 6 and was largely complete by Day 10.

Stem cell markers Oct4, Nanog, and Sox2 are known for their role in maintaining pluripotency in embryonic stem cells (ESCs). In this study, we investigated the expression levels of these markers in fibroblast cells reprogrammed during 10 days of lateral confinement. Our results demonstrate that the expression levels of these markers significantly increased from Day 3 to Day 6, rising further by Day 10. Notably, the expression on Day 6 and Day 10 more closely resembled previously published mouse ESC data than fibroblast cells (see methods) (Figure 2-4A-C).

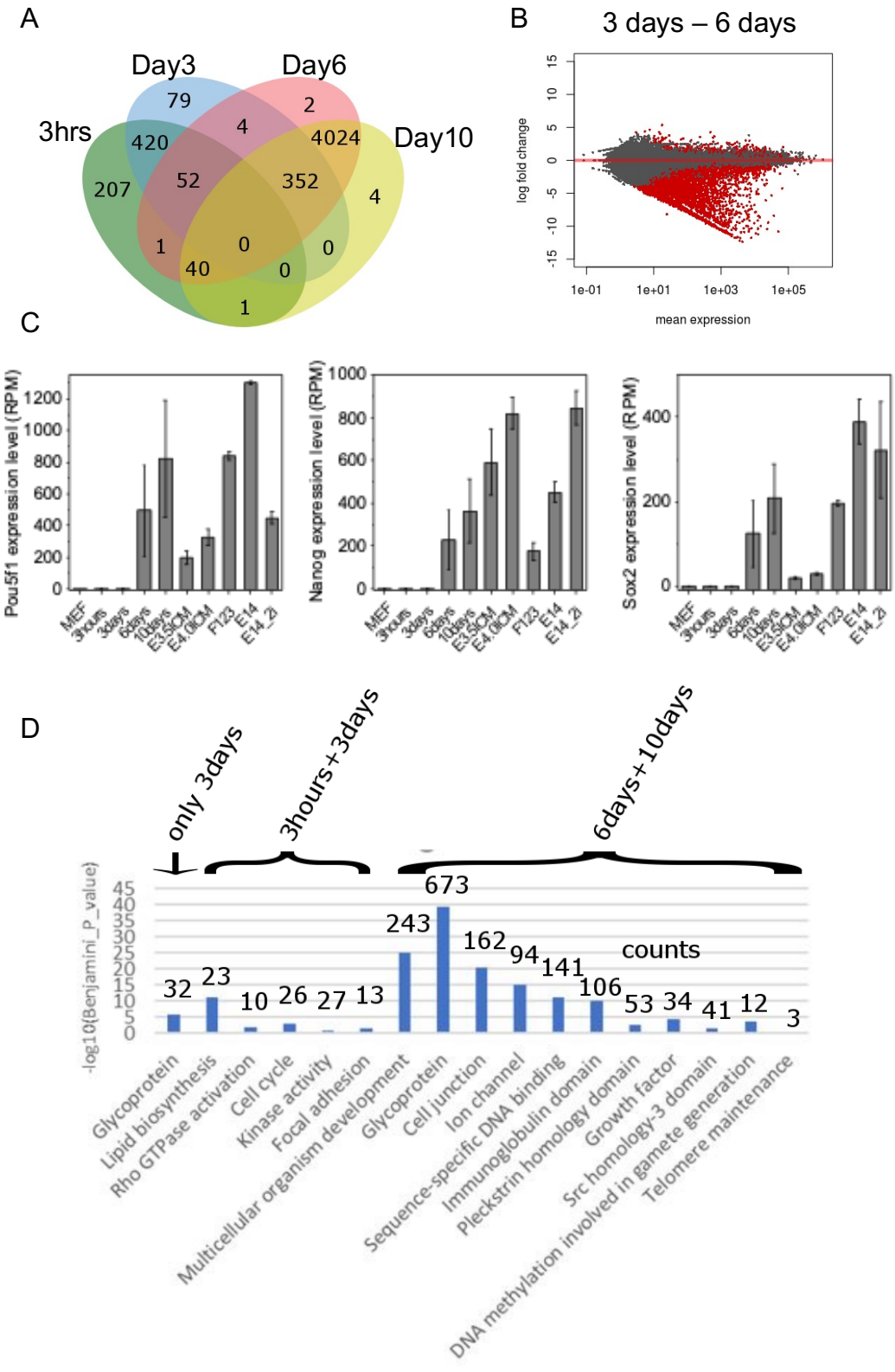

Figure 2-4. Global gene expression analysis of fibroblast cells grown under lateral confinement reveals their de-differentiation. (A) Venn diagram showing the number of up-regulated genes over the four time points during de-differentiation. For example, there are 4024 genes up-regulated on day6 and day10 compared to the 3 hours and

day3 timepoints. Up-regulated genes have FDR (adjusted p-value) < 0.01. (B) MA plot showing log fold-change versus mean expression between 3 days sample and 6 days sample. Positive value of log 2 fold change indicates genes upregulated in 3 days condition. (C) Bar plot graphs of Oct4, Nanog, or Sox2 gene expression (RPM) over four time points during de-differentiation and how it compares to other cell types. MEF: mouse embryonic fibroblasts; E3.5ICM: E3.5 inner cell mass; E4.5ICM: E4.5 inner cell mass; F123: F123 cell line; E14: ES-E14TG2a cell line cultured in mouse ES cell media; E14_2i: ES-E14TG2a cell line cultured in 2i condition. Error bars represent ± SD. (D) Functional annotation of genes that are overexpressed on the day3 timepoint (207 genes), at both 3hours and day3 timepoints (420 genes), and at both day6 and day10 timepoints (4024 genes).

To investigate changes in cellular pathways and functions during de-differentiation, we annotated and clustered the differentially expressed gene lists from the four time points (from Figure 2-4A) using the DAVID tool (D. W. Huang, Sherman, and Lempicki 2008) (Figure 2-4D). Among the 420 DE genes down-regulated in both the Day 6 and Day 10 time points, 26 were focal adhesion genes, including Talin (Tln1) and Integrin (e.g., Itga2, Itgav), suggesting that cells were progressively losing fibroblast properties while forming spheroid-like colonies. Among the 4,000 DE genes up-regulated in later time points (Day 6 and Day 10), over 200 transcription factors were annotated, including POU domain proteins (Pou2f1, Pou3f1, Pou5f1, etc.), Kruppel-like factors (Klf2, Klf5, Klf11, etc.), and SOX gene family proteins (Sox2, Sox3, Sox6, etc.). This suggests that cells acquired stem cell-like properties, consistent with Oct4 staining (Figure 2-2A: inset).

To understand potential changes in cell types over the 10-day culture period, we included published RNA-seq datasets from various mouse cell types for comparison (additional 12 conditions, 29 samples) (Figure 2-5A) (Barutcu et al. 2018; Joshi et al. 2015; Y. Zhang et al. 2018; Yan et al. 2018). Focusing on the 3,959 DE genes (FDR < 0.01 and |log2 Fold change| > 2) identified in our RNA-seq dataset, we conducted a principal component analysis (PCA), reducing dimensions from 3,959 to 2. The resulting visualization (Figure 2-5B) revealed that global gene expression on Day 6 and Day 10 more closely resembled that of mouse embryonic stem cells. These findings collectively suggest that cell growth under lateral confinement can induce the

de-differentiation of fibroblasts (NIH 3T3 cell line), with the most significant changes in gene expression occurring between Day 3 and Day 6 of confinement.

A

SRA ID	Description	SRA ID	Description
SRR3083897	RNASeq-E3.5ICM_rep1	SRR2658589	RNASeq-E14_rep1
SRR3083898	RNASeq-E3.5ICM_rep2	SRR2658612	RNASeq-E14_rep2
SRR3083901	RNASeq-E4.0ICM_rep1	SRR2173784	RNASeq-E14_serum_rep1
SRR3083902	RNASeq-E4.0ICM_rep2	SRR2173785	RNASeq-E14_serum_rep2
SRR3083903	RNASeq-E5.5Epi_rep1_part1	SRR2173786	RNASeq-E14_2i_rep1
SRR3083904	RNASeq-E5.5Epi_rep1_part2	SRR2173787	RNASeq-E14_2i_rep2
SRR3083905	RNASeq-E5.5Epi_rep2_part1	SRR5227280	RNASeq-F123_rep1
SRR3083906	RNASeq-E5.5Epi_rep2_part2	SRR5227281	RNASeq-F123_rep2
SRR3083907	RNASeq-E5.5VE_rep1	SRR6117986	RNASeq-MEF_Female_rep1
SRR3083908	RNASeq-E5.5VE_rep2	SRR6117987	RNASeq-MEF_Female_rep2
SRR3083909	RNASeq-E6.5Epi_rep1	SRR6117988	RNASeq-MEF_Female_rep3
SRR3083910	RNASeq-E6.5Epi_rep2	SRR6117992	RNASeq-MEF_Male_rep1
SRR3083911	RNASeq-E6.5VE_rep1_part1	SRR6117993	RNASeq-MEF_Male_rep2
SRR3083912	RNASeq-E6.5VE_rep1_part2	SRR6117994	RNASeq-MEF_Male_rep3
SRR3083913	RNASeq-E6.5VE_rep2		

B

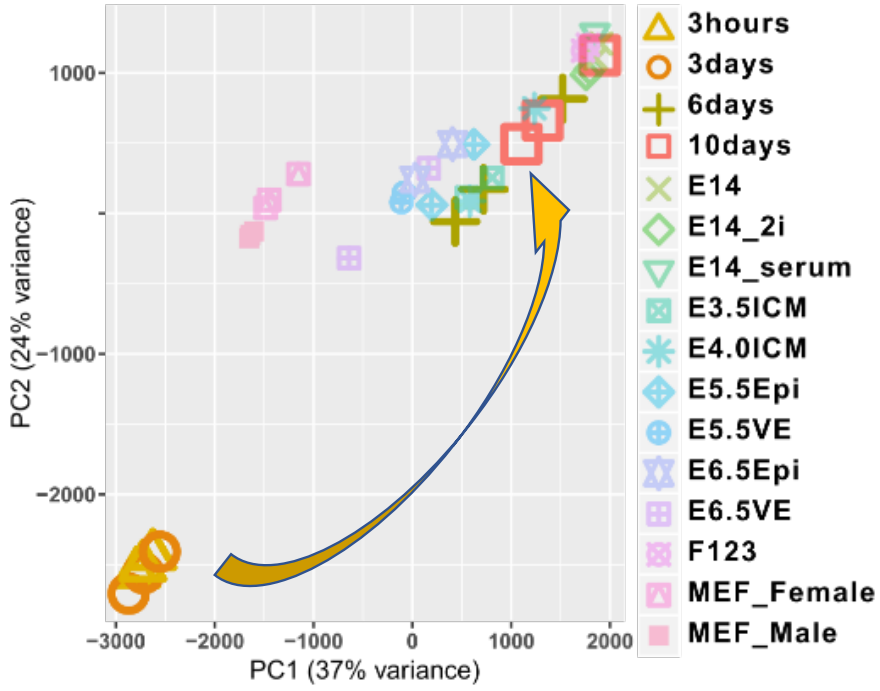

Figure 2-5. Mapping global gene expression pattern to known cell states using public available RNAseq dataset and PCA method. (A) RNAseq datasets from NCBI-SRA databased used in this study. (B) Principal Component Analysis of the gene expression profile shows change of cell states through de-differentiation. Genes

involved in this analysis are differentially expressed with adjusted p-value < 0.01 and |log2 Fold change| > 2.

Prize-Collecting Steiner Tree analysis highlights Lef1 dependent signaling during laterally confined growth of fibroblasts

To identify regulatory mechanisms that lead to gene expression changes from day3 to day6, we analyzed the functions of the genes up-regulated on day3, compared to 3hours. Our hypothesis posited that these genes might play a pivotal role in mediating the gene expression transitions observed between day 3 and day 6. To elucidate their functions, we performed gene ontology enrichment analysis on the 675 up-regulated differentially expressed (DE) genes at day 3 using pantherDB (Mi et al. 2019). This analysis linked these genes to processes governing cell motility, proliferation, and histone acetylation, all exhibiting a false discovery rate (FDR) less than 0.05. Intriguingly, among these genes, we identified thirty transcription factors, including Lef1 and Klf11, six of which possessed enhancer binding capabilities (Figure 2-6 A-D).

To gain further insight into the reprogramming process, we examined the expression patterns of established reprogramming factors – Nanog, Sox2, and Oct4 – at later time points (Theunissen and Jaenisch 2014). found that all but c-Myc showed significant up-regulation at either the day6 or day10 timepoint (Figure 2-6 E). Our analysis revealed significant up-regulation of all these factors at either day 6 or day 10 (Figure 2-6 E), suggesting their role in driving the shift toward a de-differentiated gene expression profile. However, the mechanical cues triggering the activation of these reprogramming factors remained elusive.

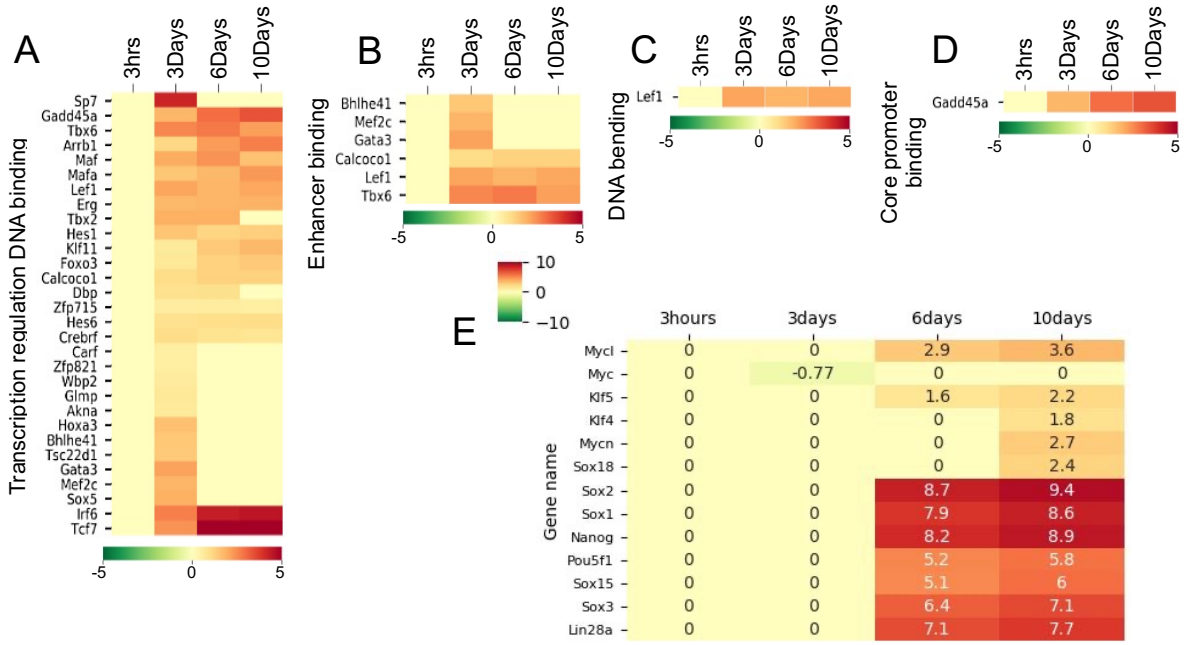

Figure 2-6. Gene expression changes during lateral confinement growth. (A-D) The heatmaps show the expression changes of transcriptional regulators which were found by gene ontology annotation. They contain the terms GO:0044212 (transcription regulatory region DNA binding), GO:0035326 (enhancer binding), GO:0008301 (DNA binding and bending), and GO:0001047 (core promoter binding). The values refer to the log2 fold change compared to the 3 hours sample. (E) Heatmap showing log2 fold changes in gene expression of reprogramming factors.

Moving forward, we constructed a comprehensive transcriptional regulatory network to uncover potential regulatory events transpiring between day 3 and day 6. To establish the transcriptional regulatory network, we employed the Prize-Collecting Steiner Tree analysis method (S. -s. C. Huang and Fraenkel 2009). This method identifies a subnetwork that elucidates the gene expression changes characterizing the de-differentiation process. Within this method, proteins from the PPI dataset and TFs from the TF-target gene relationships represented protein nodes. Target genes from TF-target gene relationships were designated as RNA nodes. Prizes for protein nodes were defined by the log2 fold change in gene expression between day 3 and the 3-hour time point, while prizes for RNA nodes were determined by the log2 fold change between day 3 and day 6. Edge costs represented the reliability of relationships in the PPI dataset. The Prize-Collecting Steiner Tree method then seeks

to maximize the prizes of nodes in the network while subtracting the costs of edges, enabling us to predict the underlying transcriptional regulatory network.

We first evaluated gene expression changes between the 3-hour and day 3 time points, identifying proteins up-regulated at day 3 and representing them as nodes (depicted as orange, red, and pink nodes in the left and middle sections of Figure 2-7 A). These proteins were connected based on PPI data. Subsequently, we added genes up-regulated between day 3 and day 6 as RNA nodes (depicted as blue and turquoise nodes on the right side of the network), connecting them based on TF-target gene relationships. By optimizing trees from the global interactome (comprising both PPI and TF-target data), we constructed the transcriptional regulatory network by connecting edges in the optimized trees, an advantage over PPI networks filtered solely by differentially expressed genes. This approach allowed us to include important intermediate genes in the Prize-Collecting Steiner Tree network, even if no expression changes were detected, as seen with Beta-catenin and Smad4 (see Figure 2-7 B).

In this constructed network, transcriptional regulators were represented by protein nodes with direct relationships with RNA nodes. These regulators encompassed transcription factors, such as Lef1 and Myc, and genes involved in epigenetic modification, such as Ep300 and Hdac1. Among these transcriptional regulators, we identified those that targeted reprogramming factors (depicted as turquoise nodes in Figure 2-7 C). Prioritizing this subset of transcriptional regulators based on their gene expression changes between the 3-hour and day 3 time points, we pinpointed Lef1 as a potential key regulator of fibroblast de-differentiation. Lef1 stood out not only for its high up-regulation but also for its potential control over thousands of genes that exhibit up-regulation between day 3 and day 6 (see Figure 2-7 D). Intriguingly, the up-regulation of Lef1 preceded that of reprogramming factors, hinting at an early dedifferentiation stage when cells primed themselves for the expression of reprogramming factors.

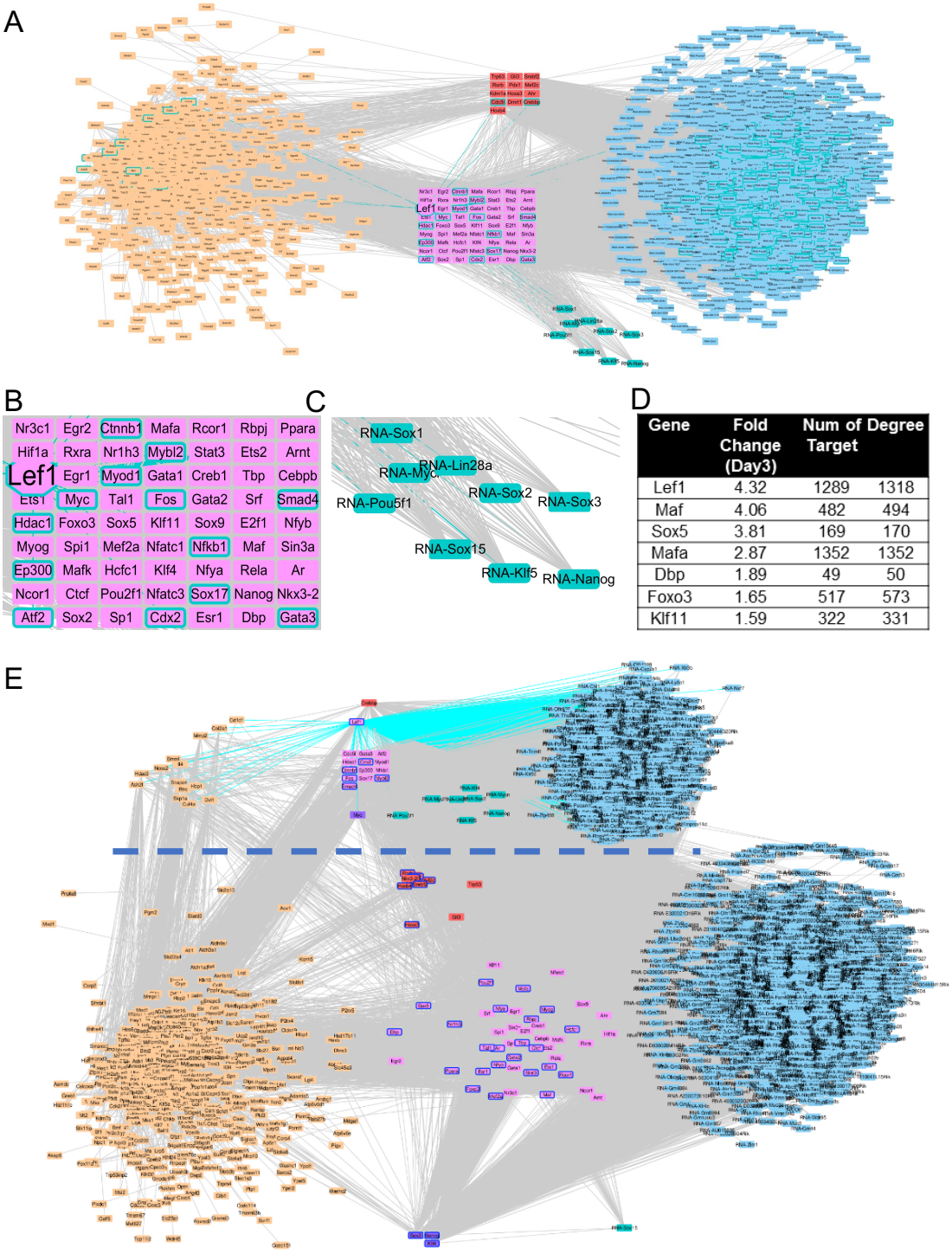

Gene	Fold Change (Day3)	Num of Degree	Target
Lef1	4.32	1289	1318
Maf	4.06	482	494
Sox5	3.81	169	170
Mafa	2.87	1352	1352
Dbp	1.89	49	50
Foxo3	1.65	517	573
Klf11	1.59	322	331

Figure 2-7. Prize-Collecting Steiner Tree analysis highlights Lef1 dependent signaling during laterally confined growth of fibroblasts. (A) Transcriptional regulatory network derived using the Prize-Collecting Steiner Tree method. Nodes in orange, red, and pink represent genes up-regulated on day3 and important intermediates that connect them. Nodes shown in red and pink are transcriptional regulators. Nodes in blue and turquoise represent genes up-regulated on day6. Within these, turquoise nodes represent reprogramming factors. (B, C) Enlarged pictures of (A) showing

transcriptional regulators (in pink and Lef1 and its interactors with turquoise border) that can regulate the expression or bind to the gene loci of reprogramming factors (in turquoise). (D) Ranking of the transcriptional regulators (pink nodes in (A)). (E) This rearranged network from (A) shows the importance of Lef1 in the early de-differentiation stages. Proteins physically interacting with Lef1; the target genes of Lef1 were shifted up and separated from the remaining proteins by dashed lines. Transcriptional regulators that can be regulated by Lef1 are represented by blue borders.

To delve deeper into Lef1's role, we scrutinized its interactions with other transcriptional regulators. Fifteen out of seventy-six transcriptional regulators, including Beta-catenin, Smad4, and Ep300, physically interacted with Lef1. Additionally, thirty-eight transcription regulators were identified as potential Lef1 targets (depicted as red and pink nodes with blue borders in Figure 2-7 E). Collectively, these findings emphasize the pivotal role of Lef1 as a key transcription factor in the early de-differentiation induced by lateral confinement and fibroblast growth.

Knockdown of Lef1 and time course studies of Lef1 and Oct4 reveal Lef1's critical role in fibroblast de-differentiation

To dissect the characteristics of early de-differentiation, we closely examined the dynamic changes in the transcription factor Lef1 and the stem cell marker Oct4. Quantitative PCR assays were used to measure the RNA levels of these two genes. In line with the RNA-seq data, we observed significantly higher expression levels of Lef1 on days 2, 4, and 6 compared to control cells in 2D culture (Figure 2-8 A). Notably, Oct4 also exhibited an upregulation trend starting from day 4 (Figure 2-8 B).

To visualize the heterogeneity in marker expression within the cell population during the early de-differentiation stage on day 4, we performed immunostaining for Lef1 and Oct4 (Figure 2-8 D, F). The results indicated an increase in the number of nuclei with a high Oct4 concentration, defined by an average Oct4 fluorescence intensity exceeding 300 per pixel, throughout the de-differentiation process. Specifically, 10% of all nuclei exhibited high Oct4 concentration on day 4, which increased to 20% on

day 6 and 22% on day 10 (Figure 2-8 C). On day 6, a significant increase in the population mean of the Oct4 signal was also observed (Figure 2-8 G). Concerning Lef1 staining, a significant upregulation was noted on day 4 in comparison to earlier time points (Figure 2-8 E).

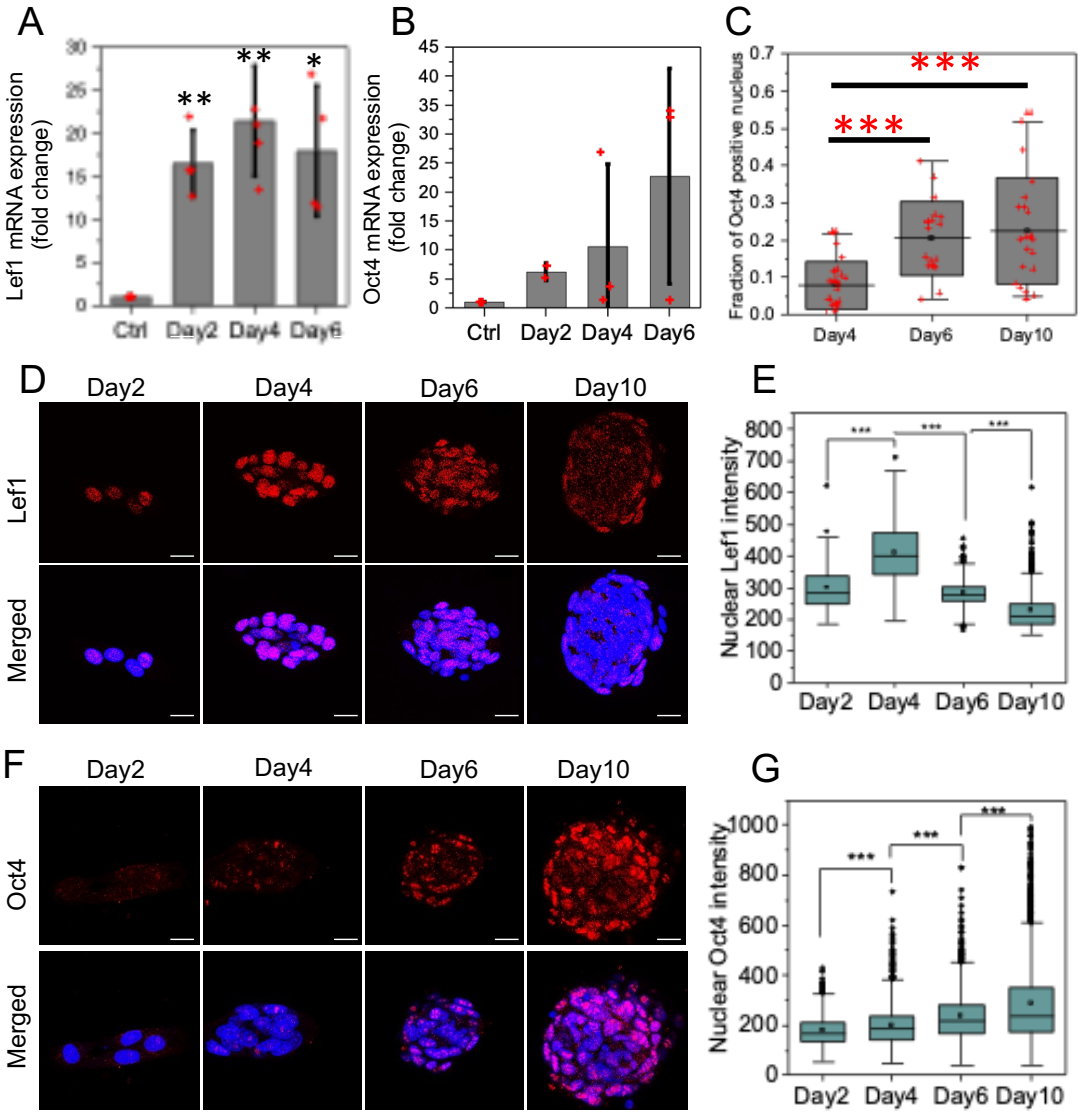

Figure 2-8. Time course studies of Lef1 and Oct4. (A, B) Bar plot graphs of Lef1 and Oct4 mRNA expression level over time, error bars represent ± SD. (C) Boxplot showing increase of Oct4 positive nucleus in colonies during laterally confined growth. *** P < 0.001. (D) The fluorescence images of Lef1 (in red) and nucleus (in blue) for cells at day2, 4, 6, and 10. Scale bar is 20 um. (E) The box plot shows the quantification of average nuclear Lef1 intensity over time; n=244, 279, and 673 respectively. (F) The fluorescence images of Oct4 (in red) and nucleus (in blue) for cells at day2, 4, 6, and 10. Scale bar is 20 um. (G) The box plot shows the

quantification of average nuclear Oct4 intensity over time; n=481, 1486, 1248 and 2472 respectively.

To validate the role of Lef1 in the de-differentiation process, we knocked down the expression of Lef1 using siRNA. When Lef1 siRNA was added two hours after cell seeding, a considerable reduction in Lef1 nuclear fluorescence intensity was observed up to five days post-seeding compared to cells without Lef1 siRNA (Figure 2-9 A-C).

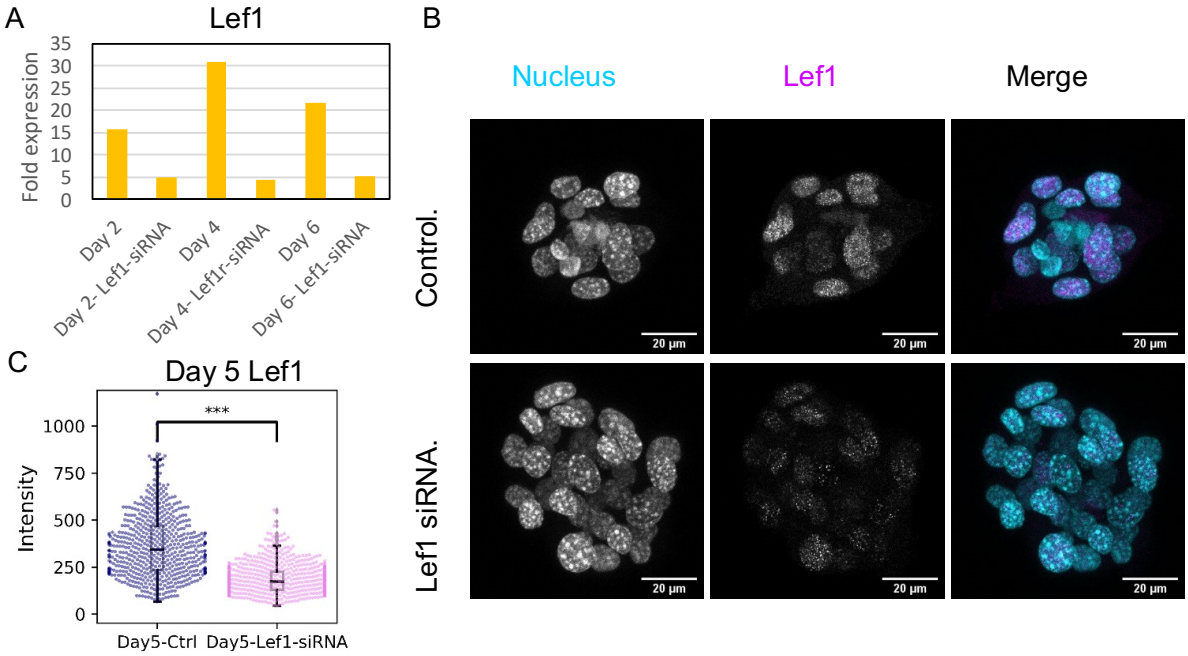

Figure 2-9. Efficiency of Lef1 siRNA knockdown experiments. (A) Quantitative qRT-PCR showing reduction in mRNA levels of Lef1 after siRNA knockdown. (B) Immunostaining and imaging of Lef1 shows reduction in protein levels on day5 under siRNA knockdown conditions. Scale bar is 20 um. (C) Boxplot showing significant reduction in Lef1 nuclear fluorescence intensity after siRNA knockdown as compared to control siRNA sample on day5; *** $P < 0.001$; n= 628, 722 nuclei for control and knockdown conditions, respectively.

We examined the de-differentiation efficiency through immunostaining of Oct4 at day10. The distribution of Oct4 nuclear intensity for cells with or without negative control (NC) siRNA (i.e. no recognized sequences in the mouse and human transcriptomes) treatment appeared nearly identical, with no significant difference in

the mean Oct4 intensity between these two conditions (Figure 2-10 C). However, cells subjected to Lef1 siRNA knockdown displayed significantly lower Oct4 intensity compared to those treated with NC siRNA (Figure 2-10 A, B, D, E). Notably, the distribution of Oct4 nuclear intensity between these two conditions showed distinct differences, with a greater proportion of nuclei displaying high Oct4 staining following NC siRNA treatment than with Lef1 siRNA treatment. qPCR experiments further supported these findings, indicating a reduction in Oct4 RNA levels in Day 10 spheroids under Lef1 siRNA treatment (Figure 2-10B).

Additionally, we conducted alkaline phosphatase staining to assess stem cell-like properties. The staining procedure was performed as described in reference (Roy et al. 2018). Notably, we observed a significant reduction in spheroid number under Lef1 siRNA treatment (Figure 2-10 F-H), with a decreased ratio of positively stained spheroids. These results suggest that Lef1 is an important regulator in the fibroblast de-differentiation process.

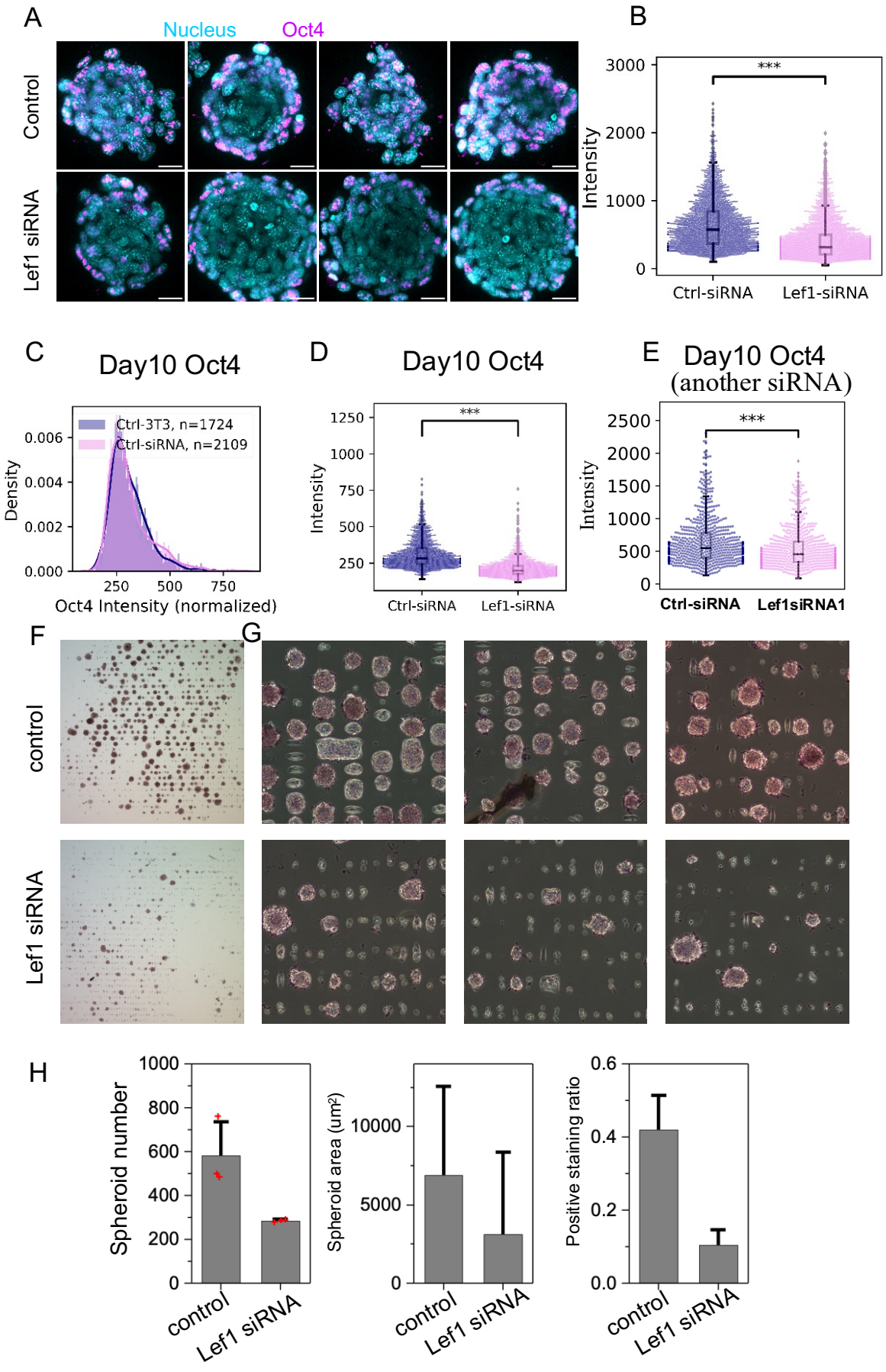
A
Nucleus
Oct4
Control
Lef1 siRNA
B
Intensity
3000
2000
1000
0
***
Ctrl-siRNA
Lef1-siRNA
C
Day10 Oct4
Ctrl-3T3, n=1724
Ctrl-siRNA, n=2109
Density
0.006
0.004
0.002
0.000
250
500
750
Oct4 Intensity (normalized)
D
Day10 Oct4
Intensity
1250
1000
750
500
250
***
Ctrl-siRNA
Lef1-siRNA
E
Day10 Oct4
(another siRNA)
Intensity
2500
2000
1500
1000
500
0
***
Ctrl-siRNA
Lef1siRNA1
F
G
control
Lef1 siRNA
H
Spheroid number
1000
800
600
400
200
0
control
Lef1 siRNA
Spheroid area (um²)
10000
5000
0
control
Lef1 siRNA
Positive staining ratio
0.6
0.4
0.2
0.0
control
Lef1 siRNA

Figure 2-10. Knockdown of Lef1 shows the critical role of Lef1 in fibroblast de-differentiation. (A) The fluorescence images of Oct4 (in magenta) and nucleus (in cyan) for control and Lef1 siRNA treated cells. Scale bar is 50 um. (B) Quantification of Oct4 nuclear intensity shows distinct distributions for control and Lef1 siRNA samples; *** $P < 0.001$; n=2708 and 3171 respectively. (C) Histogram showing no difference in de-differentiation efficiency in control samples (without siRNA added) (n=1724) as compared to NC siRNA treatment (n=2109) measured by Oct4 nuclear fluorescence intensities. (D) Boxplot showing changes in de-differentiation efficiency (measured by Oct4 nuclear intensities) between Lef1 siRNA and control siRNA samples in another repeat experiment; n=2109, 2144, respectively. This siRNA targets exon 7 and 8. (E) Boxplot showing changes in Oct4 nuclear intensities between a different Lef1 siRNA and control siRNA samples. This siRNA targets exon 10 and 12. (F) staining of the Day10 spheroid on the dishes. (G) higher resolution image showing that positive spheroids can be distinguished from negative stained ones. (H) Barplots shows the quantification of number of spheroids, area of the spheroids and the ratio of positive stained spheroids in control and Lef1 siRNA samples (data for three replicates are shown). Barplots shows standard deviation and the mean.

Lef1 binds to the gene loci of the reprogramming factors during the mechanically induced fibroblast de-differentiation

Next, we studied whether Lef1 could directly regulate the expression of reprogramming factors. We used the commercially available Chromatin Immunoprecipitation (ChIP) qPCR primer array designed for the promoter regions of mouse stem cell transcription factors (in collaboration with Dr. Prasuna Ratna). This array contains homeobox genes, GATA binding proteins and TFs that could induce de-differentiation. Based on our TF-target gene relationship data, 23 genes in this array were identified as potential targets of Lef1.

Using a ChIP-grade antibody (Merck 17-604) to precipitate Lef1-bound genomic DNA fragments, we set out to identify which of these stem cell transcription factors were directly regulated by Lef1. Our analysis unveiled that Lef1 directly bound to the promoter regions of six genes, most notably Nanog and Oct4 (also called Pou5f1),

which exhibited consistent and significant promoter occupancy during the early de-differentiation stage (Figure 2-11 A, B). To further validate these findings, we designed primers targeting the Nanog and Oct4 promoter regions and performed ChIP-qPCR experiments. The results corroborated our earlier observations, confirming that Lef1 exhibited increased binding to the promoter regions of Nanog and Oct4 during the course of lateral confinement culture from Day 2 to Day 4 (Figure 2-11 C, D).

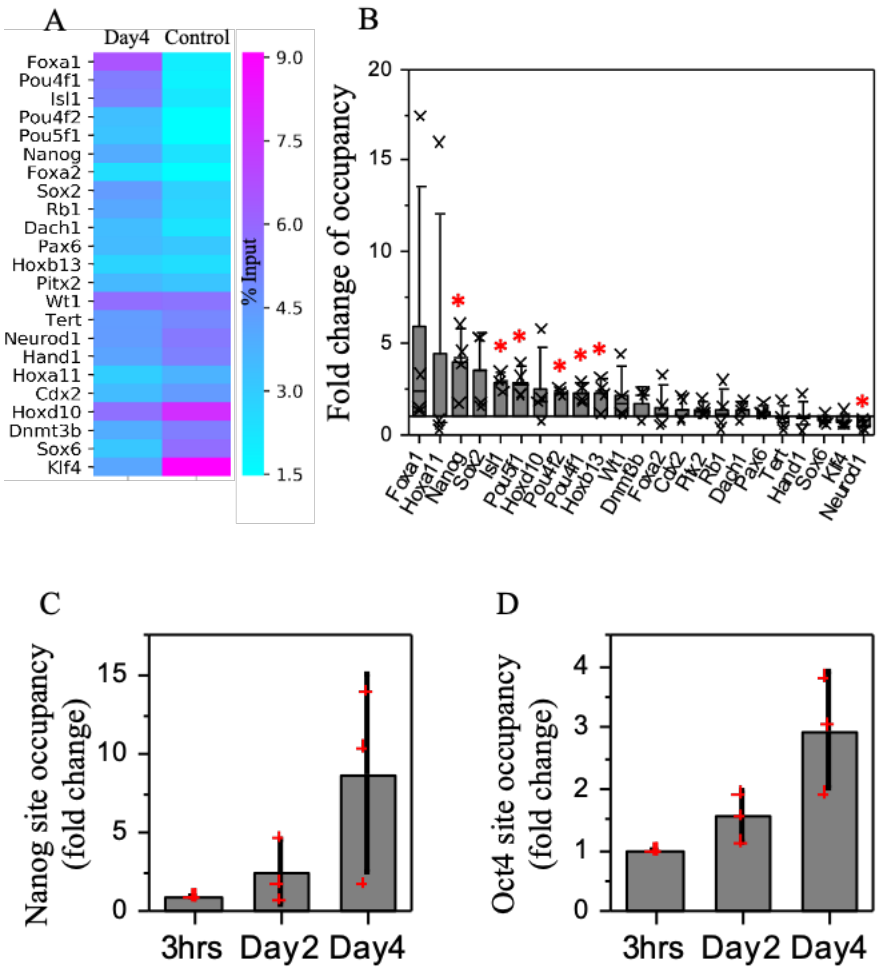

Figure 2-11. Lef1 binds to the gene loci of the reprogramming factors during the mechanically induced fibroblast de-differentiation. (A) The heatmap shows binding of Lef1 to the promoter regions of selected genes in Day4. Control cells grown on 2D culture are also shown. The unit is percentage of input. (B) Fold change of Lef1 promoter occupancy comparing Day4 sample to control sample. *P < 0.05. (C/D) The bar plot shows the increase of binding of Lef1 to Nanog and Oct4 promoter regions at 3hrs, Day2 and Day4.

We extended our investigation by examining the spatial distribution of Lef1 in correlation with histone modifications within the cell nucleus. Our analysis revealed a significant decrease in Lef1's colocalization with the inactive histone mark H3K9me3 and a simultaneous increase in colocalization with the active histone mark H3K4me3 on Day 4 comparing to 2D cultured fibroblasts as the control (Figure 2-12 A, B). Additionally, Lef1 showed a significant increase in colocalization with RNA polymerase II (RNA pol II) (Figure 2-12 C). Collectively, these findings suggest that Lef1 plays a direct role in regulating the expression of key reprogramming factors, Oct4 and Nanog, during fibroblast de-differentiation.

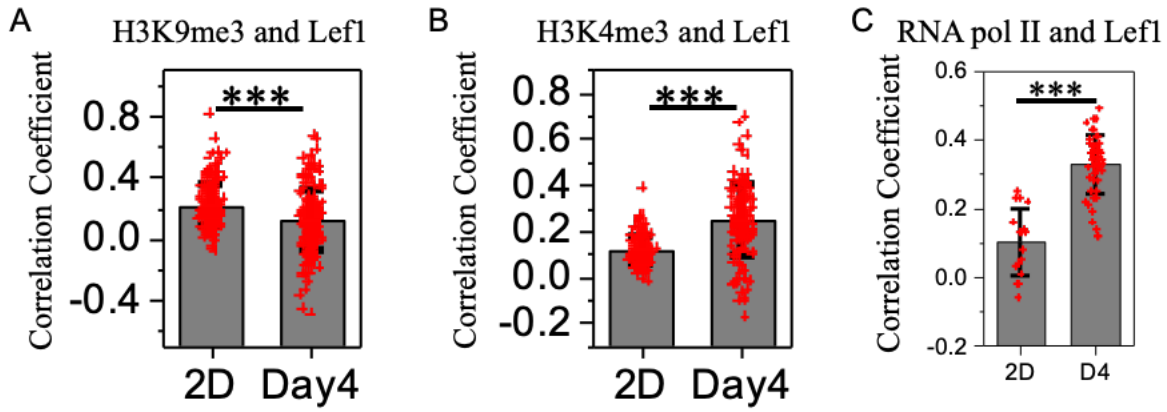

Figure 2-12. Colocalization studies of Lef1 with histone modifications. (A-C) Correlation coefficient on pixel wise basis for Lef1 and H3K9me3, Lef1 and H3K4me3, Lef1 and RNA pol II. ***P < 0.001.

Lef1 activation is potentially regulated by Smad4 and Atf2 pathways

To understand the molecular mechanisms governing Lef1 activation during early de-differentiation, we explored the expression and localization of potential Lef1 activators. Previous studies have indicated that Lef1 requires association with other DNA-binding proteins for transcriptional regulation (Giese, Cox, and Grosschedl 1992; Hsu, Galceran, and Grosschedl 1998). Hence, we focused our investigation on transcriptional regulators that can interact with Lef1. Based on the collected TF-target gene relationships and constructed transcriptional regulation network mentioned above, we identified 15 transcriptional regulators that not only interacted with Lef1 but also shared many up-regulated targets at day6 as compared to day3 (Table 2-3,

Figure 2-13). Three of the identified regulators, Smad4, Atf2, and Beta-catenin, can activate Lef1 transcription (Nawshad and Hay 2003; Lim and Hoffmann 2006; Grumolato et al. 2013). Interestingly, only Smad4 and Atf2 had Nanog, Oct4 or Sox2, as shared targets with Lef1 (Table 2-3).

TF	Shared Targets	Shared Reprogramming Factors
Myc	1200	Klf4,Klf5,Lin28a,Mycl,Mycn,Nanog,Pou5f1,Sox2
Ep300	1192	Klf4,Klf5,Lin28a,Mycl,Mycn,Nanog,Sox2
Gata3	950	Klf4,Klf5,Lin28a,Mycl,Pou5f1,Sox2
Hdac1	725	Klf4,Klf5,Lin28a,Mycn
Fos	703	Klf4,Klf5,Mycl,Nanog
Smad4	679	Klf4,Klf5,Mycl,Nanog,Pou5f1
Atf2	561	Lin28a,Mycl,Mycn,Sox2
Mybl2	502	Klf5,Mycn,Nanog,Sox2
Nfkb1	462	Klf4,Lin28a,Mycl,Mycn
Myod1	455	Klf4,Klf5,Lin28a,Mycl,Sox2
Cdx2	415	Klf4,Lin28a,Mycn
Sox17	231	Klf4,Lin28a,Mycn,Sox2
Ctnnb1	119	--
Crebbp	69	--
Cdc5l	32	Klf4

Table 2-3. List of investigated transcription factors, which could physically interact with Lef1. The number of targets and number of reprogramming factors as targets shared between each transcription factor and Lef1.

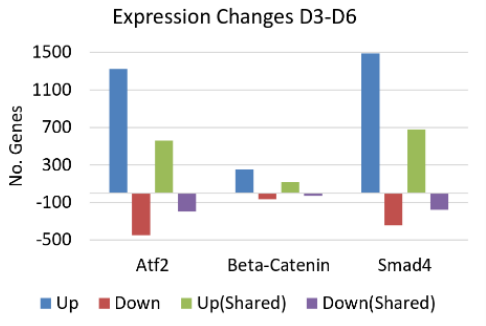

Figure 2-13. Bar plot showing the number of genes up-regulated or down-regulated from day3 to day6. Up (Shared): shared targets with Lef1 that are up-regulated. Down (Shared): shared targets with Lef1 that are down-regulated. These targets are differentially expressed with adjusted p-value < 0.01.

We immunostained Lef1 with the three identified regulators in cells from the day4 timepoint to observe their localization. Smad4 and Atf2 both co-localized with Lef1 in the cell nucleus, whereas Beta-catenin remained mostly in the cytoplasm (Figure 2-14 A, C, E). This co-localization was quantified at the cellular level by segmenting individual nuclei using the DAPI staining, followed by calculation of the average fluorescence intensity for each protein of interest. The correlation was 0.88 between Smad4 and Lef1 and 0.68 between Atf2 and Lef1, while the correlation between Beta-catenin and Lef1 was only 0.2 (Figure 2-14B, D, F). These results suggested that Lef1 was more likely to be associated with Smad4 and Atf2 than with Beta-catenin in the de-differentiation stage. However, quantifying the nuclear fractions of Beta-catenin will not be sufficient to exclude the roles of Beta-catenin in Lef1 dependent signaling.

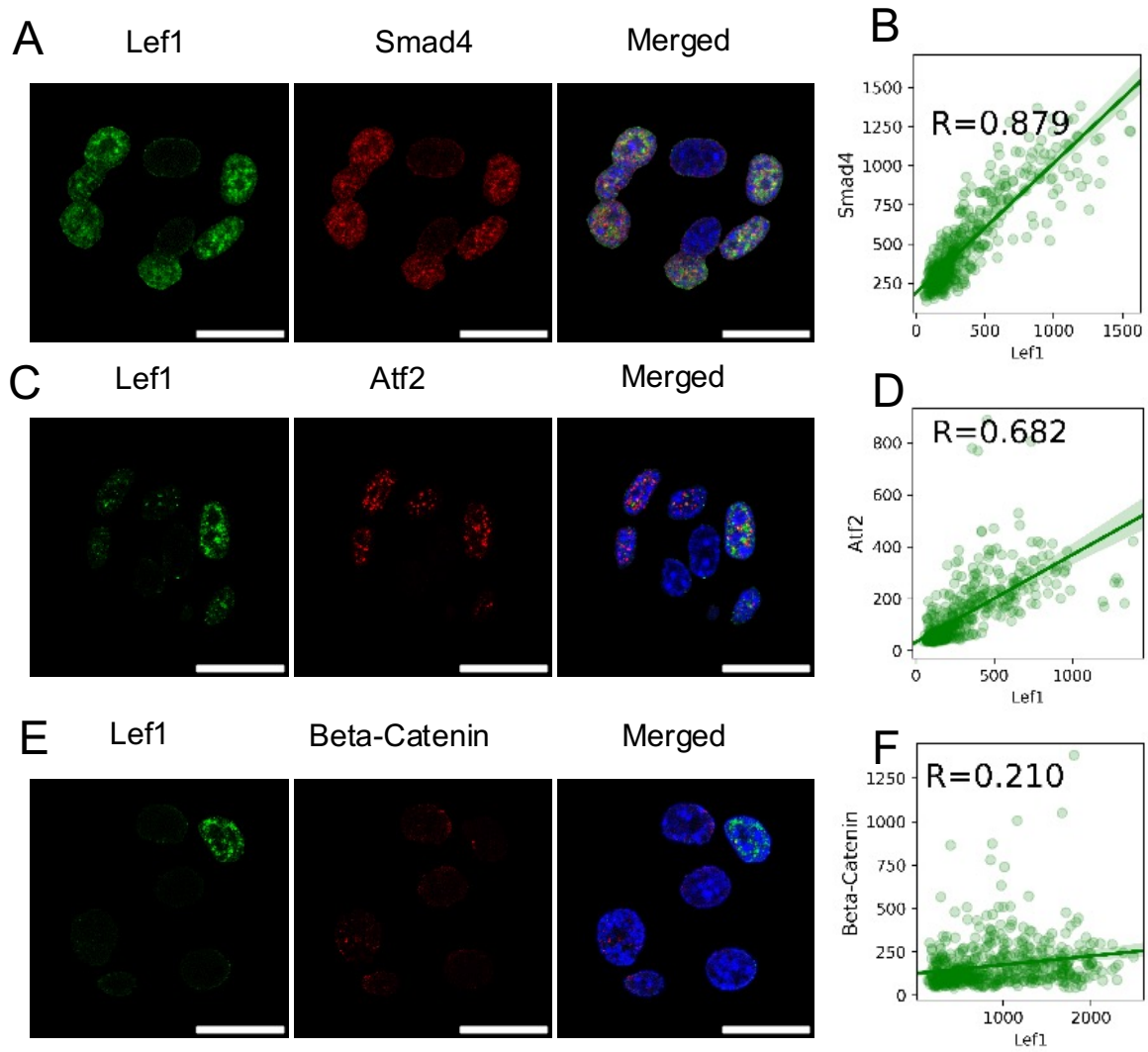

Figure 2-14. (A, C, E) The staining of Lef1, Smad4, and Nucleus; Lef1, Atf2 and Nucleus; and Lef1, Beta-catenin and Nucleus in day4 sample. Scale bar is 20 um. (F, G, H) Scatter plots showing the averaged nuclear fluorescence intensity of Lef1 and Smad4; Lef1 and Atf2; and Lef1 and Beta-catenin along with linear fits and the corresponding Pearson correlation coefficients.

To explore the role of Lef1 association with Atf2 or Smad4, we co-stained Lef1/Atf2/RNA pol II or Lef1/Smad4/RNA pol II. The reasoning of this colocalization studies is the following: the colocalization of a transcription factor and the phosphorylated RNA polymerase II C-terminal domain (activated form) indicates the transcriptional activity of this current transcription factor. When a transcriptional factor and its coactivator colocalize with active RNA pol II, it gives further evidence of the activation mechanisms of the transcription factor. Using confocal imaging, we found

the colocalization of Lef1 and its coactivator (Atf2 or Smad4) with active RNA pol II (Figure 2-19 AB). When comparing the colocalization among these transcription factors and RNA pol II for 2D cultured fibroblasts sample and Day4 colonies, we found that RNA pol II tends to significantly localize to the Lef1 and Smad4 on Day 4 (Figure 2-19 C).

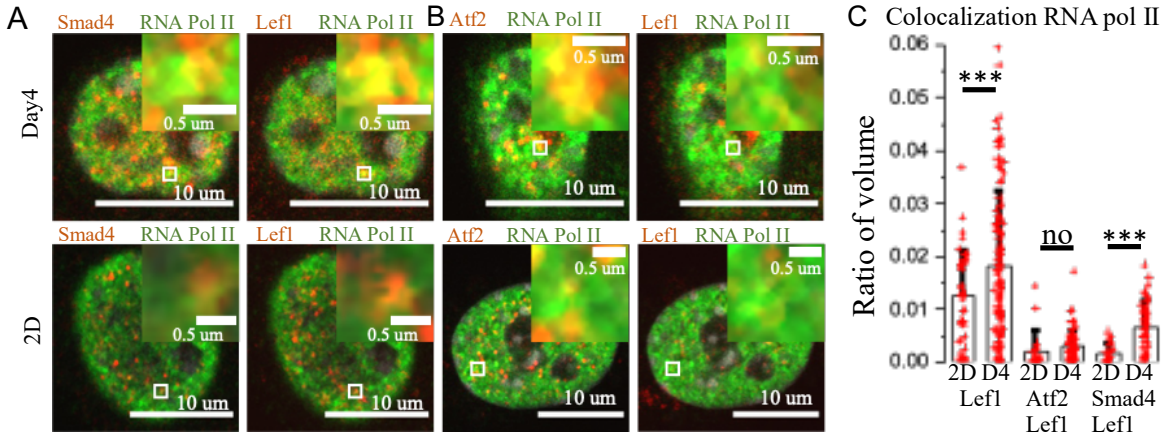

Figure 2-19. Colocalization studies of Lef1, Atf2, Smad4 and RNA polymerase II. (A) Representative images of co-staining with Lef1/Smad4/RNA pol II. (B) Representative images of co-staining with Lef1/Atf2/RNA pol II. The insets are the zoom of small white box regions from the respective images. (C) Barplot shows the change of colocalization from 2D culture conditions to D4 (Day4 sample). The unit is the ratio of colocalized volume and the nucleus volume. Each dot represents one nucleus. The first two bars are the colocalization of Lef1 and RNA pol II. The middle two bars are the colocalization of Lef1, Atf2 and RNA pol II. The last two bars are the colocalization of Lef1, Smad4 and RNA pol II.

We conducted qPCR experiments to evaluate the combined effect of Lef1, Atf2, and Smad4 on reprogramming. The results indicated that the triple knockdown led to a more pronounced reduction in Oct4 mRNA levels compared to Lef1 knockdown alone (Figure 2-20).

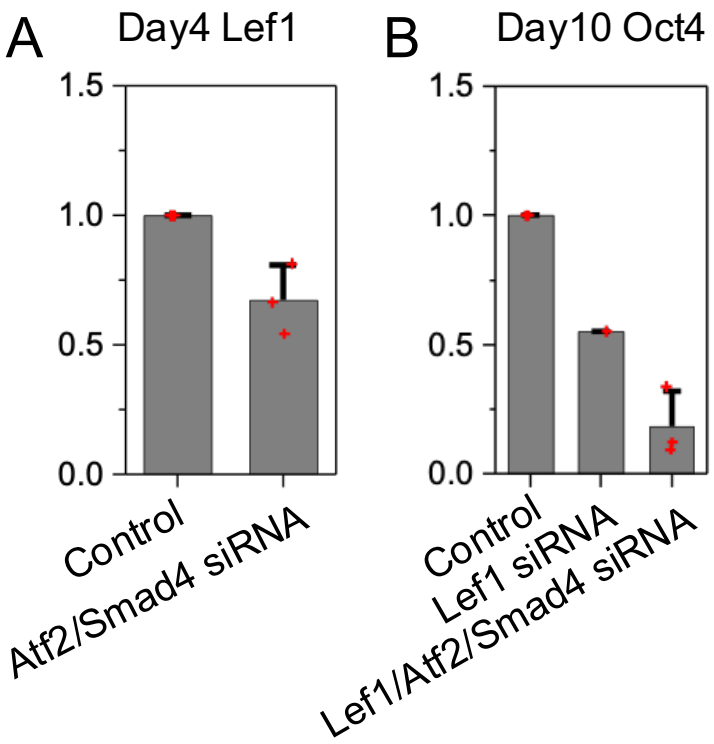

Figure 2-20. qPCR experiments on the knockdown effect of Lef1, Atf2 and Smad4. (A) Barplot showing the fold change of Lef1 mRNA level under Atf2 and Smad4 siRNA treatment (at first two days) for the Day4 colonies sample. (B) Barplot showing the fold change of Oct4 mRNA level under Lef1 siRNA knockdown or Lef1 together with Atf2 and Smad4 siRNA treatment (at first two days) for the Day10 colonies sample.

To further test the role of Beta-catenin in Lef1 activation, we blocked the interaction between Lef1 and Beta-catenin using the inhibitor iCRT3. To block the interaction between Beta-catenin and TCF family transcription factors, 25 uM iCRT3 was used (using the same volume of DMSO as control). Interestingly, iCRT3 inhibition led to a significant increase in de-differentiation, as measured with Oct4 staining at the Day10 timepoint, suggesting that the Beta-catenin pathway may play a distinct role in mechanically induced fibroblast de-differentiation (Figure 2-21 A, B). Collectively, these results identified Smad4 and Atf2 as potential activators of Lef1.

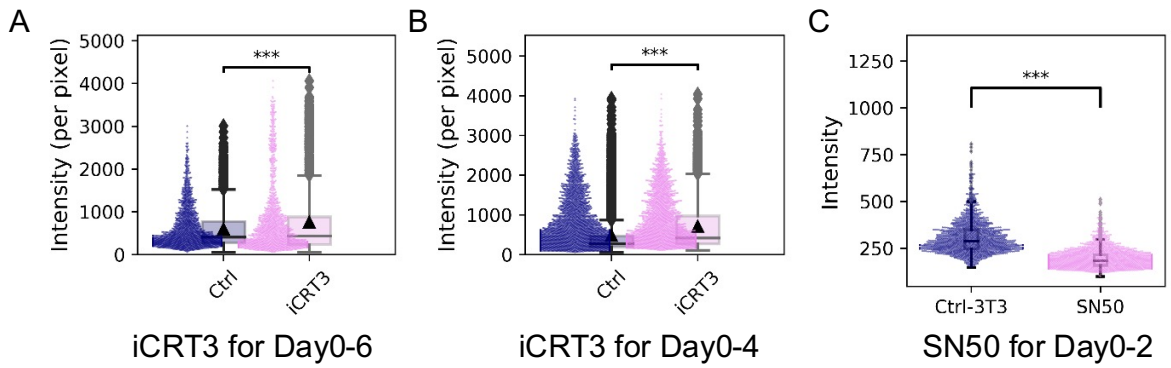

Figure 2-21. Testing Beta-Catenin, NFkB pathway using pharmaceutical compound. (A, B) The effect of iCRT3 on de-differentiation efficiency measured by nuclear Oct4 fluorescence intensity (day10); n= 1971, 1589, 7251, 3693 respectively. (C) The effect of NFkB inhibitor SN50 on de-differentiation efficiency (day10); n= 1724, 2320 respectively.

Other regulatory mechanisms in laterally confined growth induced reprogramming

Next, we also explore other possible mechanisms leading to reprogramming in this laterally confined growth process. Based on RNAseq data analysis, we observed a downregulation of several genes associated with the actin cytoskeleton (as depicted in Figure 2-21 D). Conversely, we observed an upregulation of various genes related to cell-cell junctions (as illustrated in Figure 2-22 E). Furthermore, our investigation unveiled an upregulation of several genes involved in the Wnt signaling pathway (as shown in Figure 2-22 F).

To determine whether the activation of Lef1 is associated with microtubule alterations, we employed immunostaining techniques to examine the abundance of cellular microtubules and nuclear Lef1 within the same cells. To calculate the mean intensity of microtubule for each cell, we performed an 8 um expansion of the segmentation mask around each nucleus. Our staining protocol involved Lef1, α-tubulin, and GEF-H1. Intriguingly, this analysis revealed a strong correlation between the level of nuclear Lef1 and the cytoplasmic abundance of GEF-H1 (as depicted in Figure 2-22 A). However, the correlation between Lef1 and α-tubulin, as well as GEF-H1 and α-tubulin, was relatively weak (as shown in Figure 2-22 BC).

Previous studies have highlighted the sensitivity of NFkB to local mechanical perturbations and its potential role as an upstream transcription factor for Lef1 (Jain et al. 2013; Yun et al. 2007). In our investigations, we observed that the inhibition of p65, a subunit of NFkB, using 50 µg/mL of SN50 led to a reduction in the efficiency of dedifferentiation (as illustrated in Figure 2-21 C). This effect could arise from NFkB's ability to either inhibit Lef1 or directly control the expression of downstream factors.

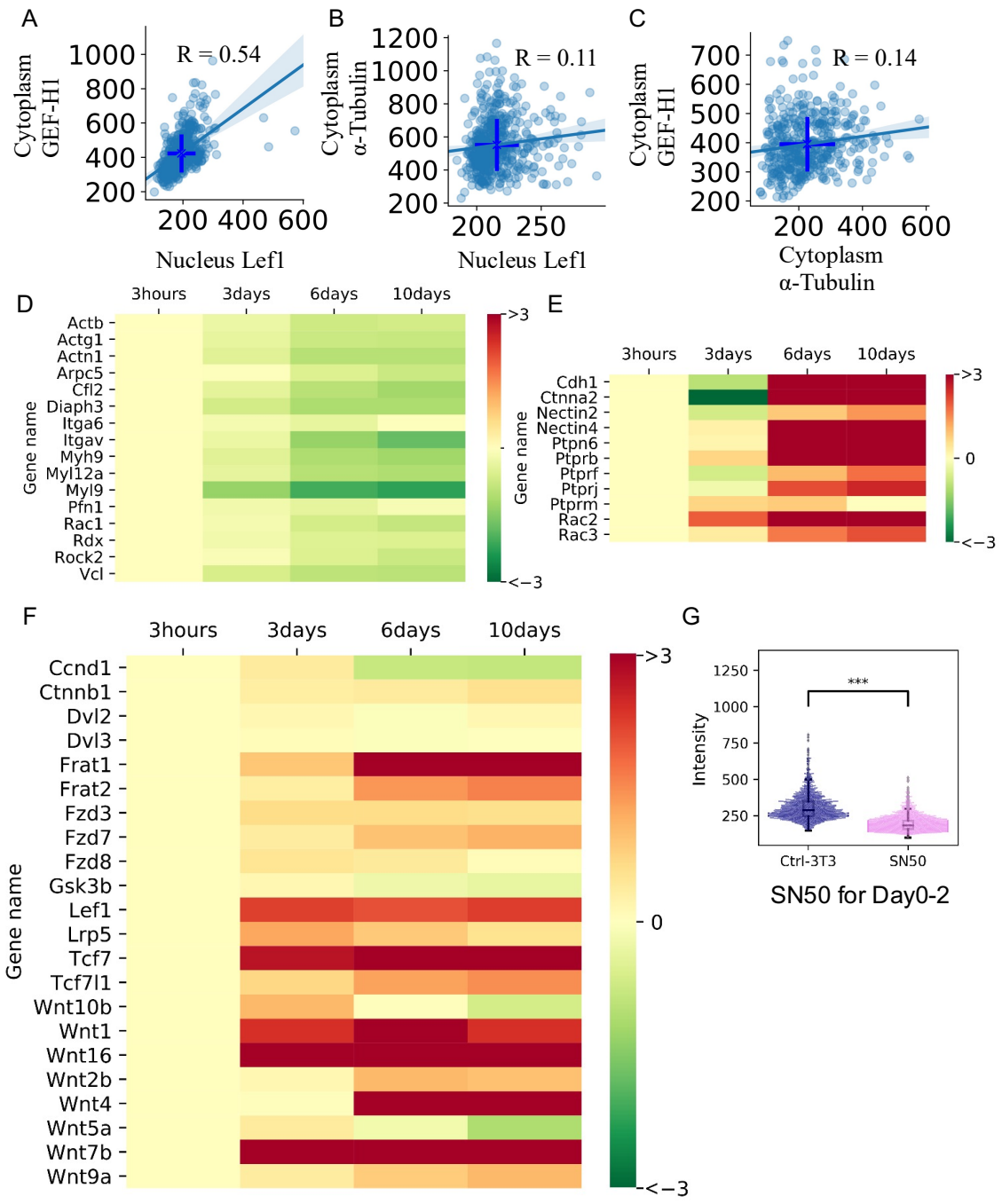

Figure 2-22. (A-C) the scatterplot shows the correlation among nucleus level of Lef1, cytoplasm level of GEF-H1 and α-Tubulin. Heatmap of gene expression changes of proteins in (D) actin cytoskeleton regulation pathway, (E) cell adherence junction pathway, and (F) WNT signaling pathway. Values are log2 fold change. (G) The effect of NFkB inhibitor SN50 on de-differentiation efficiency (day10); n= 1724, 2320 respectively.

Discussion

The process of nuclear reprogramming, which involves the introduction of exogenous transcription factors or the use of small molecules, has shed light on the remarkable plasticity of cell-states (Theunissen and Jaenisch 2014). Surprisingly, recent findings have demonstrated that cell-state transitions can also be triggered solely by mechanical changes in the extracellular environment, without the need for external transcription factors (Roy et al. 2018). This phenomenon is realized through the use of micropatterns that impose geometric constraints, acting as boundary conditions, thereby facilitating changes in both the mechanical and transcriptional profiles of cells during laterally confined growth. These observations strongly suggest a close relationship between the extracellular mechanical environment and somatic transcription factors, which can activate mechanotransduction pathways and induce cell-state transitions.

To identify the key somatic factors responsible for mechanically induced fibroblast cell-state transitions, we employed time-course RNA-seq data. Through an integrated analysis combining RNA-seq data with the STRING protein interaction database and the TRANSFAC and JASPAR transcription factor-target gene databases, we employed the Prize-Collecting Steiner Tree network optimization method (Schiebinger et al. 2019; Szklarczyk et al. 2015; Rouillard et al. 2016; S. -s. C. Huang and Fraenkel 2009). The gene ontologies data provides candidates of transcriptional regulators showing upregulation on Day3. Since some of the potentially important transcriptional factors enhancing dedifferentiation may not change at mRNA level, we used the Prize-Collecting Steiner tree method to identify them. This method combined PPI and TF-target datasets to identify transcription factors when three time points of RNAseq data were considered. The genes upregulated on Day3 which appears as protein nodes can link genes upregulated on Day6 which appears as RNA nodes through transcriptional regulators which may or may not show expression changes. Lef1 was selected based on the expression fold change and number of upregulated downstream targets. Intriguingly, we also uncovered potential coactivators of Lef1, specifically Atf2, Beta-Catenin, and Smad4, despite the absence of significant

changes in their expression profiles. Subsequent validation experiments supported the role of Lef1 in orchestrating fibroblast cell-state transitions, as evidenced by the reduced efficiency observed upon Lef1 downregulation. Furthermore, many reprogramming genes were identified as putative targets of Lef1.

Recent research has uncovered additional facets of Lef1's activity, including its role in enhancing oncogenic effects in hepatocellular carcinoma (HCC) cells through the Notch signaling pathway (Fang et al. 2019). In addition, Lef1 has been implicated in promoting the tumorigenicity of esophageal squamous cell carcinoma (ESCC) through the TGF-β signaling pathway (Zhao et al. 2019). Furthermore, Lef1 has been shown to regulate Nanog and Oct4 expression in mouse embryonic stem cells (C. Huang and Qin 2010; C. G. Kim et al. 2011). Earlier experiments related to lateral inhibition in cell specification mediated through mechanical signalling highlighted the role of YAP and TAZ (Xia et al. 2019). However, in our experiments, we did not observe significant changes in the gene expression of YAP and TAZ in 3-day cultures compared to the control, and these genes were notably absent in the network model. Notch4, which exhibited upregulation on Day 3 and demonstrated potential interactions with Atf2 and Beta-catenin, could serve as an upstream factor for Lef1 activation. Since the dedifferentiated cells tend to locate at the outer layer of the colonies, the cell state transitions could be driven by both mechanical as well as spatial signals. The outer cells, during laterally confined growth, are in privileged positions without being fully surrounded by other cells which could also be a potential spatial signal for outer cells to undergo dedifferentiation. Collectively, these studies suggest that Lef1 could enhance dedifferentiation through distinct pathways in different functional contexts including the laterally confined dedifferentiation of fibroblast.

Furthermore, ChIP-qPCR promoter occupancy assays revealed not only the nuclear localization of Lef1 but also its direct binding to the promoter sites of Nanog and Oct4, two pivotal reprogramming factors. Time-course analysis of Lef1, Oct4, and Nanog provided support for the hypothesis that Lef1 activation precedes the downstream expression of Nanog and Oct4. These findings emphasize the significant role played by somatic transcription factors in mechanically induced cell-state transitions.

To delve into the molecular pathways governing Lef1 activation, we scrutinized the involvement of the NFkB, Beta-catenin, Smad4, and Atf2 pathways. Previous investigations had indicated that NFkB is responsive to local mechanical perturbations and can function as an upstream transcription factor for Lef1 (Jain et al. 2013; Yun et al. 2007). In our experiments, inhibiting p65, an NFkB subunit, using SN50 led to a notable reduction in dedifferentiation efficiency. This effect could be attributed to NFkB either inhibiting Lef1 or directly controlling the expression of downstream factors. Additionally, Beta-catenin is known to bind and activate Lef1 through the Wnt signaling pathway, potentially facilitated by cadherin junctions (Behrens et al. 1996; J. Sun and Weis 2011; Howard et al. 2011). However, our time-course correlation analysis between Beta-catenin and Lef1 revealed only weak nuclear localization correlation. Furthermore, inhibiting their physical interaction failed to establish a significant link between Beta-catenin and Lef1 in the regulation of downstream pathways. Nevertheless, the upregulation of the Wnt signaling pathway during the reprogramming process suggests that Lef1's role may be independent of the Beta-catenin/Wnt signaling pathway.

Previous studies suggested that Lef1 can switch partner from Beta-catenin to other activators (Aloysius, DasGupta, and Dhawan 2018). Intriguingly, a meticulous analysis of Lef1's upstream interaction partners pinpointed Smad4 and Atf2 as potential candidates for the regulation of Lef1 activation during fibroblast cell-state transitions. Earlier studies have demonstrated that Smad4 and Atf2 can activate Lef1 (Lim and Hoffmann 2006; Grumolato et al. 2013). Consistent with this, we found that Smad4 and Atf2 were colocalized with Lef1 in the nucleus during mechanically induced cell-state transitions. The TGF-beta/SMAD pathway has been shown to be regulated by mechanical signals in the environment, such as ECM perturbations (X. Xu et al. 2018). In addition, activated Smad proteins can interact with different DNA binding cofactors, which might include Lef1, to target a unique group of genes (Kang, Chen, and Massagué 2003). These results collectively suggest that Lef1 dependent pathways, in consort with Atf2/Beta-Catenin/Smad4, are transiently activated to regulate the downstream transcription factors. The non-monotonic kinetics of Lef1 might be determined by the differential role of upstream signaling, e.g. Wnt pathway, in dedifferentiation process as reported in some studies (Ho et al. 2013).

Considering that fibroblast identity wanes as cell-cell contacts are established, we also explored the potential role of cytoskeleton-related processes. Intriguingly, we observed a strong correlation between nuclear Lef1 levels and cytoplasmic GEF-H1 levels. In addition, a recent study from our lab unveiled the regulatory role of actomyosin contractile forces in cell-fate decisions during laterally confined growth-induced reprogramming (Venkatachalapathy et al. 2022). These findings collectively suggest that multiple mechanotransduction pathways may converge to activate Lef1, initiating the expression of downstream transcription factors.

In conclusion, this project has illuminated the capacity of the local mechanical microenvironment, in the absence of exogenous factors, to induce cell-state transitions through Lef1-dependent signaling pathways. The application of the Prize-Collecting Steiner Tree analysis has unveiled other somatic transcriptional regulators that could be pivotal in driving cell-state transitions. These findings imply that somatic cells in vivo downregulate key somatic transcription factors or their regulatory pathways as a mechanism to maintain cellular homeostasis. The aberrant activation of these transcriptional regulators over multiple cell divisions may serve as precursors for dedifferentiation and transdifferentiation pathways. Given that fibroblast dedifferentiation necessitates a biphasic cell-state transition, it is conceivable that these transitions, though infrequent, may contribute not only to dedifferentiation programs but also to the development of various disease states.

Chapter 3: Cytoskeleton pathways and chromatin reorganization in mechanically induced reprogramming and rejuvenation

This part of the result section is adapted from two papers:
Bibhas Roy, **Luezhen Yuan**, Yaelim Lee, Aradhana Bharti, Aninda Mitra, G.V. Shivashankar, Fibroblast rejuvenation by mechanical reprogramming and redifferentiation, PNAS 2020.
DOI: 10.1073/pnas.1911497117

Trinadha Rao Sornapudi*, **Luezhen Yuan***, Jana Muriel Braunger, Caroline Uhler and G.V. Shivashankar, Transcription-associated chromatin reorganization during cellular rejuvenation, under review 2023. (*equal first author)

As a second author, I contributed to the PNAS publication by planning and conducting experiments and data analysis, including live cell imaging, image analysis, RNAseq analysis and statistical analysis.

I contributed to the second publication equally with T.R.S. (Postdoctoral fellow in our group) by planning and conducting experiments, data analysis and writing the manuscript. I carried out cell culture, immunostaining and imaging experiments related to chromatin organization and gene expression at the nuclear envelope region and imaging-based cytoskeleton-heterochromatin colocalization analysis. The data analysis that I contributed to included image analysis, RNAseq analysis and HiC analysis.

Introduction

In complex organisms like humans, cells undergo two types of aging: chronological aging and replicative aging. Chronological aging at the organismal level encompasses the natural, time-driven aging process, while replicative aging arises from cell division and the gradual erosion of replicative capacity. Aging is accompanied by epigenetic changes, such as accumulation of DNA damage, telomere attrition, increased reactive oxygen production (ROS) and mitochondrial dysfunction (López-Otín et al. 2023;

Rossi et al. 2007; H.-W. Lee et al. 1998; Correia-Melo et al. 2016). These changes collectively culminate in the decline of cellular function and cell-cycle arrest. Recent studies have revealed the alteration of links between the cytoskeleton and the nuclear envelope during aging, with young cells primarily featuring actin-nuclear envelope links, while their older counterparts exhibit relatively more microtubule-nuclear connections (Chang et al. 2019).

A concrete illustration of this aging process is observed in the dwindling population of skin fibroblasts, accompanied by their diminished capacity to proliferate and synthesize essential components of the dermal extracellular matrix. The extracellular matrix plays a pivotal role in upholding the skin's mechanical integrity and homeostasis. However, as aging advances, both the quantity and quality of the extracellular matrix undergo a steady decline (López-Otín et al. 2013; Dimri et al. 1995; A. S. Wang and Dreesen 2018).

Fibroblasts are indispensable constituents of the skin, tasked with facilitating the remodeling of the extracellular matrix. Conventional approaches to skin rejuvenation involve the injection of autologous dermal fibroblasts into the skin. Nevertheless, emerging personalized cell therapies are garnering attention as more stable treatment options. These innovative therapies leverage autologous stem cells and induced pluripotent stem cells (iPSCs) to rejuvenate the skin (Takahashi and Yamanaka 2006; Dinella, Koster, and Koch 2014). By harnessing the regenerative potential of these cells, it becomes possible to reinstate the youthful characteristics of the skin. It is worth noting that while these interventions rejuvenate cells, they are not exempt from acquiring genomic mutations that might elevate the risk of cancer development. Consequently, extensive efforts are currently underway to enhance the safety and address the limitations of these methods.

In the quest for effective therapeutic strategies, an ideal approach would involve resetting the aging process through non-genetic means while preserving the cell's differentiation program. This approach holds the promise of reversing aging-related changes without introducing potentially harmful genetic modifications. By focusing on non-genetic interventions, researchers aspire to develop safer and more precise methods to combat the effects of aging.

Moreover, aging is often accompanied by epigenetic changes, such as the integration of histone variants into the genome, global DNA methylation alterations, and global heterochromatin modifications at the nuclear envelope (Robin and Magdinier 2016; Bollati et al. 2009). Furthermore, chromosomal abnormalities tend to increase rapidly during aging, contributing to the induction of cellular senescence. Numerous studies have demonstrated that global chromatin organization undergoes alterations during replicative senescence and oncogene-induced senescence (OIS) (Criscione, Teo, and Neretti 2016). Specifically, it has been observed that Lamina-associated domains (LAD), typically tethered to the nuclear periphery in young cells, tend to relocate more towards the interior of the nucleus in aging cells due to a partial loss of Lamin proteins. This phenomenon leads to the formation of senescence-associated heterochromatin foci (SAHF) (Criscione et al. 2016). Apart from changes in chromatin spatial organization, aging is also associated with global alterations in transcriptional programs (Ibañez-Solé et al. 2022; Y. Lee and Shivashankar 2020).

Recently, our research group unveiled an intriguing discovery: sustained laterally confined growth of fibroblasts on micropatterned substrates could induce their reprogramming into stem cell-like cells, all without the need for any genetic or biochemical interventions (Roy et al. 2018). However, it’s unclear that whether we can adapt this approach to reverse the aged cellular phenotype. While these partially reprogrammed cells displayed stem cell-like characteristics, they may retain elements of their differentiation states, making them a potential model for rejuvenating fibroblasts in connective tissues. In this chapter, with RNA sequencing, we uncovered a shift in the transcriptome, transitioning from a fibroblastic state to an intermediate reprogrammed state upon lateral confinement, which subsequently reverted to the fibroblastic transcriptome, marked by enhanced expression of genes related to contractile cytoskeletal pathways, upon redifferentiation within the collagen matrix. Regarding changes in nuclear architecture, the partially reprogrammed cells exhibited a relatively more open chromatin compaction state, termed the "chromatin poise state", in contrast to the parental fibroblasts. Such open chromatin cell state renders them more prone to differentiate into contractile fibroblasts in response to cues from the extracellular matrix (ECM) present in the 3D-collagen matrix.

Furthermore, it's unclear that whether mechanical-induced rejuvenation can reset epigenetic changes in aging. We embarked on a thorough analysis, characterizing the 3D chromatin alterations during cellular aging and rejuvenation induced through mechanical reprogramming. To achieve this, we employed patient-derived human dermal young fibroblasts (10 years old), aged fibroblasts (75 years old), as well as rejuvenated aged fibroblasts. Through experiments involving cellular contractility, cytoskeletal-nuclear links, chromatin morphometric analysis, and RNA sequencing, we observed highly efficient rejuvenation of aged fibroblasts. Immunofluorescence analysis illuminated an augmented colocalization of microtubules and heterochromatin during aging, a phenomenon mitigated through cellular rejuvenation. For a global-scale analysis of chromatin reorganization during rejuvenation, we conducted chromatin conformation capture (Hi-C) experiments. Several recent works have shown the alteration in global chromatin structure and promoter-enhancer interactions in aging (Meng et al. 2023; Yang et al. 2023). However, the detailed investigation on chromatin organization at nuclear envelope in aged fibroblasts is still lacking. The amalgamation of publicly available DAM-ID data with Hi-C and gene expression data revealed aging-dependent alterations in LAD regions at the nuclear envelope, which were subsequently reset during rejuvenation. These findings paint a promising picture of mechanically rejuvenated cells, with far-reaching implications in the realm of regenerative medicine.

Material and Methods

Partial reprogramming of fibroblasts and redifferentiation

In this project, we used NIH3T3 mouse embryonic fibroblasts, human primary old skin fibroblasts (GM08401, 75 years old, male origin) and young skin fibroblasts (GM09503, 10 years old, male origin) to explore the potential of cellular rejuvenation. NIH3T3 cells were cultured in high-glucose DMEM (Gibco) supplemented with 10% (vol/vol) FBS (Gibco) and 1% penicillin-streptomycin (Gibco). Human primary skin fibroblasts were sourced from the NIGMS Human Genetic Cell Repository at the Coriell Institute for Medical Research and expanded in minimum essential medium (MEM) containing 15%

FBS, 1% non-essential amino acids (NEAA), 1% penicillin-streptomycin, and 1% glutaMax, all maintained under 5% CO2 conditions at 37°C.

For the mechanical rejuvenation of NIH3T3 mouse embryonic fibroblasts, our experimental procedures encompassed microcontact printing, cell seeding, partial reprogramming, collagen gel embedding for dedifferentiation, and the subsequent retrieval of cells from the collagen gel using collagenase.

These cells were cultured on fibronectin micropatterns and grown under laterally confined conditions as described in previous chapter (Roy et al. 2018). To elaborate, rectangular micropatterns with an aspect ratio of 1:5, measuring 1,800 μm2 and spaced 150 μm apart, were established on uncoated Ibidi dishes (81151) through the stamping of fibronectin (F1141, Sigma)-coated PDMS micropillars, a product of soft lithography.

Approximately 7,000 cells were seeded on a fibronectin-micropatterned dish to attain a density of one cell per fibronectin island. These single cells were cultured under laterally confined conditions for 6 days in the previously mentioned culture medium, with fresh media replacements every alternate day, unless specified otherwise. To initiate redifferentiation, spheroids or cells derived from trypsinized spheroids were embedded in a 3D rat tail Collagen-I gel at a concentration of 1 mg/mL following the manufacturer's protocol (Thermofisher). In this 3D collagen matrix, cells were cultured for 48 hours in the aforementioned medium for rejuvenation assays.

For partial reprogramming and rejuvenation of human old fibroblasts, cells were exposed to 10,000 μm2 (58*174 um2, spaced 174 um apart) micropatterns with an aspect ratio of 1:3. Subsequently, the micropatterned dish was surface-passivated with 0.2% Pluronic acid (Sigma P2443) for 10 minutes. Approximately 7,000 cells were seeded per dish. Single cells were grown for 8 days in the cell culture medium to achieve the partially reprogrammed state. The old medium was replaced with fresh medium every other day, taking care not to disrupt the spheres until day 8. On day 9, the spheres were carefully collected in a fresh complete growth medium using a sterile scrapper. The spheres were subsequently centrifuged at 800 rpm for 3 minutes at room temperature, and excess growth medium was removed. Finally, these spheres

were embedded in a 3D rat-tail collagen type I gel at a concentration of 1 mg/ml for their redifferentiation. Cells were then cultured in the collagen gel for 2 days.

To retrieve cells from the 3D collagen matrix for RNAseq sample preparation or imaging studies for 2D cultured cells, collagenase was employed to digest the collagen matrix. After 48 hours in the collagen, gels were subjected to digestion with 2 mg/ml collagenase enzyme for 25 minutes in a 37°C culture incubator. The cells were subsequently collected in a fresh complete growth medium to inactivate or dilute the collagenase activity and then centrifuged at 1000 rpm for 4 minutes. The cells were resuspended in 1 ml of fresh complete growth medium in a 60 mm petri dish coated with collagen (50 µg/ml). Control GM09503 and GM08401 cells were cultured as monolayers on collagen-coated petri dishes on the same day when the rejuvenated cells were collected.

RNA-seq sample preparation and analysis

For the mouse cell sample, total RNA was isolated from cells grown on patterns for varying durations using the RNeasy Plus Micro Kit (Qiagen). Cells grown in 3D Collagen-I gel were treated with collagenase for 15 minutes prior to RNA isolation. mRNA libraries (Illumina Stranded) were prepared, and sequencing was conducted on a HiSeq 2000 platform at the Genome Institute Singapore. In essence, four conditions were examined: FC (3T3 clumps grown overnight on micropatterns without gel), FCG (3T3 clumps grown in Collagen-I gel for 48 hours), PR (partially reprogrammed spheroids without gel), and RF (6-day samples grown in Collagen-I gel for 48 hours). Each condition comprised three biological replicates and four technical replicates (run on four different lanes).

Reads were aligned to Mus musculus GRCm38.p6 soft-masked genomic DNA (with GenBank Assembly ID GCA_000001635.8, downloaded from Ensembl) using the tophat sequence alignment tool (D. Kim et al. 2013). The annotation file (GTF format) used for tophat sequence alignment was downloaded from Ensembl (for GRCm38.p6 assembly) (Martin et al. 2023). Default parameters were used in Tophat (v2.1.1) (D. Kim et al. 2013). Following alignment, four technical replicates for each biological sample (accepted_hits.bam files from Tophat output) were combined for downstream

analysis. The Cufflinks (v2.2.1) software was employed to assemble transcripts and determine the number of reads for each transcript (Trapnell et al. 2013). The number of reads for transcripts from the same gene were summed to get the count number (reads per million, RPM). Count numbers for all expressed genes were used in differential expression analysis via DESeq2 (Version 1.20.0) (Love, Huber, and Anders 2014). Differentially expressed genes were defined as those with adjusted p values (Benjamini–Hochberg) below a 0.1 false discovery rate.

For human cell sample, total RNA was isolated from replicates of young, old and rejuvenated cells cultured on 2D collagen coated surface using Qiagen RNeasy mini kit according to manufacturer's protocol. RNA quality was measured with a high sensitivity RNA kit using the agilent Bioanalyzer. Illumina paired-end library was then prepared using NEBNext® Ultra™ RNA Library Prep Kit. All samples were sequenced in the D-BSSE facility at ETH Zurich in a single flow cell with a yield of 350-450 million reads with a read length of PE 38*2.

Paired end reads were aligned to Homo sapiens GRCh38.84 reference genomic indexes using the HISAT2 sequence-alignment tool (version 2.2.1) (D. Kim et al. 2019). The cloud indexes (grch38_trans) for HISAT2 were accessed on June 25th 2020 from https://registry.opendata.aws/jhu-indexes. Four technical replicates for each biological sample (in batch 2) were combined as input of HISAT2. Default parameters were used in HISAT2. Single aligned reads were counted by htseq-count (1.99.2). Count numbers for all expressed genes were used in differential expression analysis using DESeq2 (Version 1.36.0) . Differentially expressed genes had adjusted P values (Benjamini–Hochberg) below a 0.1 false discovery rate (FDR) and fold change higher than 1.4. Enrichment analysis was conducted using the David database using a gene list with log2 fold change ≥ 1 and p-adjusted value ≤ 0.05 for upregulated genes (Sherman et al. 2022). Similarly, for downregulated genes, log2 fold change ≤ −1 and p-adjusted value ≤ 0.05 was used.

Chromatin transcriptional activity

To assess the transcriptional activity of each chromosome, we leveraged RNA-seq data obtained from young and old fibroblasts cultured in 2D and followed the methodology outlined in our lab's previous work (Y. Wang et al. 2017). Initially, we

computed the Transcripts Per Million (TPM) values for each gene using the Salmon software, which achieved a mapping rate of approximately 90%. Subsequently, we calculated the z-scores for the TPM values of each gene, normalizing them across all biological conditions and replicates. The chromosome activity for each biological sample was determined by summing the z-scores of genes located on that specific chromosome and dividing by the total number of genes on the chromosome. This calculated chromosome activity provided an average measure of the transcriptional activity of genes within that chromosome.

Prize-Collecting Steiner Tree analysis

Network analysis was done as previously described with enlarged human network dataset. Human protein-protein interaction data were downloaded from the STRING database (version 11.5), comprising 17,804 genes and 937,906 interactions (Szklarczyk et al. 2015). Transcriptional regulator and target genes relationships were combined from both the hTFtarget database and previous datasets (downloaded from Harmonizome and Enrichr database as described in previous chapter), including 774 transcriptional regulators, 19,382 protein-coding genes as targets and 4,419,504 interactions (Rouillard et al. 2016; Z. Xie et al. 2021; Q. Zhang et al. 2020). Transcriptional regulators with protein-protein interaction information were designated transcriptional regulator nodes, while other proteins in the protein-protein interaction data were classified as protein nodes. Target genes of the transcriptional regulators were termed RNA nodes.

The costs on the edges of the network (representing interactions between nodes) were calculated as -log(score/1000), with the score being derived from the quality of links between proteins stored in the STRING database (multiplied by a factor of 1000 upon download). Edges linking transcriptional regulators and targets were assigned a cost of zero. For the analysis in Figure 3-13, prizes were given to 1210 genes upregulated in young fibroblasts compared to the old cells. For the analysis in Figure 3-15, prizes were allocated to 1974 protein and transcriptional regulator nodes based on their log2 fold change for upregulated genes in rejuvenated cells compared to old fibroblasts. Prizes were also assigned to 167 RNA nodes, utilizing their averaged log2 fold change comparing young fibroblasts with old fibroblasts and rejuvenated cells with old fibroblasts based on RNA-seq analysis. Network optimization using Prize-Collecting

Steiner Tree was performed to derive a regulatory network connecting potential upstream protein and transcriptional regulator nodes with their targets (S. -s. C. Huang and Fraenkel 2009).

Hi-C processing

Hi-C sequencing reads were mapped to the human genome (GRCh38) downloaded from the ensemble database (release 104) using the bwa software (version 0.7.17) (Martin et al. 2023; Heng Li and Durbin 2009). Pairtools software (version 0.3.0) was used to filter Hi-C mapped reads, removing PCR/optical duplicates and retaining UU, UR, RU reads (U refers to unique mapped reads, R refers to rescued multiple mapped reads coming from sequencing through the ligation junction).

Chromatin organization at the nuclear periphery

The pairtools file output (i.e., .pairs file) was binned into a 10 kb resolution contact matrix using the cooler python library (Abdennur and Mirny 2020). Genomic regions belonging to nuclear Lamina-associated domains (LADs) were obtained from the UCSC genome browser (Guelen et al. 2008; Karolchik 2004). These LAD regions were extended by 0.5 Mb upstream and downstream. For each 10 kb bin within an extended LAD region, we calculated the contacts between the bin and all non-LAD regions on the same chromosome. This value represented the contact strength for each bin within an extended LAD region. The number of LAD loci with increased or decreased contact strength with non-LAD in young and/or rejuvenated cells compared to old samples was determined. The DESeq2 package (version 1.36.0) with padj < 0.01 was used to obtain the contact bins that significantly differed between the different states (Love, Huber, and Anders 2014). In this analysis, the values of the summed contacts were used as the count input to DESeq2. Differential contact LAD loci were analyzed in conjunction with RNA-seq data to identify LAD genes exhibiting transcriptional changes. Functional annotation using the DAVID database was performed to identify pathways associated with these selected LAD genes. Transcriptional regulatory pathways were studied using the Prize-Collecting Steiner tree method.

Immunostaining on 2D and 3D culture conditions

Cells from 2D culture were fixed with 4% paraformaldehyde prepared in PBS for 15 minutes followed by three PBS washes for 5 minutes each. Similarly, cells embedded

in 3D collagen-I gels were fixed for 25 minutes and then washed with PBS containing 100mM glycine three times, each wash lasting 5 minutes. Subsequently, cells were permeabilized using 0.5% Triton X-100 for 15 minutes (2D) or 20 minutes (3D) and washed with PBS three times. For 2D cells, a blocking solution consisting of 1% BSA in PBS with 0.1% tween was applied and incubated for one hour at room temperature. For 3D dishes, a blocking solution consisting of 10% goat serum and immunofluorescence (IF) wash solution (0.2% Triton X100, 0.2% tween in PBS) was used and incubated for three hours at room temperature. Primary antibodies were diluted in a 1% BSA blocking solution for 2D samples, while for 3D samples, primary antibodies were diluted in 5% goat serum and incubated overnight, followed by three IF washes of 10 minutes each. Secondary antibodies for 2D samples were diluted in a 1% BSA blocking solution, and for 3D samples, they were diluted in 5% goat serum in IF solution. After secondary antibody staining, stained dishes were washed with IF solution three times each for 10 minutes and the nuclei were stained with Nucblue from Thermo Scientific readymade solution by dissolving one drop of it in 1ml PBS and incubating it for 10 minutes at room temperature. Filamentous actin labeling was done using actin green from Thermo Scientific by dissolving one drop of it in 1 ml PBS and incubating it for three hours at 4°C.

Imaging and image analysis

All fluorescent images of cells cultured on 2D and 3D embedded in collagen-I gel were acquired using a Nikon A1 confocal laser scanning microscope with 20x magnification, 60x magnification or 100x magnification with the following acquisition settings. For imaging whole cells, a x-y pixel size of 0.43 µm with 1 or 2 µm z step size was used. For 2D cultured cells, the z-direction was captured for a thickness of 5 µm, whereas cells embedded in 3D collagen-I gel were imaged up to the thickness of 25 µm. With these settings, confocal images of either 512×512 or 1,024×1,024 pixels were obtained. Nuclei were segmented based on the Otsu thresholding method. Nuclear features were calculated on the DAPI stained nuclei images using tools published previously by our group (https://github.com/GVS-Lab/chrometrics) (Venkatachalapathy, Jokhun, and Shivashankar 2020). For the quantification of cytoskeleton features, the cytoskeleton was segmented using the Otsu thresholding method. The volume of cytoskeleton close to the nucleus (2 um expansion of the

segmented 3D nucleus masks) was calculated. The mean intensity of the cytoskeleton close to the nucleus was also measured.

Nuclear dynamics were analyzed from the decorrelation of the nuclear images in time. Time-lapse live-imaging of nucleus stained with Hoechst 33342 (ThermoFisher Scientific) was done in confocal mode with time intervals of one minute for up to 32 minutes in PR, FC and FC+TSA conditions. Pearson correlation coefficient (PCC) value was calculated from two lists of pixel intensity of the same nucleus captured in different time points with a certain time lag. For each cell, one PCC curve was drawn which connecting all PCCs (as y) with the increasing time lags (as x) as represented in dim color in Figure 3-14A. The mean PCC curves for all cells in each condition, were drawn in bright color in Figure 3-14A. The mean PCC curves in each condition were fitted by equation $y = (1-\alpha) + \alpha \exp(-t/\tau) - \eta$, where y refers to PCC value, t is time lags, fitting parameter α is drop rate, τ is time constant, η is noise.

To study the colocalization of the cytoskeleton and heterochromatin or telomere markers, we used the 60X objective NA1.4 with a pixel size of 0.08 μm and z step size 0.2 μm. Chromatic aberration (in 3D) was corrected based on the images of 100 nm fluorescent beads under the same imaging settings. Nucleus (DAPI) was segmented to get a 3D volume mask using the Otsu thresholding method. To study the top surface of the nucleus, a projected (flattened) image for the top surface (1 voxel per xy coordinate) on the segmented 3D volume of the nucleus with corresponding cytoskeleton and heterochromatin or telomere marker channels was derived. A similar process was performed to study the bottom surface of the nucleus (using the bottom surface on the segmented 3D volume). The mean intensity of the chromatin markers in the top and bottom surface images was measured. Next, in the images of top or bottom surfaces, actin, microtubule, HP1a and TRF2 within the segmented nucleus mask were further segmented using the Otsu thresholding method to get their localization. To quantify the colocalization of cytoskeleton and chromatin markers, two ratios were measured. First, the number of overlapping pixels from the two segmented masks (i.e., the region of cytoskeleton and the region of chromatin marker that are overlapping) divided by the number of pixels in the cytoskeleton mask was calculated. Second, the number of overlapping pixels from the two masks divided by the number of pixels in the chromatin marker mask was calculated.

Chromosome painting of interphase chromosomes

Cells from the three cell states (young, old and rejuvenated) were cultured with complete growth medium up to 70% confluence. Cells were then trypsinized and fixed using carnoy fixation as described in the previous section. Finally the cell number was adjusted and a few drops of cells were spotted on the slide and left for air drying. Metasystem Xcyting FISH probes for chromosomes chr4 (green) and chr18 (red) were premixed in a Eppendorf tube and spotted exactly on to the slide without bubbles. A cover slip was placed and sealed with rubber cement and incubated for a denaturation step at 75°C for 2 minutes. The slides were kept in a humidified chamber protected from light for hybridization overnight at 37°C in a water bath. For post hybridization on the next day, rubber cement was carefully removed and the slides were washed with 0.4x SSC buffer (3M sodium chloride and 30mM sodium citrate adjusted pH-7.2) at 72°C for 2 minutes followed by 2X SSC buffer with 0.05% triton X-100 for 30 seconds at room temperature. Finally, the slides were washed with water once and allowed to air-dry for a few minutes followed by adding antifade mounting medium with DAPI. All slides were scanned under a confocal microscope with 100X objective for chromosome spots.

Results

Redifferentiation of fibroblasts from partially reprogrammed spheroids

In our preceding investigation into mechanically-induced nuclear reprogramming, conducted in the absence of exogenous biochemical factors, we observed that mouse embryonic fibroblasts subjected to laterally confined growth on micropatterns for 6 days (as described in the previous chapter) began to exhibit partially stem cell-like gene expression. These 6-day-old spheroids were subsequently embedded in collagen gels and cultured for an additional 2 days (Fig 3-1). Remarkably, within mere hours, cells derived from these spheroids initiated a progressive invasion of the collagen matrix. They migrated individually as unicellular sprouts or collectively formed complex capillary-like structures. In addition to cell invasion, we noted morphological alterations in the spheroid core itself. While the spheroids initially presented as

compact structures, subsequent cell migration led to spheroid expansion and breaches in the spheroid core.

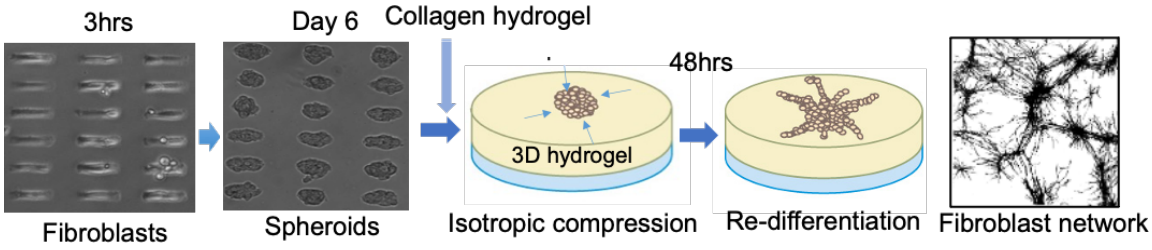

Figure 3-1. Schematic representation of the effect of geometry-driven laterally confined growth of fibroblasts on reprogramming, followed by their redifferentiation within the embedded 3D collagen matrix.

Redifferentiated fibroblasts are characterized by activation of cytoskeleton pathways and enhanced cell contractility

To comprehensively assess the gene expression profiles in redifferentiated fibroblasts (RF) and compare them to various control conditions, including partially reprogrammed cells obtained from 6 days of laterally confined growth on micropatterns (PR), fibroblasts grown overnight on micropatterns and forming clumps (FC), and fibroblasts grown in clumps overnight and subsequently embedded in collagen for 48 hours (FCG), we conducted RNA-seq experiments.

Thousands of genes, including key pluripotency markers Bmp4, Cdx2, Fgf4, Gdf3, Nanog, Nodal, Nt5e, Sall4 and Sox2, were solely upregulated in the PR cells (Figure 3-2A). When the gene expression profiles in these four conditions were analysed together with a previous RNAseq dataset generated for the reprogramming process, two drastically different cell states were revealed by clustering analysis (Figure 3-2 B). PR cells shifted away from the parental fibroblast-like state (FC) to a stem-like state from day 6 to day10, as a result of lateral confinement. Embedding these day 8 partially reprogrammed cells in a 3D collagen environment resulted in a reversion of their gene expression profiles back to the parental 3T3 fibroblast–like state, as observed in RF cells.

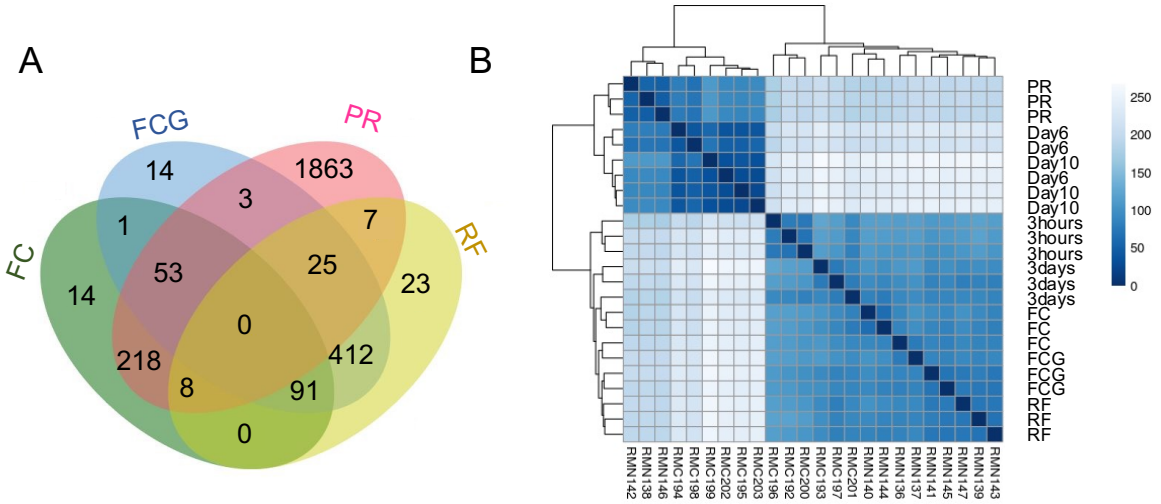

Figure 3-2. Differential expression analysis for partially reprogrammed cells (PR) and redifferentiated cells (RF). (A) Venn diagram showing the number of upregulated genes in 14 ($2^n - 2$, n is 4 conditions) comparisons. FDR (adjusted p value) < 0.1. (B) Heatmap showing the similarities between the samples based on the sample-to-sample Euclidean distance defined on gene expression profiles, calculated on the count matrix.

Based on the comparisons outlined in the Venn diagram above, we identified two sets of genes: those selectively overexpressed (23 genes) and those downregulated (53 genes) in RF compared to all the other conditions. The genes upregulated in RF formed a molecular interaction network characterized by several central nodes, including proteins such as Rab25, Cdc42bpa, Rhoj, and Iqgap1, which are known to enhance cell migration and cell contractility (Figure 3-3 A). The network was generated using the known protein-protein interaction data from STRING databased combined with a gene list which showed upregulation in RF condition compare to the FCG control condition. The pink color nodes represent the genes which are expressed higher in RF than FCG condition. The first neighbour of these pink nodes were labeled in blue color. The hexagon nodes are ones with degree (i.e. the number of neighbours) higher than 5. The expression of selected genes regulating cell contractility was up-regulated in RF compared to FCG (Figure 3-3 B). These experiments show that PR cells can be redifferentiated into a fibroblast-like (RF) state by embedding them into a 3D collagen

matrix, and these cells are characterized by elevated expression of contractility- and fibroblast-related genes.

A

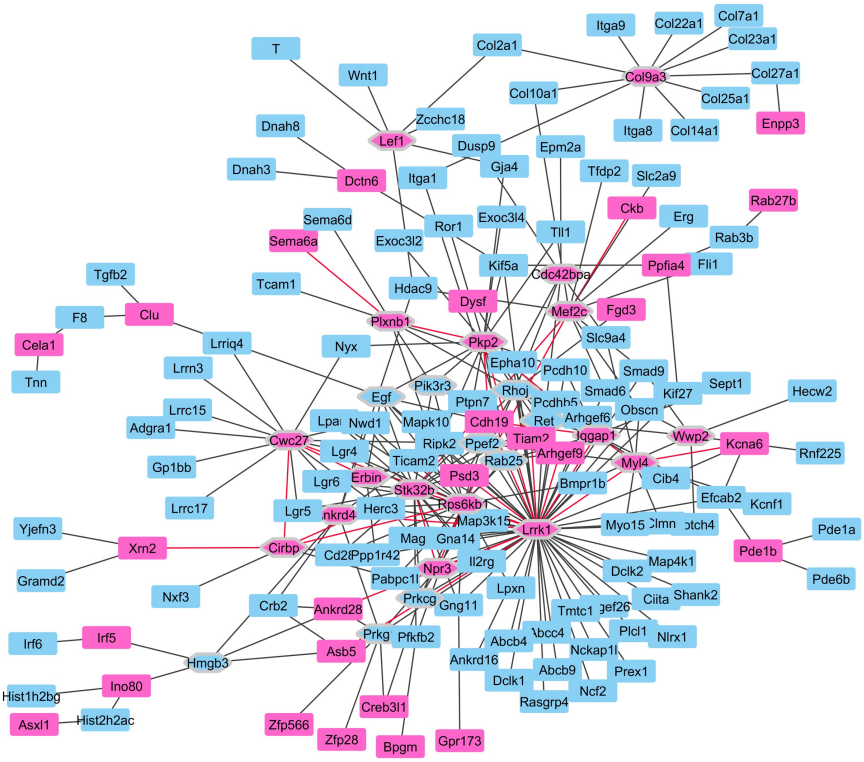

B

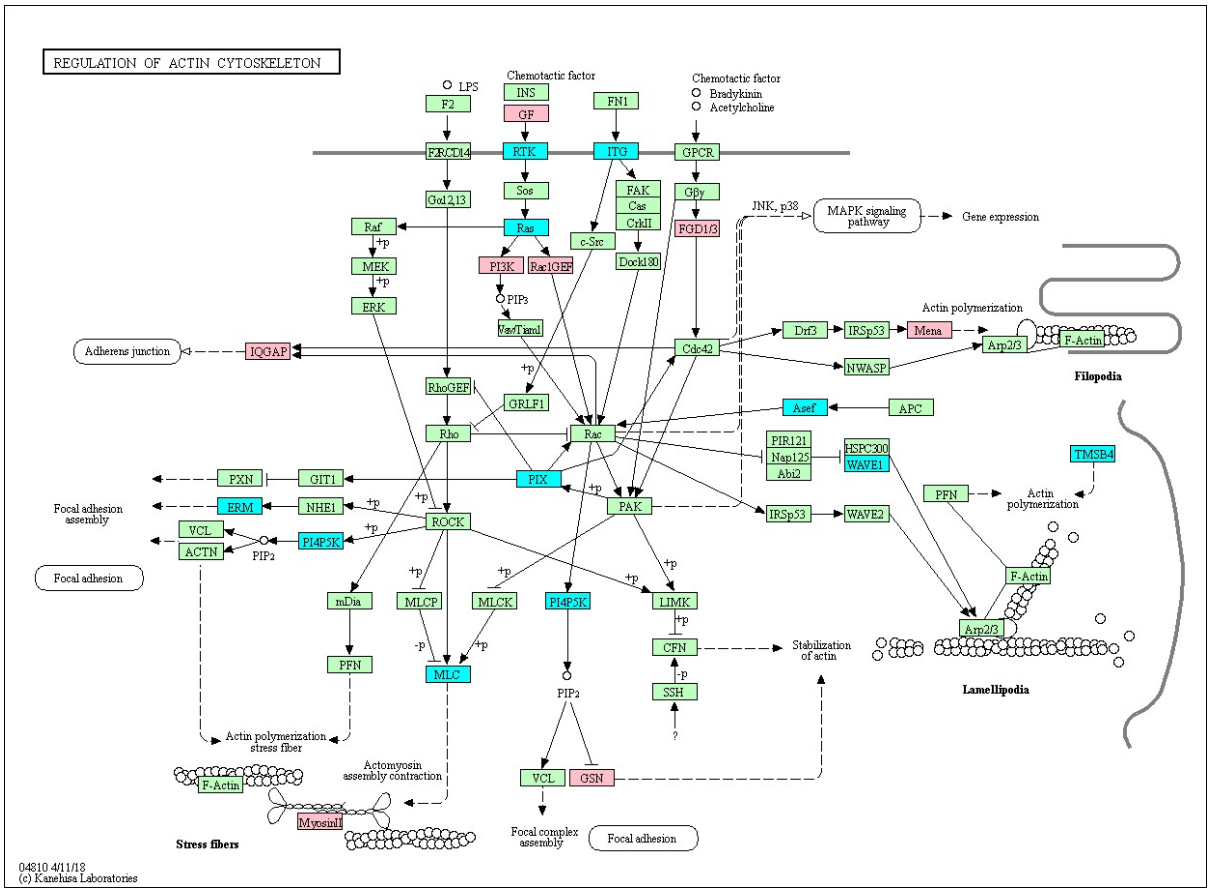

Figure 3-3. Upregulated genes in RF compared to FCG. (A) Protein-protein interaction network showing the upregulated genes in RF compared to FCG. Pink: upregulated genes. Blue: the first neighbours of the pink nodes. Hexagon shape: nodes with degree (the number of neighbours) higher than 5. (B) Pathway map showing the differentially expressed genes in the regulation of actin cytoskeleton pathway (KEGG: hsa04810). Pink: upregulated in RF. Cyan: downregulated in RF. Green: no expression changes.

Consistent with the RNA-seq results, Figure 3-4 A-C clearly demonstrates that RF exhibit enhanced actomyosin contractility compared to control fibroblasts (FCG). This observation is based on immunostaining of phosphorylated myosin light chain (pMLC) and actin staining, along with the quantification of mean pixel intensity per cell. Remarkably, this trend was similarly observed in redifferentiated partially reprogrammed human primary cells (Figure 3-4 D-F). When we examined cell contractility using pMLC immunostaining, we discovered that old fibroblasts exhibited significantly lower pMLC intensity than young fibroblasts, consistent across both 2D and 3D culture environments.

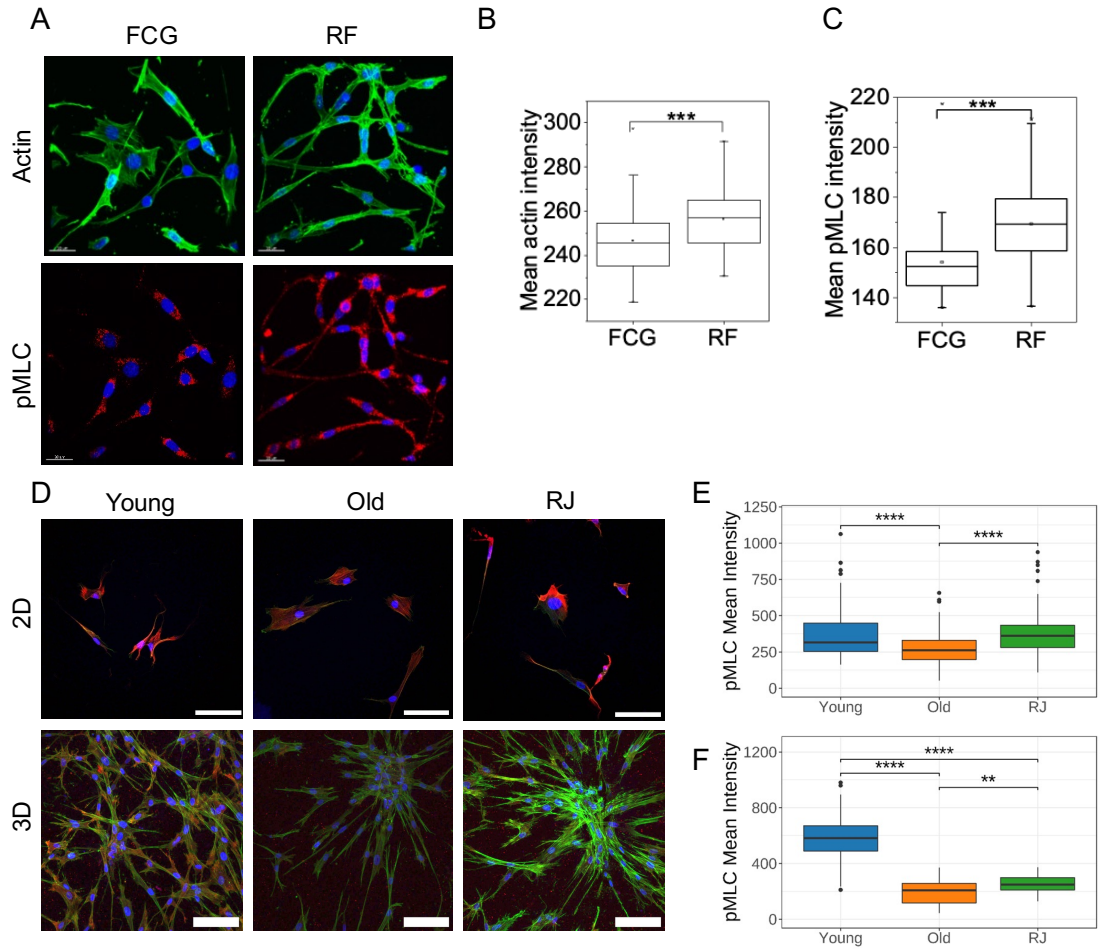

Figure 3-4. Immunostaining experiments showing the increased cell contractility in mouse redifferentiated fibroblasts (RF) and human rejuvenated cells (RJ). (A) Representative actin and pMLC immunofluorescence micrograph of RF and FCG embedded in 1mg/ml collagen matrix. (B and C) Corresponding box plots for cellular mean intensity of actin and pMLC; n=81 and 67 for FCG and RF conditions, respectively. ***P < 0.001; Two-sided Student's t-test were used. (D) Representative immunofluorescence images of actin (green) and pMLC (red) of young, old, RJ cells from 2D cultured (top panel) and 3D cultured in 1mg/ml collagen matrix (bottom panel). Scale bar is 100 um. (E and F) Box plot representing corresponding cellular mean pMLC intensity (A.U.) for these three cell states in the 2D and 3D culture condition.

To further investigate the relationship between the cytoskeleton, nuclear morphology, and transcriptional regulation in the context of aging and rejuvenation, we focused on human primary cells, specifically, young fibroblasts, old fibroblasts, and rejuvenated fibroblasts (RJ). Using 3D confocal microscopy, we examined the morphological

differences in the nucleus among these three cell states. As shown in the figures, the height of the nucleus averaged around 5.2 μm, with significant differences observed in the nucleus volume across these three cell types (Figure 3-5 A and B). Such variations may be attributed to alterations in cytoskeleton organization and could potentially impact chromatin compaction..

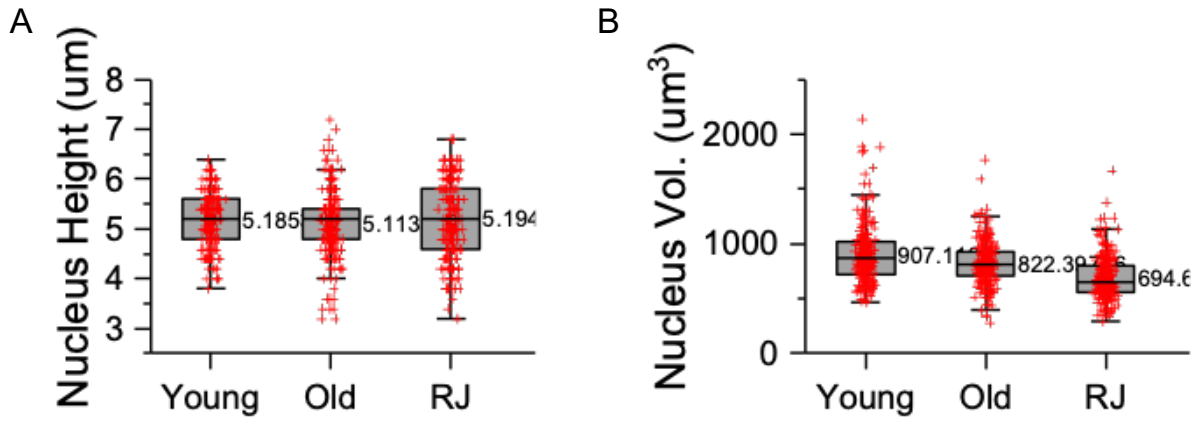

Figure 3-5. Nucleus size in young fibroblasts, old fibroblast and rejuvenated cells (RJ) in 2D culture condition. (A) Boxplot showing the nucleus height distribution in micron unit. (B) Boxplot showing the nucleus volume (um^3 unit).

Cytoskeleton reorganization in proximity to the nucleus

To explore potential correlations between changes in cytoskeletal contractility and chromatin organization, we employed high-resolution 3D confocal microscopy to visualize actin, microtubules, the heterochromatin marker HP1a, and the telomere marker TRF2 (Figure 3-6 A, D, E). Our analysis revealed that the amount of microtubules in close proximity to the nucleus (within a 2 μm distance) increased during the aging process but decreased in rejuvenated fibroblasts (Figure 3-6 B). Additionally, the amount of heterochromatin decreased during aging but increased in the rejuvenated state (Figure 3-6 C).

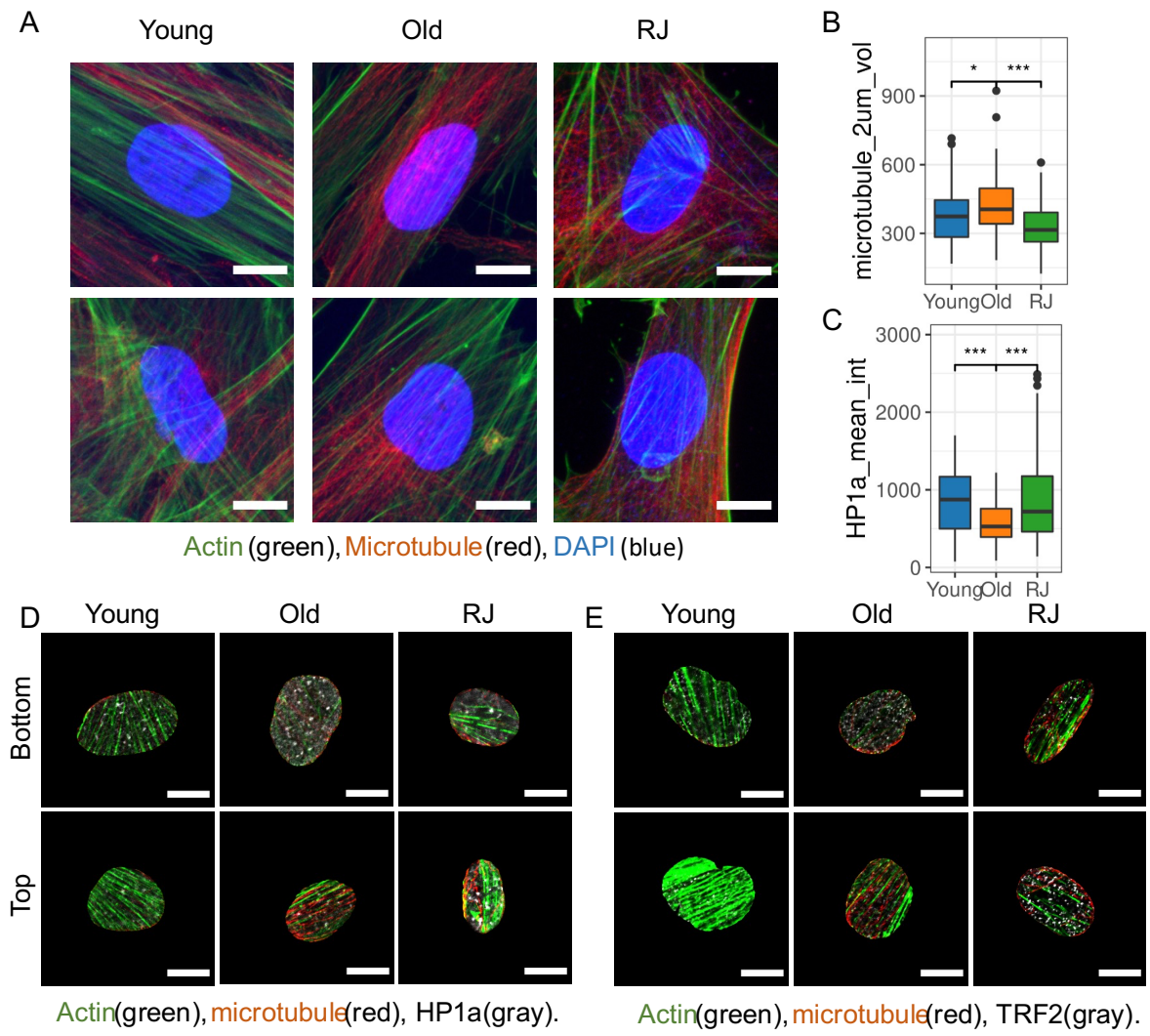

Figure 3-6. Representative 2D projected immunofluorescent images of actin (green), microtubule (red) and nucleus (blue). Scale bar is 10 um. (B) Boxplot showing the volume of microtubule close to the nucleus (within 2 um distance) (n = 105 nuclei for young, 111 nuclei for old, 113 nuclei for RJ, combined from three biological replicates). (C) Boxplot showing the mean intensity of HP1a per nucleus (n = 105 nuclei for young, 111 nuclei for old, 113 nuclei for RJ). (D) Representative immunofluorescence images of actin (red), microtubule (green), heterochromatin protein HP1a (gray) of the three cell states. Scale bar is 10 um. (E) Representative immunofluorescence images of actin (red), microtubule (green), telomere marker TRF2 (gray). Scale bar is 10 um.

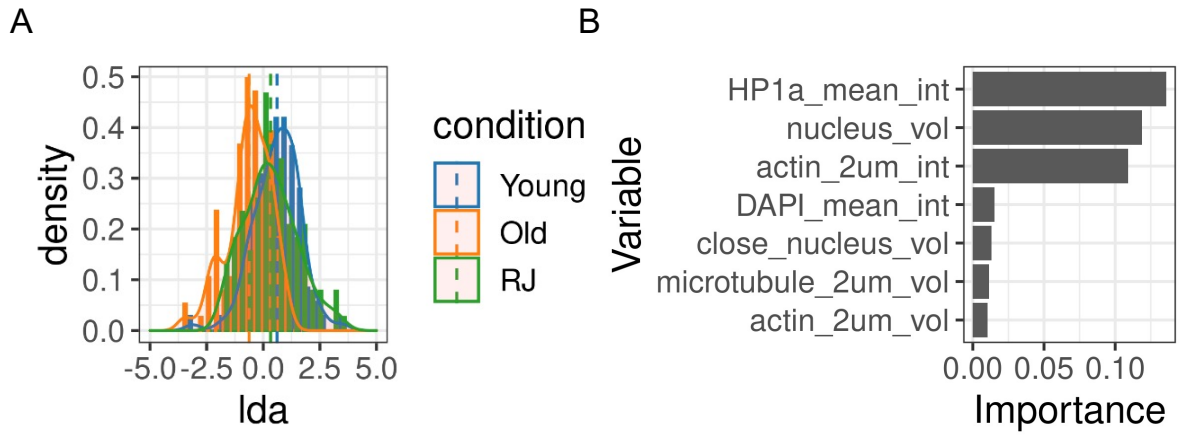

Figure 3-7. Linear discriminant analysis showing changes in cytoskeleton amount and heterochromatin amount in young, old and rejuvenated cells. (A) Distribution of Linear Discriminant Analysis (LDA) scores for classifying young and old cells based on cytoskeleton, DAPI and HP1a staining features. The classification accuracy was 73 % (balanced dataset). Nine features were used: HP1a mean intensity, DAPI mean intensity, nuclear volume, volume close to the nucleus (2 um distances), height of the nucleus, actin volume close to the nucleus, microtubule volume close to the nucleus, mean actin intensity close to the nucleus, mean microtubule intensity close to the nucleus. 100 nuclei for each condition were used in the analysis. (B) Top features used for classifying young and old fibroblasts used in (A).

For a more comprehensive understanding of the roles played by cytoskeletal and nuclear phenotypes within the context of aging and rejuvenation, we quantified the mean fluorescence intensity and volume of the actin and microtubule cytoskeleton, DAPI-stained nucleus, and HP1a-stained heterochromatin, using 3D fluorescent images rather than 2D projected images. Employing the Linear Discriminant Analysis (LDA) model, trained with derived features obtained from young and old fibroblast data, we identified the utmost significance of the actin cytoskeleton, 3D nuclear volumes, and heterochromatin intensity in distinguishing between young and old fibroblasts (Figure 3-7 B). Applying this trained model to previously unseen 3D images of rejuvenated cells revealed that their distribution fell between that of young and old cells (Figure 3-7 A). Collectively, these findings indicate that aging corresponds to alterations in cytoskeletal quantity, nuclear morphology, and chromatin arrangement, which are subsequently reversed in rejuvenated cells.

Nuclear morphometric features revealing the similarities between rejuvenated and young fibroblasts

To delve deeper into the chromatin organization within these three distinct cell states, we conducted an analysis of 2D projected DAPI-stained nuclear images. This comprehensive assessment encompassed various aspects, including nuclear shape features (e.g. the aspect ratio of the nucleus), nuclear boundary features (e.g. the length of the nuclear boundary with positive or negative curvature), chromatin texture features (e.g. the correlation coefficient of DAPI pixel intensity within a fixed distance) and chromatin intensity features (e.g. the amount of heterochromatin) (Figure 3-8 B). For the classification of nuclear images from young and old fibroblasts, we employed a Linear Discriminant Analysis (LDA) model. Post-training, LDA scores were computed for previously unseen nuclear images from rejuvenated fibroblasts. Interestingly, these rejuvenated cells exhibited a distribution of LDA scores akin to that of young fibroblasts (Figure 3-8 A). The selection of the top 15 crucial features for distinguishing between young and old fibroblasts encompassed nuclear shape features (e.g., aspect ratio denoted as "a_r"), nuclear boundary characteristics (e.g., "frac_peri_w_neg_curvature" representing the ratio of boundary length with negative curvature to total perimeter), chromatin texture properties (e.g., "correlation_5" indicating correlation of co-occurrence matrix for a 5-pixel lag), and chromatin condensation attributes (e.g., "hc_content_dna_content" representing the ratio of summed intensity in heterochromatin regions normalized by total area, and "hc_area_nuc_area" denoting heterochromatin content area normalized by total area) (Figure 3-8 B). Notably, the aspect ratio of the nucleus, a significant indicator of mechanical stretching, was examined for rejuvenated cells, revealing their more elongated morphology compared to old cells and a similarity to young cells (Figure 3-8 C).

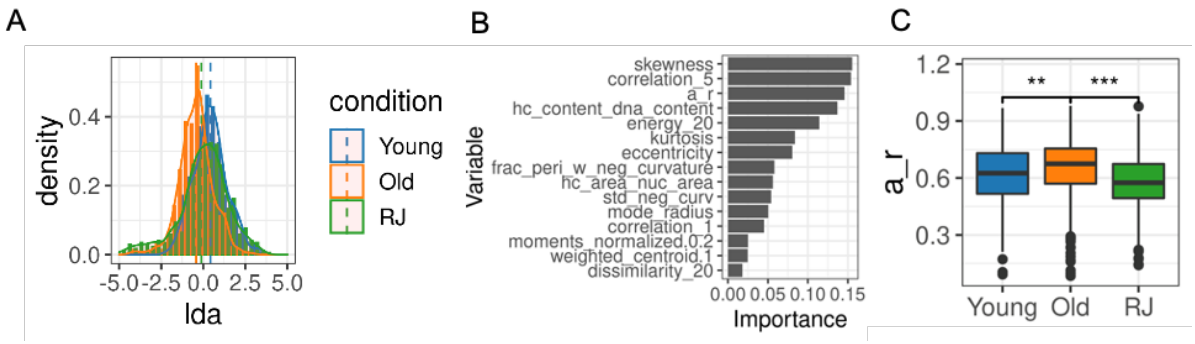

Figure 3-8. Linear discriminant analysis showing the nuclear morphometric features changes in aging and rejuvenation. (A) Distribution of Linear Discriminant Analysis (LDA) scores for classifying young and old cells based on the nuclear features derived from 2D projected nuclear images. Classification accuracy (young and old samples) was 70% (balanced dataset). Sample size was 400 cells per condition. 46 chromatin features were used for the analysis (see Methods). (B) Top nuclear features used for classifying young and old cells based on the LDA model. (C) Boxplot showing the aspect ratio per nucleus for these three cell states (n = 448 nuclei for young, 429 nuclei for old, 562 nuclei for RJ).

Differential colocalization of the microtubule cytoskeleton with heterochromatin and telomeres

To explore whether chromatin organization correlated with cytoskeleton localization, we examined the top and bottom surfaces of the nucleus for colocalization of cytoskeleton (outside the nucleus) with heterochromatin and telomere markers (inside the nucleus) (Figure 3-6 D and E, Figure 3-9). Both top and bottom surfaces of the nucleus showed decreased amounts of heterochromatin of old fibroblasts compared to the young and the rejuvenated fibroblasts (Figure 3-10 I and J). Even though the amount of telomere at the top and bottom surfaces of the nucleus did not change (Figure 3-10 D and H), the ratio of heterochromatin and telomere associated with microtubules increased in the old cells (Figure 3-10 C/G/K). In addition, the density of telomeres colocalized with actin and microtubule on both, the top and bottom nuclear surfaces, increased in the old fibroblasts (Figure 3-10 A/B/E/F). This indicated that the differential colocalization of the cytoskeleton with heterochromatin and telomeres during aging and rejuvenation may contribute to changes in 3D chromatin organization at the nuclear envelope.

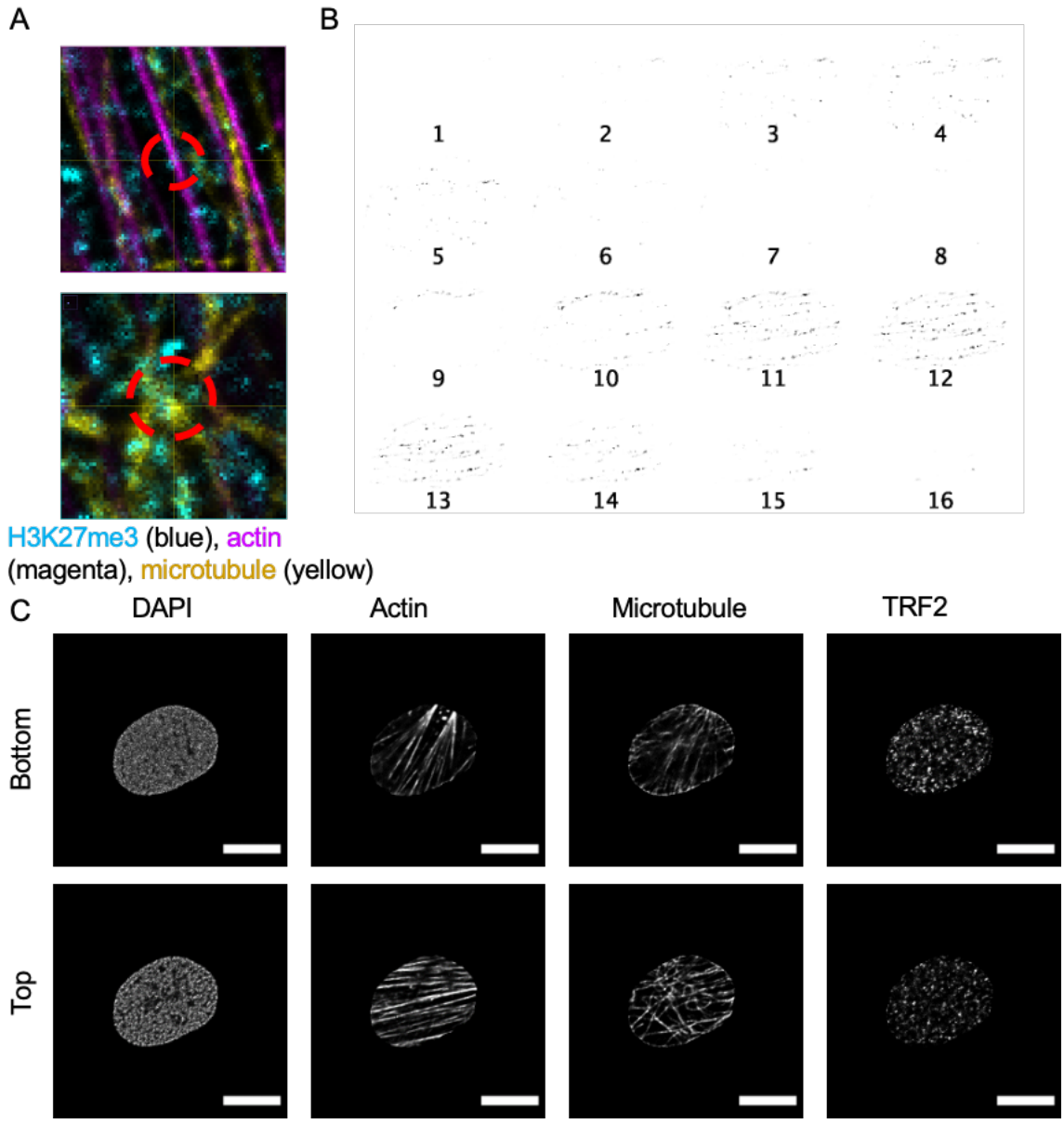

Figure 3-9. Colocalization of cytoskeleton and heterochromatin in fibroblasts. (A) Representative images of the colocalization of heterochromatin (H3K27me3 in cyan), actin (magenta) and microtubule (yellow). These images were from the z-plane of the corresponding nuclei surface. (B) Representative image showing the montage of the colocalized heterochromatin region (stained with HP1a antibody) and microtubule for one nucleus. Different number showing different z planes. (C) Representative images of the top and bottom surfaces of the nucleus stained with DAPI, actin, microtubule (a-Tubulin) and telomere (TRF2). Scale bar is 10 um.

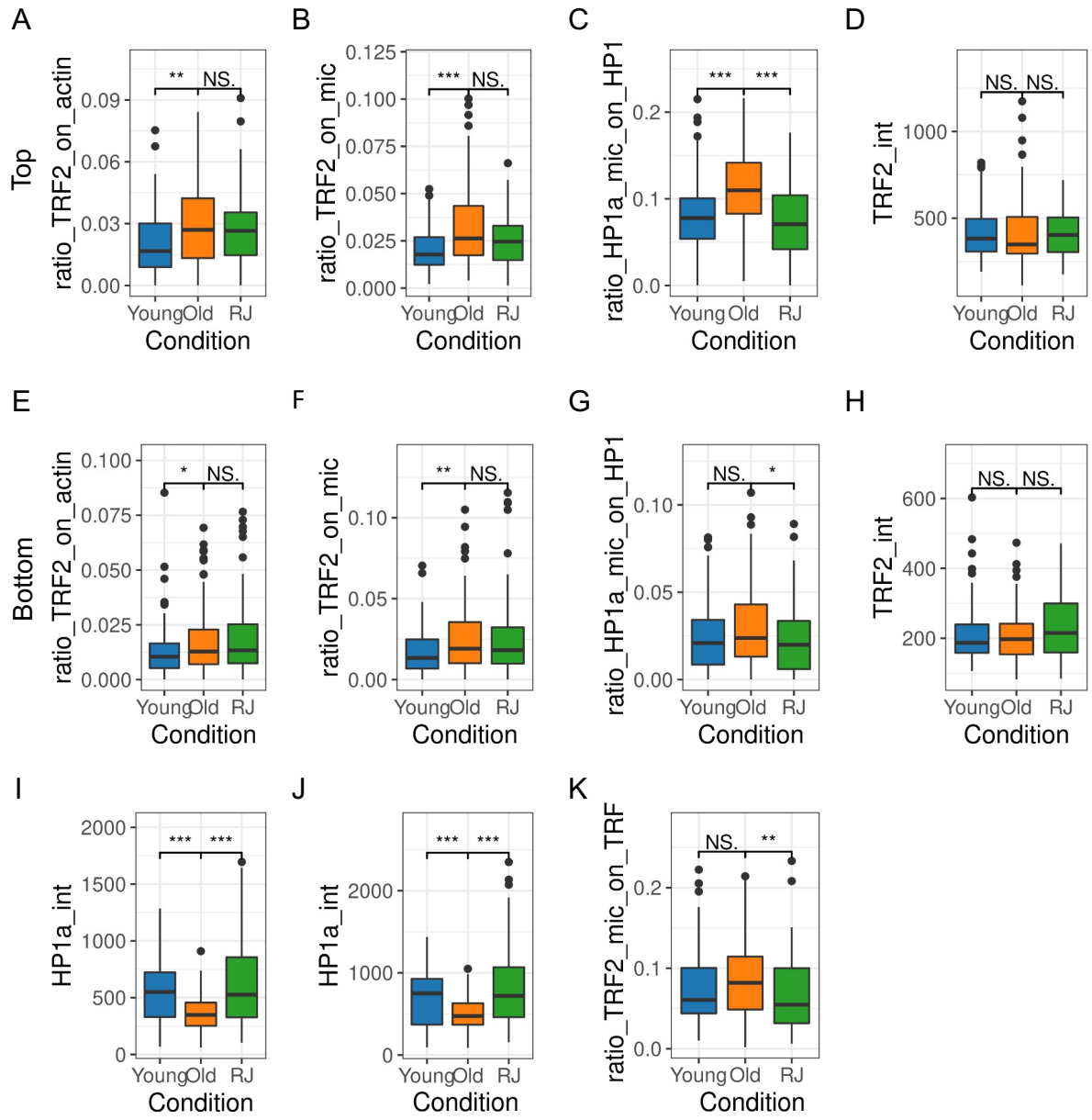

Figure 3-10. Quantification of the cytoskeleton and chromatin features in young, old and rejuvenated cells. (A) Boxplot showing the ratio (i.e. density) of the telomeres on the actin at the top nuclear surface for young (n = 113), old (n = 111) and RJ cells (n = 108) combined from three replicates. (B) Boxplot showing the ratio (i.e. density) of the telomeres on the microtubule at the top nuclear surface for these three cell states. (C) Ratio of heterochromatin HP1a colocalized with microtubule compared to the overall amount of HP1a region at the top nuclear surface. n = 105, 111, 113 combined from three replicates. (D) Intensity of telomere at the top nuclear surface. (E) Ratio (i.e. density) of the telomeres on the actin at the bottom nuclear surface for young, old and RJ cells. (F) Ratio (i.e. density) of the telomeres on the microtubule at the bottom nuclear surface for these three cell states. (G) Ratio of heterochromatin HP1a

colocalized with microtubule compared to the overall amount of HP1a region at the bottom nuclear surface. (H) Intensity of telomere at the bottom nuclear surface. (I) Amount of HP1a at the bottom nuclear surface. (J) Boxplot showing the mean intensity of HP1a per nucleus at the top nucleus surface for three cell states. (K) Boxplot showing the ratio of TRF2 stained telomere region colocalized with microtubule at the top nucleus surface compared to the overall TRF2 region at the top nucleus surface (n = 113 nuclei for young, 111 nuclei for old, 108 nuclei for RJ, combined from three replicates).

Chromatin reorganization at the nuclear periphery

In light of the observed changes in heterochromatin associated with aging, we embarked on a comparative analysis of chromatin transcriptional activity and radial localization between young and old fibroblasts. Using differential expression gene lists obtained from RNAseq dataset and quantification on chromatin transcriptional activity, we wanted to measure changes of gene transcription at the chromosome level (see method). A comparison of the chromatin transcriptional activity between old and young fibroblasts revealed notable differences, with chromosome 6 and 17 exhibiting higher activity in young cells, while chromosome 16 displayed lower activity in the same cells (Figure 3-11D). To delve deeper into these observations, we explored the correlation suggested by our lab's prior research between chromosome activity and radial distance from the nuclear centroid, which led us to conduct fluorescence in situ hybridization (FISH) on these chromosomes (Y. Wang et al. 2017).

Through confocal 3D imaging, we discerned distinct patterns of chromosomal localization. Particularly noteworthy was the relocation of chromosome 4 and 17, which were inclined to occupy central positions in young fibroblasts but shifted towards the nuclear periphery in old fibroblasts. Conversely, chromosome 16 exhibited a tendency for central localization in old fibroblasts but displayed peripheral positioning in young fibroblasts. Furthermore, we unveiled variations in the copy number of chromosomes 4 and 17, with certain imaged old fibroblasts showcasing 3 copies of chromosome 4 and 1 copy of chromosome 17. We proceeded to quantify the normalized radial distance of each chromosome within the imaged nuclei, achieved

by segmenting the labelled chromosomes and calculating their volume within 2/3 of the nucleus divided by their whole volume (Figure 3-11 B). Our results indicated that chromosomes 4 and 17 tended to localize closer to the nucleus's inner regions in young fibroblasts compared to older ones. In contrast, chromosomes 13, 16, and 18 exhibited a propensity for peripheral localization in young fibroblasts when contrasted with their positions in older fibroblasts. These findings strongly indicate changes in the radial localization of chromosomes as cells undergo aging.

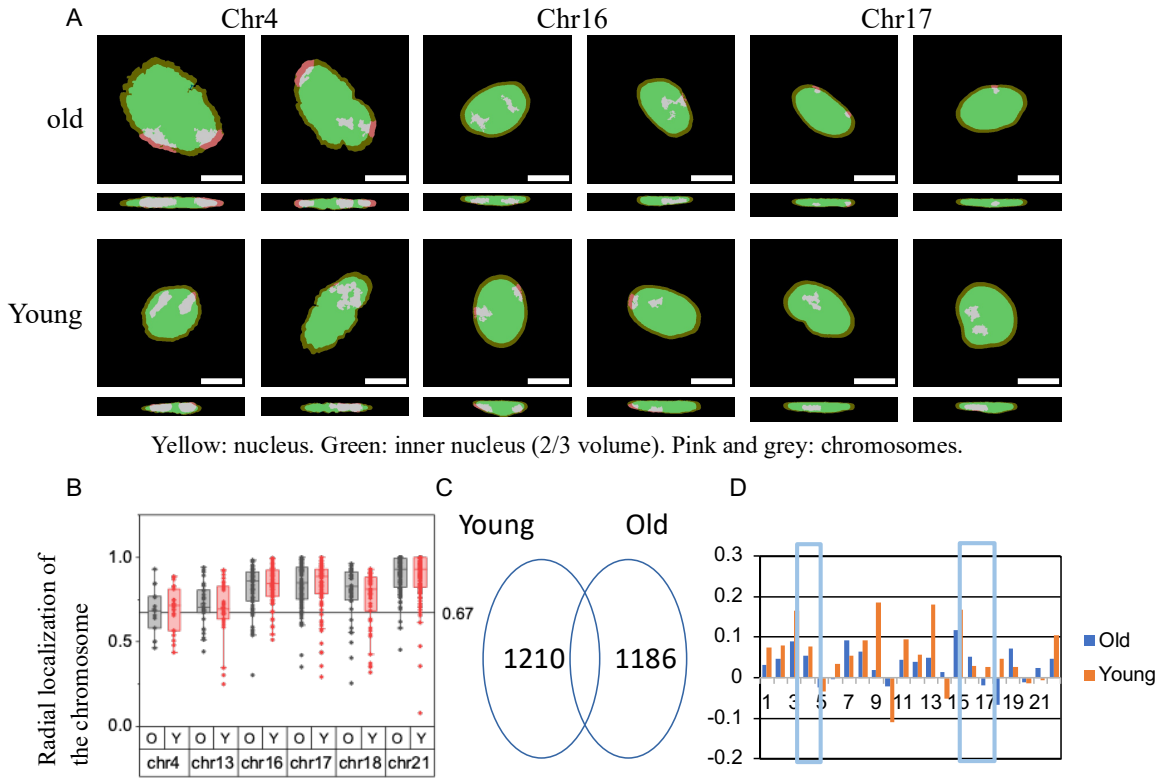

Figure 3-11. Radial distribution changes of chromatin in old fibroblasts compared to young fibroblasts. (A) Representative images of the painted chromatin 4, 16 and 17 in young and old fibroblasts. Z project image and X projected image for the same nucleus are shown. Dark yellow color region is the nucleus, blue color region is 2/3 volume of the nucleus shrinking to the center of the nucleus, pink color regions are the painted chromosomes. (B) Boxplot showing the radial localization of painted chromosome 4, 13, 16, 17, 18, 21 for old and young fibroblasts. (C) Venn graph showing the differentially expressed genes comparing old and young fibroblasts. 1210 genes are upregulated in young cells, 1186 genes are upregulated in old fibroblasts. (D) Barplot showing the normalized chromosome transcriptional activity for young and old fibroblasts.

To delve even deeper into the chromatin organization in aging and rejuvenation, Dr. Triandha Rao Sornapudi generated and sequenced in-nucleus Hi-C libraries from the three cell states using approximately 200 thousand cells and the low-input Hi-C method (Díaz et al. 2018) (Figure 3-12 A, Table 3-1).

sample	Total number of sequences	Mapping rate (bwa)	mapped to different chr (mapQ>5)	Number of reads after filtering (pairtools)	Ratio of remaining reads
Old_B1R1	652329304	0.99231	0.075973	375287436	0.57530366
Old_B2R2	797125811	0.98945	0.077163	444355982	0.55744774
Young_B1R1	553876884	0.99359	0.077738	272124166	0.49130804
Young_B1R2	528030894	0.99317	0.087871	295413589	0.5594627
RJ_B1	581092062	0.98994	0.064834	202706128	0.34883651
RJ_B2	37052694	0.99307	0.088438	20647182	0.55723835

Table 3-1. Descriptive table of Hi-C data for young, old and rejuvenated cells in replicates. The table shows the total number of sequences, the mapping rate, the number of reads that were mapped to different chromosomes (i.e. trans-chromosomal interactions), the number of reads after filtering, as well as the percentage of reads that remained after filtering.

The correlation of expression changes with alteration in LAD gene organization.

In light of our previous findings regarding the changes in heterochromatin organization at the nuclear envelope during aging and rejuvenation, we turned our attention to the genomic regions at the nuclear periphery in the three cell states. To pinpoint chromatin regions in proximity to the nuclear periphery, we employed Lamina-associated domains (LADs) data obtained from Lamin B1 DamID-seq of human fibroblasts (Guelen et al. 2008) (Figure 3-12 B).

The genomic regions within nuclear Lamina-associated domains (LADs), defined by the Lamin B1 DamID track, were extended by 0.5 Mb upstream and downstream. For each 10 kb bin within these extended LAD regions, we calculated the contacts between the bin and all non-LAD regions on the same chromosome, resulting in a contact strength value for each 10 kb bin within the extended LAD region. This approach facilitated the determination of contact strengths for the extended LAD regions while compensating for the absence of many potential contacts in the 10 kb resolution Hi-C matrix (Figure 3-12 C and D). The contact strength distribution appeared relatively smooth considering the high resolution of the 10 kb Hi-C data. Notably, in this analysis, an increase in the contact strength of a LAD locus with inner located chromatin (non-LAD locus) suggests its potential detachment from the nuclear Lamina.

Interestingly, statistical testing of the contact strength using the DEseq2 software, based on the Hi-C data, showed significantly changed LAD loci, which we call differential contact (DC) loci (Figure 3-12 E). To gain a comprehensive understanding of the transcription-dependent reorganization of LAD loci, we conducted an integrated analysis that included Hi-C, DamID-seq, and RNA-seq data. In young cells, we identified 516 genes that were transcriptionally upregulated and exhibited higher contact strength within LAD regions (Figure 3-12 F). Functional annotation of these 516 genes using the DAVID database revealed their involvement in pathways regulating cell migration, cytoskeleton organization, BMP signaling, and TGFb signaling (Figure 3-12 H) (D. W. Huang, Sherman, and Lempicki 2008). On the other hand, in old cells, we detected 165 genes that were transcriptionally upregulated and exhibited higher contact strength within LAD regions associated with cell adhesion pathways. Notably, most LAD loci with increased contact strength in young fibroblasts also exhibited increased contact strength in rejuvenated cells (Figure 3-12 G). Similarly, LAD loci with decreased contact strength in young cells also displayed decreased contact strength in rejuvenated cells compared to old fibroblasts. These results suggest that chromatin reorganization at the nuclear Lamina may play a role in the activation of cell type-specific pathways, particularly in the context of aging and rejuvenation.

To delve deeper into the potential transcriptional regulators of LAD loci at the nuclear periphery, we employed the Prize-Collecting Steiner Tree method as described previously. Prizes were assigned to protein nodes, transcriptional regulators, and RNA nodes that were transcriptionally upregulated in young fibroblasts compared to old fibroblasts (Figure 3-13). Among the genes belonging to the LAD gene list (516 genes) identified earlier for young cells, a small group of those associated with the annotated pathways in Figure 3-12H were designated as RNA nodes in the constructed network's bottom right section (Figure 3-13C). Among the identified transcriptional regulators for these LAD genes, the top hit was PPARG (Table 3-3). This finding aligns with previous studies highlighting the role of PPARG in aging (Miard et al. 2009). In summary, our analysis of chromatin reorganization at the nuclear periphery, integrating DamID-seq, Hi-C, and RNA-seq, sheds light on a significant transcriptional regulatory mechanism for LAD genes in aging and rejuvenation.

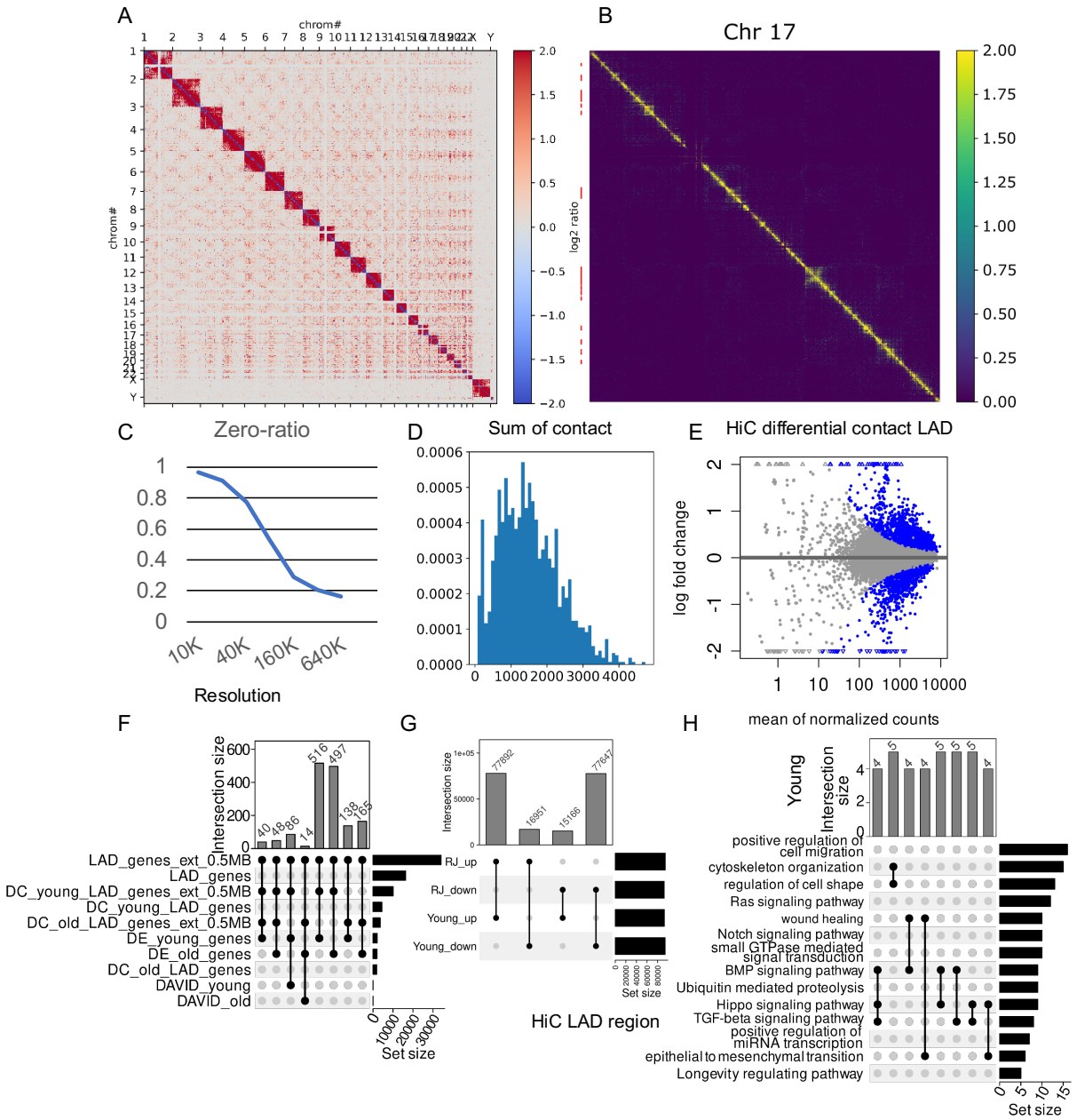

Figure 3-12. Spatial reorganization of Lamina-associated domains are reset in rejuvenation. (A) Differential HiC matrix showing the log2 fold change of the Young and Old's observed divided by expected HiC matrix (obtained using FAN-C software). (B) The contact matrix of chromosome 17 along with annotated LAD regions (left red bar) using resolution 10 kb. (C) Percentage of locus-locus interactions in the chromosome 17 intrachromosomal contact matrix that has zero value (y axis) with the change of HiC resolution (x axis). (D) The distribution of the sum of contacts between each LAD locus and all non-LAD loci in the same chromosome 17 using resolution 10kb. (E) MA-plot of HiC differential contacts of the LAD region. The top blue nodes refer to the LAD loci with significantly increased contact strength in the young cells

compared to the old ones (adjusted p value < 0.01). The bottom blue nodes refer to the LAD loci with decreased contact strength in the young cells. (F) Upset-plot showing the number of LAD genes with differential expression and/or differential contacts comparing young and old cells. For example, there are 516 LAD genes (within 0.5 MB upstream and downstream of the annotated LAD region) that show increased contact strength and are transcriptionally upregulated. (G) Upset-plot showing the number of shared LAD loci with increased contact strength or decreased contact strength in both RJ and young cells compared to the old cells. (H) Upset-plot showing the functional annotation of LAD genes with increased contact strength in young cells and transcriptional upregulation compared to the old ones. Numbers of LAD genes in the corresponding pathways are shown.

Gene name	Gene description
ANK1	ankyrin 1
ERBB3	erb-b2 receptor tyrosine kinase 3
PLXNA2	plexin A2
TCF7	transcription factor 7
EPB41L4B	erythrocyte membrane protein band 4.1 like 4B
ZNF423	zinc finger protein 423
HOXD3	homeobox D3
ITGA7	integrin subunit alpha 7
MYO10	myosin X
ATOH8	atonal bHLH transcription factor 8
AQP1	aquaporin 1 (Colton blood group)

Table 3-2. Subset of selected genes identified in Figure 3-12 H.

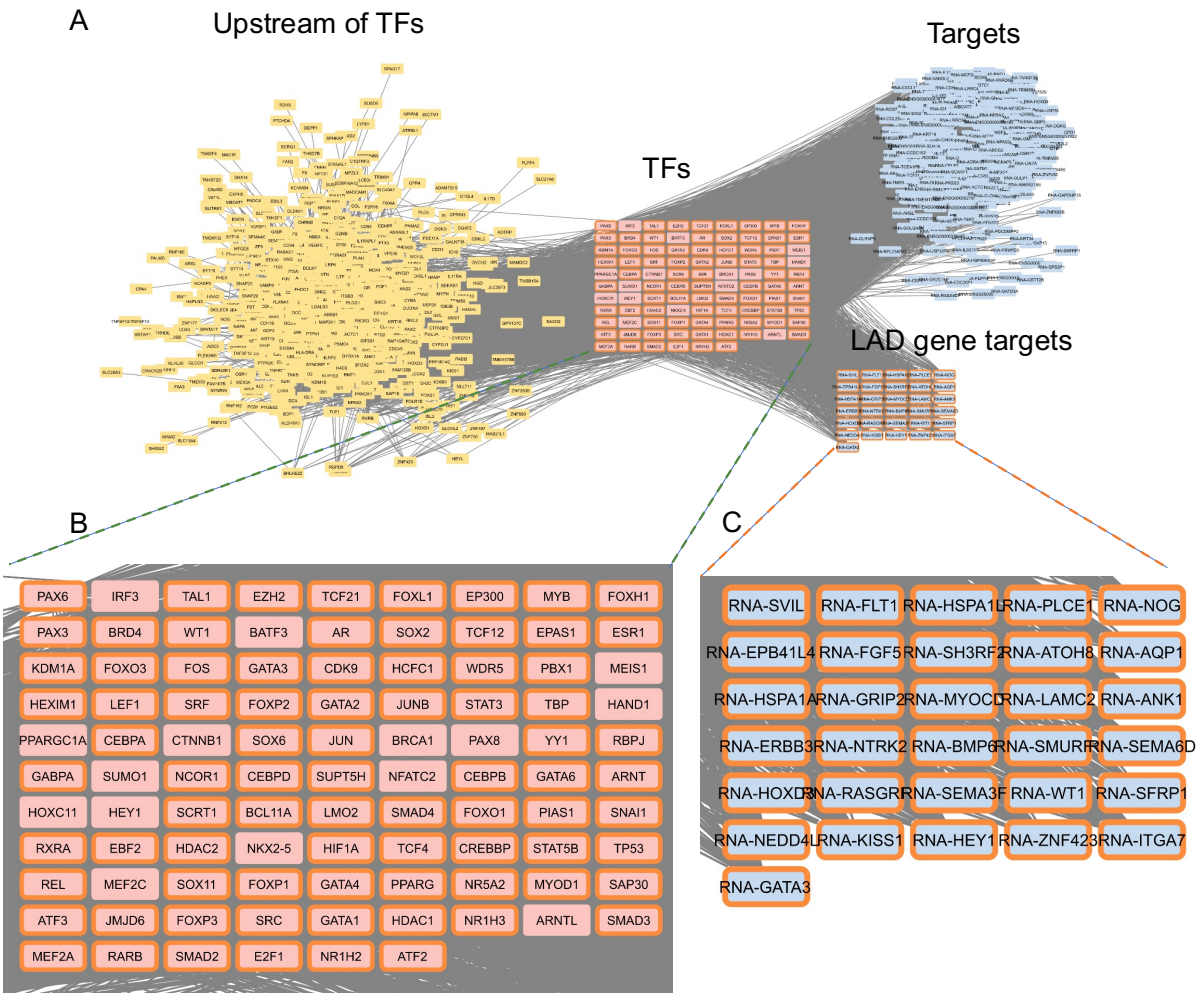

Figure 3-13. Constructed transcriptional regulatory network highlighting the regulation on LAD genes (Blue color nodes in the bottom right) and their corresponding transcriptional regulators (Pink color nodes in the bottom left).

TF	log2foldchange	num of targets
PPARG	2.74	27
AR	1.30	24
GATA2	1.05	23
GATA3	2.17	18
FOXP2	2.65	17
WT1	5.19	17
MYB	1.79	11
GATA6	2.13	10

Table 3-3. Top transcriptional regulators in (A) ranked by the expression changes comparing young and old fibroblasts and the number of targets belonging to the selected LAD genes (chosen from Figure 3-12H).

Chromatin Poised State in Partially Reprogrammed Cells

Given our observations of chromatin organization differences between young and old fibroblasts and the subsequent reset of some of these differences during rejuvenation, we delved into the role of cellular reprogramming in driving the rejuvenation process. To investigate chromatin organization changes in cellular reprogramming, we employed live cell imaging. The pluripotent genome is known for its unique epigenetic features and decondensed chromatin conformation (Gaspar-Maia et al. 2011). Therefore, we hypothesized that rejuvenation of fibroblasts might be linked to the chromatin poised state in partially reprogrammed (PR) cells. We analyzed nuclear dynamics through the decorrelation of nuclear images over time, as previously described (Makhija et al. 2014).

We conducted time-lapse live imaging of nuclei stained with Hoechst 33342 in confocal mode, with one-minute time intervals for up to 32 minutes, across PR cells, fibroblast clumps (FC), and FC+TSA conditions. TSA, a histone deacetylase (HDAC) inhibitor known to induce chromatin decondensation, was included as a positive control for comparing nuclear dynamics changes in the PR condition and FC condition. We calculated the Pearson correlation coefficient (PCC) from two lists of pixel intensity within the same nucleus, captured at different time points with specific time lags. A PCC curve was generated for each cell, connecting all PCC values with increasing time lags, as depicted in a subdued color in Figure 3-14A. The mean PCC curves for all cells in each condition were illustrated in a vivid color in Figure 3-14A. Intriguingly, we observed that Day6 and FC + TSA conditions exhibited a faster decline in PCC values over time. The mean PCC curves for each condition were fitted using the equation $y = (1-\alpha) + \alpha \exp(-t/\tau) - \eta$, where y represents the PCC value, t is the time lag, α is the drop rate, τ is the time constant, and η is noise. The drop rate quantification revealed that Day6 cells underwent more significant nuclear changes compared to the

other two conditions, suggesting that chromatin organization in Day6 cells is more open and flexible (Figure 3-14 B).

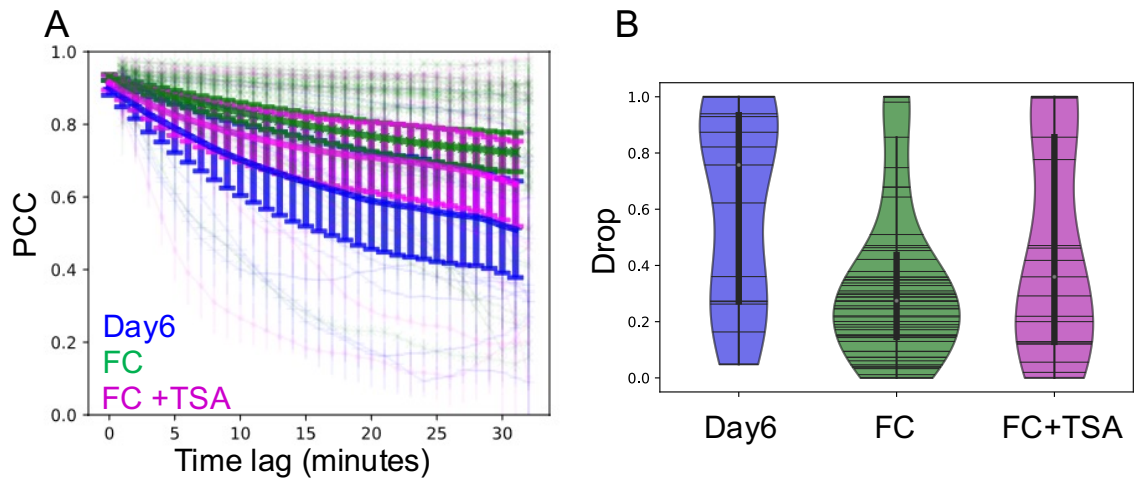

Figure 3-14. Chromatin Poised State in Partially Reprogrammed Cells. (A) Pearson correlation coefficient (PCC) curve of projected nuclear area as a function of time with mean and confidence interval of mean (as error bar). n = 38, 138, 122 for Partially reprogrammed cells (PR), fibroblasts clumps (FC) and FC+TSA conditions, respectively. (B) Drop rate obtained by fitting the nuclear area PCC curves of (A) indicating the rapid change of nuclear morphology and DNA organizations in PR and FC+TSA conditions.

Transcriptional regulation in rejuvenation process

To further explore potential transcriptional regulatory mechanisms driving rejuvenation, we employed the Prize-Collecting Steiner Tree method to analyze differentially expressed gene lists obtained from RNA-seq data (Figure 3-15A). Specifically, genes significantly upregulated in the rejuvenated cells compared to the old fibroblasts were treated as protein and transcriptional regulatory nodes (1974 genes) (Figure 3-15B). Genes significantly upregulated in both young and rejuvenated cells compared to the old ones were treated as RNA nodes (167 genes). These 167 genes are likely to be closely related to young cell state. All these nodes were used in the Prize-Collecting Steiner Tree method to create a network based on protein-protein interaction data and

transcriptional regulator-target gene relationships. Functional annotation of these three types of nodes highlighted the potential significance of NFkB and pluripotency-regulating pathways in rejuvenation (Figure 3-15E). Since rejuvenated cells undergo partial reprogramming, the upregulation of factors associated with de-differentiation may play a role in inducing rejuvenation. This hypothesis was supported by Steiner tree analysis, which identified several of these factors, such as LIF and HOXD1, as potential regulators acting upstream of a group of transcriptional regulators, including LEF1 and SOX4, known to regulate the young-specific RNA nodes described earlier (Figure 3-15C/D). These findings align with previous studies demonstrating the role of LEF1 in skin regeneration (Phan et al. 2020). In conclusion, our results shed light on potential regulatory pathways triggered by dedifferentiation, contributing to cellular rejuvenation.

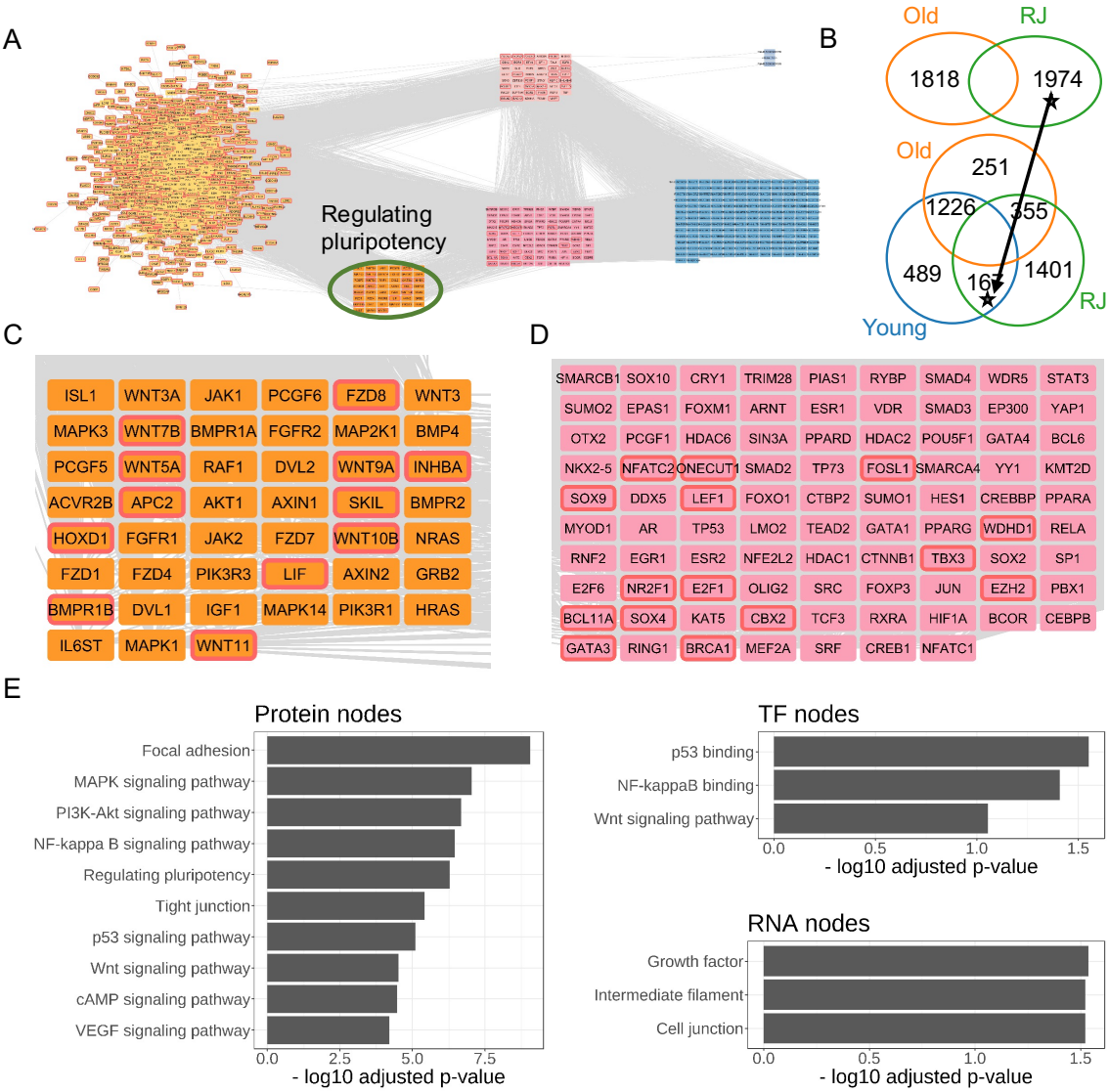

Figure 3-15. Transcriptional regulation for the rejuvenation process. (A) Constructed transcriptional regulatory network in the rejuvenation process derived from the Prize-Collecting Steiner Tree method. One upstream pathway (i.e. regulating pluripotency) of the transcription factors was highlighted. Yellow colored nodes (left) are the protein nodes. Pink colored nodes in the middle are the transcriptional regulators. Blue colored nodes (right) are the RNA nodes. (B) Differential expression gene lists used as the input of Prize-Collecting Steiner Tree. (C) Pathways regulating pluripotency in the constructed transcriptional regulatory network in (A). Genes with upregulation were marked with a red color border. (D) Transcriptional regulators in the main Figure 2 (H). Genes with upregulation were marked with a red color border. (E) Functional annotation of protein nodes, transcriptional regulator nodes and RNA nodes in the constructed transcriptional regulatory network.

Discussion

Rejuvenation of terminally differentiated cells can be achieved through various approaches, involving environmental factors, genetic modifications, or pharmacological interventions. Notably, techniques like somatic cell nuclear transfer (SCNT) and the generation of induced pluripotent stem cells (iPSCs) have been instrumental in reversing the aging process in a variety of cell types, including fibroblasts, neurons, cardiac myocytes, T-cells, macrophages, and skin cells (Takahashi and Yamanaka 2006; Gurdon 1962). While these methodologies hold immense promise, their clinical applications are hampered by drawbacks such as low efficiency and an increased risk of oncogenic transformations due to genomic mutations acquired during the dedifferentiation process (Ghosh et al. 2011; Kimbrel and Lanza 2015).

Over the past few decades, researchers have explored alternative approaches to rejuvenation that do not involve genetic manipulation. These approaches encompass environmental interventions, genetic modifications (e.g., downregulation of NF-kB signaling), and pharmacological strategies (e.g., mTOR inhibition with rapamycin), which have demonstrated the capacity to extend the lifespan of mice (Ladiges et al. 2009; Bitto et al. 2016). However, the potential of mechanically driven reprogramming,

as well as its ability to address the limitations associated with dedifferentiation, remains to be thoroughly elucidated. Additionally, the rejuvenation of physically dedifferentiated cells through their subsequent redifferentiation into a more youthful cellular state has yet to be explored.

A recent study introduced a novel method whereby the lateral confinement of fibroblasts on fibronectin micropatterns induced their reprogramming, endowing them with embryonic stem cell (ES)-like characteristics (Roy et al. 2018). Beyond its capacity to restore stem cell-like properties, this mechanical mode of reprogramming also holds significant potential in the realm of rejuvenation (Shivashankar 2019). In the present work, we harnessed these partially reprogrammed (PR) cells, which exhibited a gene expression profile reminiscent of naive ES cells, and subsequently redifferentiated them into young fibroblasts for potential applications in rejuvenation therapies. This innovative approach highlights the advantage of decoupling rejuvenation from complete dedifferentiation, with tissue microenvironment mechanical properties augmenting the redifferentiation of stem cells into specific lineages.

Our transcriptional analysis revealed the upregulation of markers associated with contractility and rejuvenation, in redifferentiated fibroblasts (RF) compared to control cells. This observation suggests that RF cells evolve into activated fibroblasts through reprogramming. Additionally, we found that treating fibroblasts with agents that promote chromatin decondensation, such as the histone deacetylase (HDAC) inhibitor Trichostatin A, resulted in chromatin structures that were more poised for activation. These cells exhibited increased contractility when exposed to extracellular matrix (ECM)-related cues.

Fibroblast aging is characterized by a collection of features, including a loss of cellular contractility, increased senescence, nuclear Lamina degradation, chromosomal aberrations, and alterations in 3D chromatin organization and transcriptional outputs. In the second part of our study, we subjected aged human fibroblasts to lateral confinement, inducing partial dedifferentiation. Subsequent redifferentiation of these cells within 3D matrix constraints led to the emergence of a rejuvenated cellular state characterized by the reversal of many age-related hallmarks. Notably, the increased

staining for phosphorylated myosin light chain (pMLC) in rejuvenated fibroblasts indicated that partial reprogramming and redifferentiation resulted in enhanced acto-myosin contractility.

Lamin-associated domains (LADs) are known to undergo alterations with aging and require resetting in rejuvenated cells. By integrating DamID-seq, RNA-seq, and Hi-C data, we identified that the majority of LAD sequences detached from the nuclear Lamina in rejuvenated cells were also detached in young cells. Pathways enriched for upregulated genes within these identified LAD regions included cell migration, cytoskeletal organization, BMP signaling, and TGFb signaling. Within these LAD regions, we also pinpointed transcription factors that regulate LAD genes, such as PPARG. This indicates that aging-dependent reorganization of LADs can be reset during the rejuvenation process.

Furthermore, our imaging-based methods allowed us to investigate the role of the cytoskeleton in regulating chromatin organization at the nuclear periphery. We analyzed the colocalization of the actin cytoskeleton or microtubules with heterochromatin or telomeres. Previous research has shown that aged fibroblasts exhibit increased association of microtubules with the nucleus and elevated levels of the Linker of Nucleoskeleton and Cytoskeleton (LINC) component SUN1 (Chang et al. 2019). Our imaging results indicated that the rejuvenation process also reset the colocalization patterns of chromatin and the cytoskeleton at the nuclear periphery. Additionally, gene expression analysis confirmed the upregulation of cytoskeleton-related pathways in the rejuvenated state.

In summary, our study has shed light on innovative approaches to rejuvenation that harness physical reprogramming, thus avoiding the limitations associated with complete dedifferentiation. The rejuvenation process involves the resetting of transcription-dependent chromatin organization, including genes related to key aging pathways and LADs. Additionally, our findings highlight the role of the cytoskeleton in regulating chromatin organization at the nuclear periphery and its involvement in the rejuvenation process. These insights open up new avenues for future research and potential applications in rejuvenation therapies.

Chapter 4: Rejuvenation of aged fibroblasts in human skin model

This part of the result section is adapted from the paper:
Bibhas Roy, Tina Pekec, **Luezhen Yuan**, G.V. Shivashankar, Implanting mechanically reprogrammed fibroblasts for aged tissue regeneration and wound healing, Aging Cell 2023 (accepted).

I contributed to all the data analysis, including image analysis, RNAseq analysis, and statistical analysis for this manuscript.

Introduction

Aging skin tissues undergo a reduction in fibroblast numbers within the dermis, accompanied by alterations in extracellular matrix (ECM) deposition. These changes result in diminished responses to tissue repair and wound healing (Cole et al. 2018; López-Otín et al. 2013; Freitas-Rodríguez, Folgueras, and López-Otín 2017; Gunin et al. 2011; Solé-Boldo et al. 2020; M. Li et al. 2021). In this context, cell-based therapies have gained popularity as a means of regenerating aging tissues and promoting wound healing clearance. Reprogramming cells holds substantial promise for cell therapy, offering the potential to treat diseases and rejuvenate aged tissues. For example, reprogrammed cells have been harnessed to enhance wound healing, a complex process comprising multiple stages, including hemostasis, inflammation, proliferation, and remodeling (Guo and DiPietro 2010). The initial phase of hemostasis involves immediate responses to wounds, including vascular constriction and fibrin clot formation to control bleeding. Subsequently, during the inflammatory phase, neutrophils, macrophages, and lymphocytes are recruited to the wound site to clear invading microbes and cellular debris. The release of cytokines activates keratinocytes, fibroblasts, and angiogenesis, facilitating tissue regeneration, which leads to the third phase of wound healing. Fibroblasts within the wound bed play a crucial role by producing collagen, glycosaminoglycans, and proteoglycans - major components of the ECM. Finally, the last phase involves ECM remodeling and the restoration of vascular density, which can extend over several years.

Three primary cell therapies have been applied for skin rejuvenation and facilitating wound healing: a) autologous, b) allogenic, and c) iPSC-based therapies. In autologous implantation, cells are derived from various tissue regions within the same patient and used as cellular implants for tissue repair and wound healing (Grether-Beck et al. 2020; B. K. Sun, Siprashvili, and Khavari 2014; Abdel-Sayed et al. 2019; Guenou et al. 2009). However, this approach faces significant limitations in aging cases due to challenges in obtaining a sufficient number of high-quality cells, especially as aging cells become senescent and exhibit senescence-associated secretory phenotypes (Wlaschek et al. 2021). Additionally, this approach involves two clinical procedures - cell isolation and re-infusion - making it logistically complex (isolation and re-infusion)(Uchida et al. 2000). Allogeneic cell therapies follow a similar production process to autologous therapies but differ in that cells are derived from healthy donors. Although allogeneic cell therapies offer numerous advantages, they still face two major challenges: immunological rejection and elimination (Yu et al. 2019).

iPSC-based therapies have shown promise, as reprogramming aging cells can erase aging hallmarks at the epigenetic level (Takahashi and Yamanaka 2006; Abraham E 2017). Implanting reprogrammed aging cells presents a unique opportunity for tissue regeneration. However, the clinical applications of iPSC-based therapies have been limited by the risk of oncogenic transformation upon implantation. While recent studies aim to address some of these limitations, alternative cell-based approaches have the potential to offer extra improvement in regenerative medicine.

In a recent study, we demonstrated that mechanically induced growth confinement of cells resulted in their partial reprogramming (Roy et al. 2018). Subsequent redifferentiation of these partially reprogrammed cells exhibited enhanced rejuvenation properties (Roy et al. 2020). Specifically, these findings indicated that laterally confined growth of fibroblasts on micropatterned substrates induced nuclear reprogramming with high efficiency, in the absence of exogenous reprogramming factors. We provided compelling evidence of the induction of stem cell-like properties, as evidenced by various assays for pluripotent markers, and demonstrated their redifferentiation potential into multiple lineages. Moreover, we efficiently redifferentiated these partially reprogrammed spheroids into fibroblasts by embedding them in three-dimensional (3D) collagen-I matrices with appropriate densities.

Intriguingly, we found that these differentiated fibroblasts exhibited rejuvenation properties, including enhanced ECM regeneration and remodelling, along with reduced DNA damage when compared to parental fibroblasts. Importantly, we successfully demonstrated this rejuvenation approach using primary human dermal fibroblasts derived from aged individuals. Collectively, rejuvenating fibroblasts through this approach holds significant promise for regenerative medicine, particularly in the context of tissue rejuvenation.

In this chapter, we explore how mechanically induced partially reprogrammed cells can serve as a robust avenue for tissue regeneration and wound healing responses. To investigate this, we implanted mechanically reprogrammed cells derived from primary aged human skin fibroblasts into in vitro reconstructed aged skin tissue models and we analyzed the ECM secretion with the aim of rejuvenating aged skin to a more youthful state and the spatial distribution of implanted cells. Additionally, we assessed the wound healing potential of these partially reprogrammed cells by implanting them into in vitro aged skin-based wound models. It has been shown that in wound healing, fibroblasts align among themselves (Laufer et al. 1974). To evaluate wound healing ability, we analyzed the spatial clustering of nuclear states. Finally, through RNAseq assays, we attempted to identify upregulated genes and signaling pathways involved in the wound healing process. Together, our findings demonstrate a non-genetic approach to tissue repair with significant implications for regenerative medicine.

Materials and Methods

Partial reprogramming of aged skin fibroblasts

Aged human primary skin fibroblasts were obtained from an aged donor (age 75) (GM08401; Coriell Institute), and young human primary skin fibroblasts were obtained from a young donor (age 11) (GM09503; Coriell Institute). All primary cells used in this study were within passages 3-10. The old and young cells were cultured in minimal essential medium (MEM) (Gibco) supplemented with 15% (vol/vol) heat-inactivated fetal bovine serum (FBS) (Gibco), 1% non-essential amino acids (NEAA), and 1% penicillin–streptomycin (Gibco). Partially reprogrammed cells derived from old cells

were obtained under similar conditions as previously described (Roy et al. 2018). In brief, old cells were cultured under laterally confined conditions on specific fibronectin micropatterns (area 9,000 µm2 with an aspect ratio of 1:4) created on uncoated culture dishes (catalog no. 81151, Ibidi) by stamping fibronectin-coated (catalog no. F1141; Sigma) PDMS micropillars fabricated through soft lithography. After 8 days of culture under laterally confined conditions in the above-mentioned culture medium, partially reprogrammed spheroids were formed. These spheroids exhibited stem-like properties and were previously characterized as partially reprogrammed (PR) cells (Roy et al. 2020). Each batch of PR cells was subjected to alkaline phosphatase assay for characterization of the reprogramming efficiency. Young and old fibroblasts were used as respective control conditions.

In vitro skin models

In this study, we used reconstructed full thickness (FT) skin model (Phenion^{TM}). The FT AGED skin model (short for AG model) mimics aged human skin and was employed as an aged skin model in our experiments. It is characterized by connective tissue with senescent fibroblasts, reduced synthesis of ECM proteins like collagen and elastin, and elevated secretion of matrix metalloproteinases (MMPs).

Cryo-sectioning and immunohistology

After 10 days of culture, the tissues are cryopreserved according to the manufacturer's protocol. Briefly, the skin model was first dissected into two nearly identical halves, and then the tissue halves were again cut parallel to the first section plane. The dissected tissues were placed in precooled cryo-tray and were frozen using tissue freezing media (OCT). After the tissue-freezing medium was frozen completely, the skin model stripes/pieces were stack side by side with the larger cutting edge facing upwards and leaving a small space between each other. The fresh tissue-freezing medium was added in time before the previous portion had been frozen completely. OCT was added slowly around the tissue before waiting for it to freeze, thereafter repeating this step until the tissues were completely embedded in the frozen medium. The frozen tissues were cryosectioned at 7µm thickness using cryomicrotome (Leica) and transferred to Superfrost Plus slides (Thermo Scientific). Tissue sections were dried after cutting and stored at -80°C until further use. For immunostaining, slides were recovered from -80°C, let dry briefly and fixed in -20°C (ice cold) acetone for 15

min. Then slides were dried for 5 minutes, and tissue sections were encircled with a PAP pen and dipped in PBS for a few minutes. From this step all the subsequent steps were performed in a humid chamber.

Tissue sections were blocked in 10% goat serum for 1 hour. The slides were incubated with primary antibody solutions diluted in 1% BSA and 0.3% Triton in PBS at 4°C overnight. Then, slides were washed in PBS three times with 5 minutes each. Then slides were incubated with Alexa Fluor plus secondary antibodies prepared in 1% BSA and 0.3% Triton. Again, slides were washed with PBS three times. After the wash, samples were stained with Hoechst 33342 (NucBlue, ThermoFisher Scientific) in PBS for 10 min at room temperature, and further mounted with mounting media (Gold antifade, Thermo Fisher Scientific), after which a coverslip was placed on top of it. Slides were left to dry for overnight at room temperature and stored at 4°C until imaging. The following primary antibodies were used in this study: Elastin (abcam ab21610), aSMA (sigma A5228), Fibronectin (abcam ab2413), Collagen I (abcam ab6308).

Image acquisition and Image analysis

Fluorescent images of immunostained histological sections were acquired by using a Nikon A1R laser-scanning confocal microscope (Nikon Instruments Inc.) at either 20× magnification (Plan Apo 20× extra-long working distance, numerical aperture [NA] 0.8) or 40× magnification (1.25-NA silicon objective) with identical acquisition settings and with a step size of 3 or 1 μm, respectively. Confocal images of either 512 × 512 or 1,024 × 1,024 pixels were obtained with an XY optical resolution of 0.84 or 0.42 μm, respectively. The fluorescence intensity of cells at the implanted region was measured for each protein in its respective channel using in-house code in Fiji (NIH). We calculated the fold change in ECM protein levels and quantified the normalized mean intensities of the PR cell-implanted region with respect to the mean normalized intensity of the old cell-implanted regions.

Nuclear feature analysis and spatial clustering analysis

Local and global Otsu thresholding was employed to segment the nucleus from the original DAPI images. Large, dim autofluorescent regions (especially in DAPI channel) were eliminated based on size and fluorescent intensity. Nucleus features were

extracted using tools previously established in our lab (https://github.com/GVS-Lab/chrometrics) (Venkatachalapathy, Jokhun, and Shivashankar 2020). Linear discriminant analysis (LDA) was used to train a classifier to distinguish between injected old and PR cells. For balanced training data, 3000-3500 nuclei were used from each condition, with 75% of nuclei used for training and the remaining 25% for testing. LDA1 values were normalized to a 0-1 range (Min-max normalization) to derive a score for each nucleus to characterize cell states. To analyze the spatial distribution of the injected cells based on nuclear features, Density-based spatial clustering of applications with noise (DBSCAN) was utilized, using nuclear features and centroid coordinates within the image. All features were normalized to the 0-1 range before clustering analysis. Python hdbscan was employed for this purpose (McInnes, Healy, and Astels 2017). Pairwise angular distances between nuclei were computed within a range of 0 to π/2 for every pair. The mean difference in angles was determined by calculating the average value of pairwise angular distances within the spatial cluster identified by the DBSCAN result.

RNA-Seq sample preparation and analysis

Total RNA was isolated from the implanted cells specifically in the wound regions. After post implantation of 10 days of culture, the AG wound models were precisely dissected to collect the tissue of the wound site and surrounding tissue regions. The epidermis of the dissected tissue was removed and the remaining sections were minced finely for further processing. The total RNA was isolated according to the manufacturer's protocol using the RNeasy Mini Kit (Qiagen, (Hilden, Germany). The preparation of the mRNA library (Illumina's TruSeq Stranded protocol) and sequencing on a HiSeq 2000 platform were performed at the Department of Biosystems Science and Engineering (DBSSE), ETH Zurich. In summary, we had two conditions: PR (implanted PR cells in AG tissue based wound model), Old (old fibroblast implanted in the AG tissue based wound model) each condition had two biological replicates and technical replicates (run on four different lanes).

RNA analysis was done as described previously (Roy et al. 2020). Paired end reads were aligned to Homo sapiens GRCh38.84 reference genomic indexes using the HISAT2 sequence-alignment tool (version 2.2.1). The cloud indexes (grch38_trans) for HISAT2 were accessed on June 25th 2020 from https://registry.opendata.aws/jhu-

indexes. Four technical replicates for each biological sample were combined as input of HISAT2. Default parameters were used in HISAT2. Single aligned reads were counted by htseq-count (1.99.2) (Anders, Pyl, and Huber 2015). Count numbers for all expressed genes were used in differential expression analysis using DESeq2 (Version 1.34.0) (Love, Huber, and Anders 2014). Differentially expressed genes had adjusted P values (Benjamini–Hochberg) below a 0.1 false discovery rate (FDR) and fold change higher than 2. Enrichment analysis was done in DAVID database (Dec. 2021 version) (D. W. Huang, Sherman, and Lempicki 2008). Gene lists for each Gene Ontology (GO) term were obtained from AmiGO (Carbon et al. 2009). Genes used in the Principal Component Analysis (PCA) are from GO:0009611, GO:0030198 and GO:0042060. For each gene, z-score of TPM value normalized within each set of experiment was used. Highly correlated genes (correlation coefficient >0.95 or <-0.95) were removed in this PCA. Principal Component (PC) one was chosen as the combined expression level.

Statistical analysis.

All data are expressed as mean ± SD or ± SEM as noted in figure legends. For box plots, the box limit represents the 25th to 75th percentile and whiskers 1.5× interquartile range. Each experiment was repeated at least three times. We evaluated the statistical significance of the mean with the Student's unpaired two-tailed t test, performed between samples of interest and corresponding control. *P < 0.05; **P < 0.01; ***P < 0.001.

Results

Implanted partially reprogrammed spheroids showing rejuvenation properties in aged skin model

In an earlier chapter of this thesis, we investigated fibroblast rejuvenation through mechanical reprogramming and redifferentiation. We observed that primary aged skin fibroblasts, when subjected to laterally confined growth and subsequent redifferentiation within a 3D collagen matrix, exhibited phenotypic characteristics akin

to young fibroblasts. These characteristics included enhanced cell size, contractility, and extracellular matrix (ECM) remodeling. Importantly, these young fibroblast-like traits are crucial for rejuvenating aged human skin by replenishing the fibroblast population, regenerating ECM proteins, and facilitating matrix remodeling. To simulate aged human skin, we utilized primary skin fibroblasts derived from an elderly donor (age 75). These cells were cultivated under laterally confined conditions on Fibronectin (FN) micropatterns for 8 days until they developed partial stem-cell-like properties, resulting in the formation of spheroids with characteristics we previously termed "partially reprogrammed cells" (PRs) (Figure 4-1A) (Roy et al. 2018; 2020).

To assess the rejuvenation potential of these PRs in human skin, Dr. Bibhas Roy and Dr. Tina Pekec implanted them into a commercially available reconstructed aged skin model (PhenionTM) and allowed them to differentiate and grow for 10 days (Figure 4-1B and Figure 4-2A). The Phenion aged skin model closely mimics the structure and physiology of mature aged human skin. Following 10 days of air-liquid culture, the skin tissues were cryo-embedded and cryosectioned for subsequent immunohistological analysis.

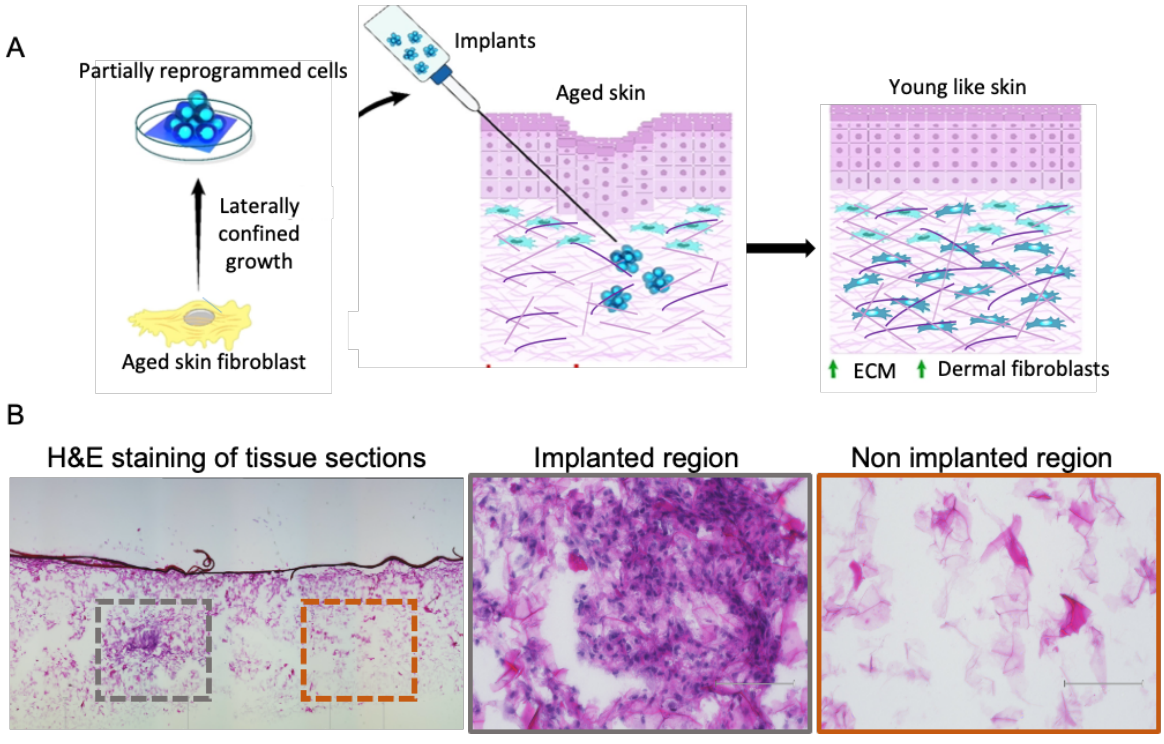

Figure 4-1. Implanting partially reprogrammed (PR) cells in human skin model. (A) Schematic representation of the in vitro skin model of tissue regeneration by mechanically reprogrammed cells. Aged skin fibroblast were culture on rectangular fibronectin coated patterns for 8 days to reach partially reprogrammed state. Collages collected from the patterns and then were injected into the skin model and culture for additional 10 days. (B) Extracellular matrix (ECM) production in aged skin by the implanted cells using H&E staining of implanted and non-implanted region.

Interestingly, we observed a significant increase in collagen I protein regeneration in the regions where PRs were implanted in the aged skin model compared to regions implanted with control old fibroblasts (Figure 4-2B/C). Moreover, the regeneration of other critical ECM proteins, such as elastin and fibronectin, was also substantially higher in the regions implanted with PRs. Quantitative image analysis revealed significantly elevated levels of collagen I, elastin, and fibronectin in the skin model produced by the implanted PRs compared to that produced by the implanted old fibroblasts.

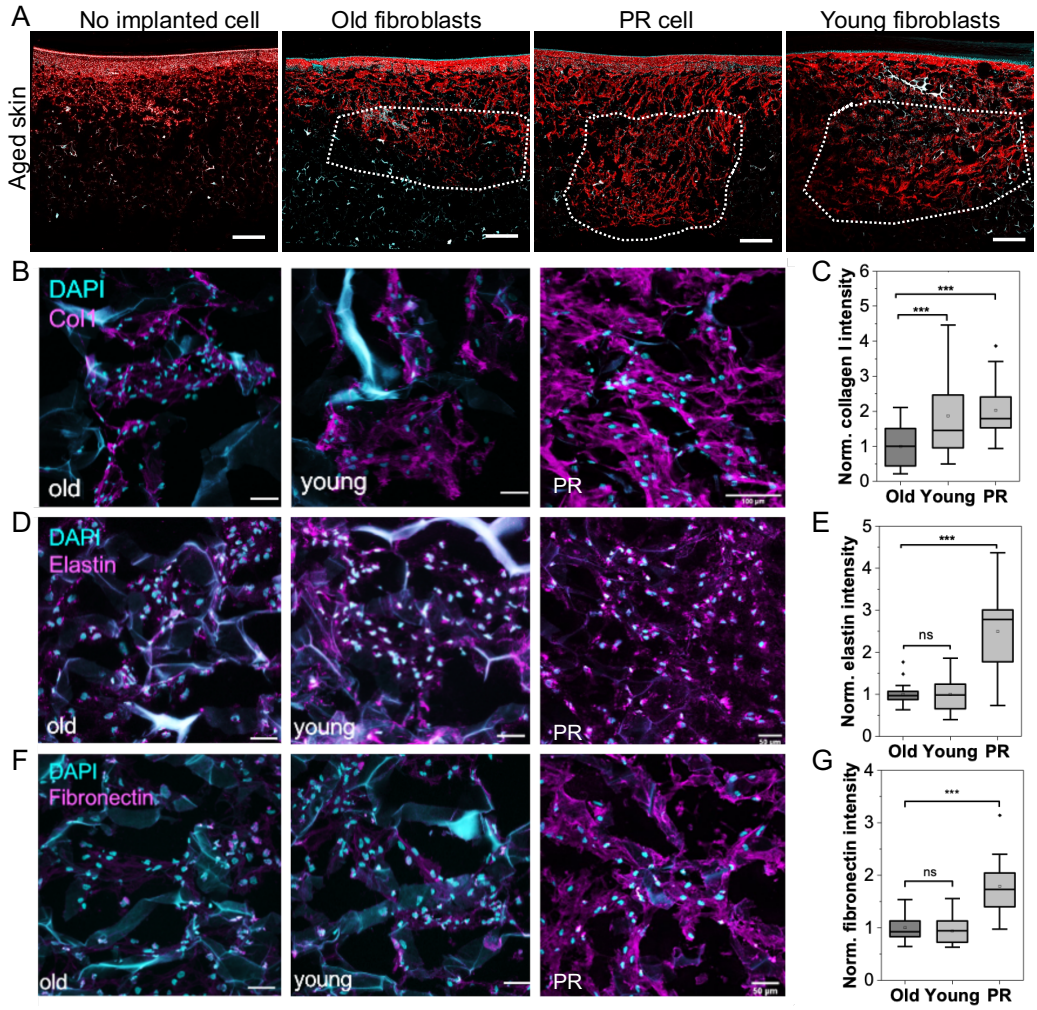

Figure 4-2. Extracellular matrix (ECM) secretion after implantation of young, old and PR cells. (A) Representative fluorescent images (10X magnification) of histological tissue sections of in vitro aged skin tissue with different implanted cells immunostained with collagen I antibodies (red color) and Hoechst (cyan color). Scale bar: 500μm. (B/D/F) Representative fluorescent images (40X magnification) of the cell implanted regions of histological in vitro aged skin tissue sections stained with collagen I, elastin, and fibronectin antibodies. Scale bar: 50μm if not mentioned. (C/E/G) Normalized intensity plots of ECM proteins collagen I, elastin and fibronectin at the cell implanted regions obtained from immunohistology of in vitro aged skin tissue sections. ***P < 0.001; two-sided Student's t tests were used.

Cell population analysis using nuclear features reveals distinct states and distribution of partially reprogrammed cells

Upon implantation of PR cells into the skin tissue models, it is essential to assess the different cell states and their spatial distribution during the rejuvenation and wound healing processes. Previous work from our group demonstrated that nuclear morphology and chromatin organization features can serve as biomarkers of cell states, with changes in cell state detectable through nuclear features (Venkatachalapathy et al. 2022). Based on linear discriminant analysis (LDA), we found that a linear combination of four groups of features - chromatin textures, 2D nuclear morphology features, global intensity profile, and nuclear boundary characteristics - could accurately distinguish PR cells from old cells, with a high accuracy rate (63%~67% for testing) for the rejuvenation process (Figure 4-3 B). Chromatin textures and 2D nuclear morphology features emerged as critical factors in this classification (Figure 4-3 C).

To study the spatial distribution of injected cells in different states within this skin rejuvenation model, we employed the density-based spatial clustering of applications with noise (DBSCAN) method to group nuclei with similar LDA scores (Figure 4-3 A) (McInnes, Healy, and Astels 2017; Campello, Moulavi, and Sander 2013). Specifically, for analyzing the spatial distribution of the injected cells, we used the nuclear features and centroid coordinate within the image. All these features were normalized to the 0-1 range before the clustering analysis. The centroid coordinates were included to get the spatial clustering of nucleus with similar nucleus features and close in space.

We observed that PR cells injected into the same local groups exhibited significantly different LDA scores compared to groups of old cells in the skin rejuvenation models (Figure 4-3 D). This indicates that injected PR cells are maintained at a different cell states compared to old cells, consistent with previous findings of differences in ECM secretion between these two cell types. Furthermore, there were no differences in cell orientation within the clusters when comparing these two types of implanted cells (Figure 4-3 E). Effective rejuvenation relies on the appropriate distribution of implanted cells to maintain local cell density and facilitate effective matrix regeneration. Interestingly, we found that implanted PR cells spread out uniformly over a larger area of in vitro aged skin tissue for more efficient ECM regeneration compared to implanted old fibroblast cells (Figure 4-3 A). Taken together, these results highlight the efficient migration and redifferentiation of implanted PR cells in the in vitro skin environment.

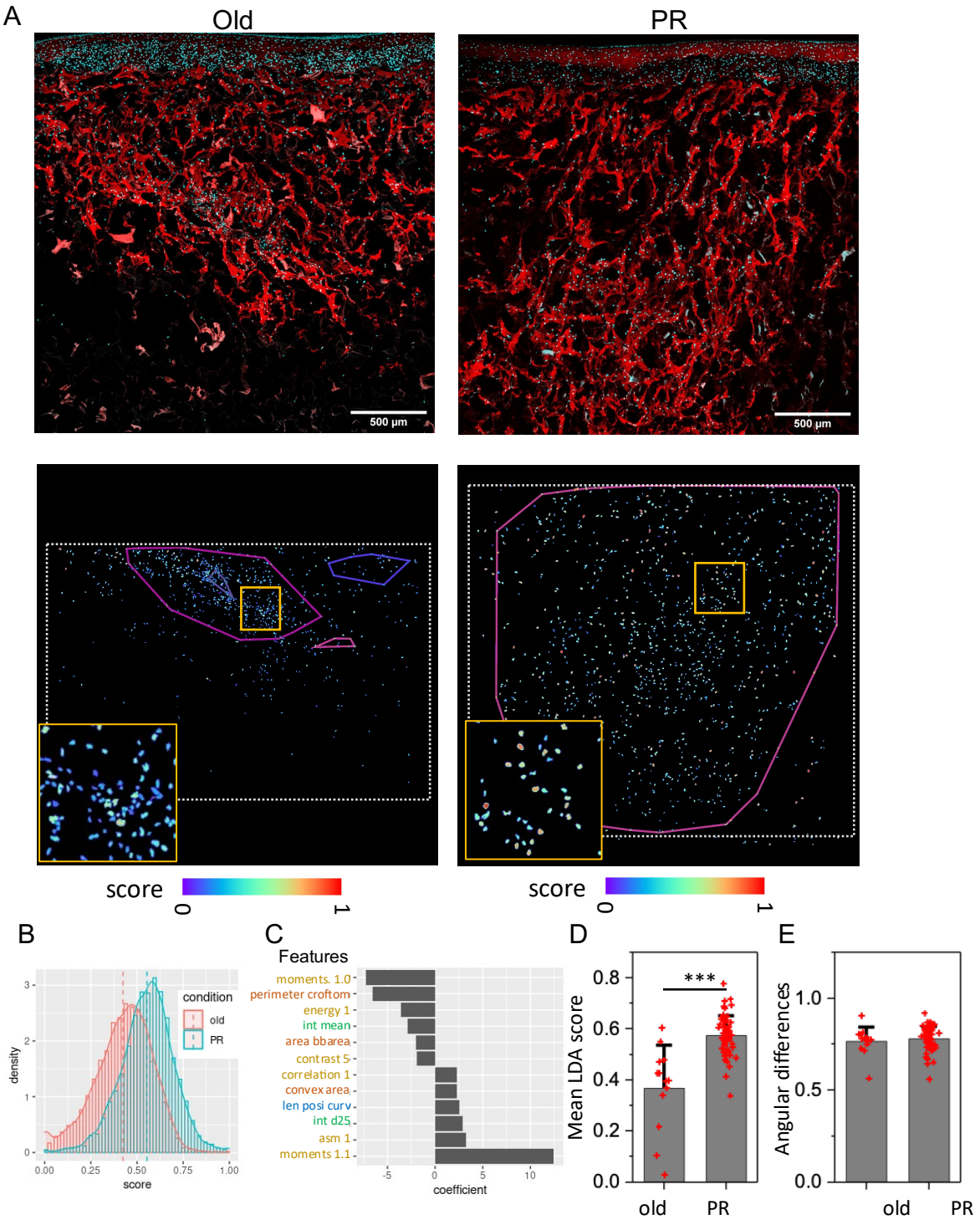

Figure 4-3. Implanted PR cells exhibit specific nuclear and chromatin features from old cells in skin rejuvenation model. (A) Representative images of the implanted regions in the skin rejuvenation model. First row: nucleus in cyan, Collagen I in red. Second row: the corresponding spatial clustering of nuclei based on their LDA scores from the same region. (B) Probability density histograms of the normalized LDA1 score for nuclei from injected old (red) or PR (blue) cells. (C) Top nuclear features used in

the LDA classifier and the related coefficients. Four groups of nuclear and chromatin features as top loading features of LDA classifier are chromatin textures (yellow), 2D nuclear morphology features (red), global intensity profile (green), nuclear boundary characteristics (blue). (D) Barplot shows the mean of the LDA scores within the local clusters for the injected old and PR cells. Each data point refers to one cluster identified by DBSCAN algorithm. (E) Barplot shows the mean of the angular difference among any two nuclei within the cluster for the implanted old and PR cells.

Implanted partially reprogrammed spheroids in wound healing model show elevated ECM secretion

The enhanced regeneration of ECM proteins and cell redifferentiation properties of PRs suggest their potential role in wound healing. To investigate this, we implanted PRs into an aged skin wound model. The wound model was created by making a deep incision in the aged skin model (Figure 4-4 A). Subsequently, PRs were implanted into the wound bed and surrounding regions of the skin, followed by a 10-day culture period and subsequent histological assays (Figure 4-4 C). The marked regions of the images from the top surfaces of the aged skins show the wound region at day 0 and day 10 after cell implantation (Figure 4-4 B). These top view images revealed that wounds with implanted PRs exhibited better healing compared to the wounds with implanted old fibroblasts, as indicated by the yellow arrowheads (Figure 4-4 B). However, the wound regions without implanted cells, marked with blue arrowheads, showed minimal change even after 10 days. Furthermore, we observed that implanted cells facilitated matrix regeneration at the wound site through immunohistological assays, whereas ECM regeneration was absent in regions without implanted cells (Figure 4-4 C). Similar to the tissue rejuvenation model, we also noted a significantly higher regeneration of ECM proteins, including collagen I, elastin, and fibronectin, by PRs compared to old cells within the wound bed (Figure 4-4 D). This heightened ability of ECM regeneration by PRs in the wound bed is essential for facilitating the wound healing process.

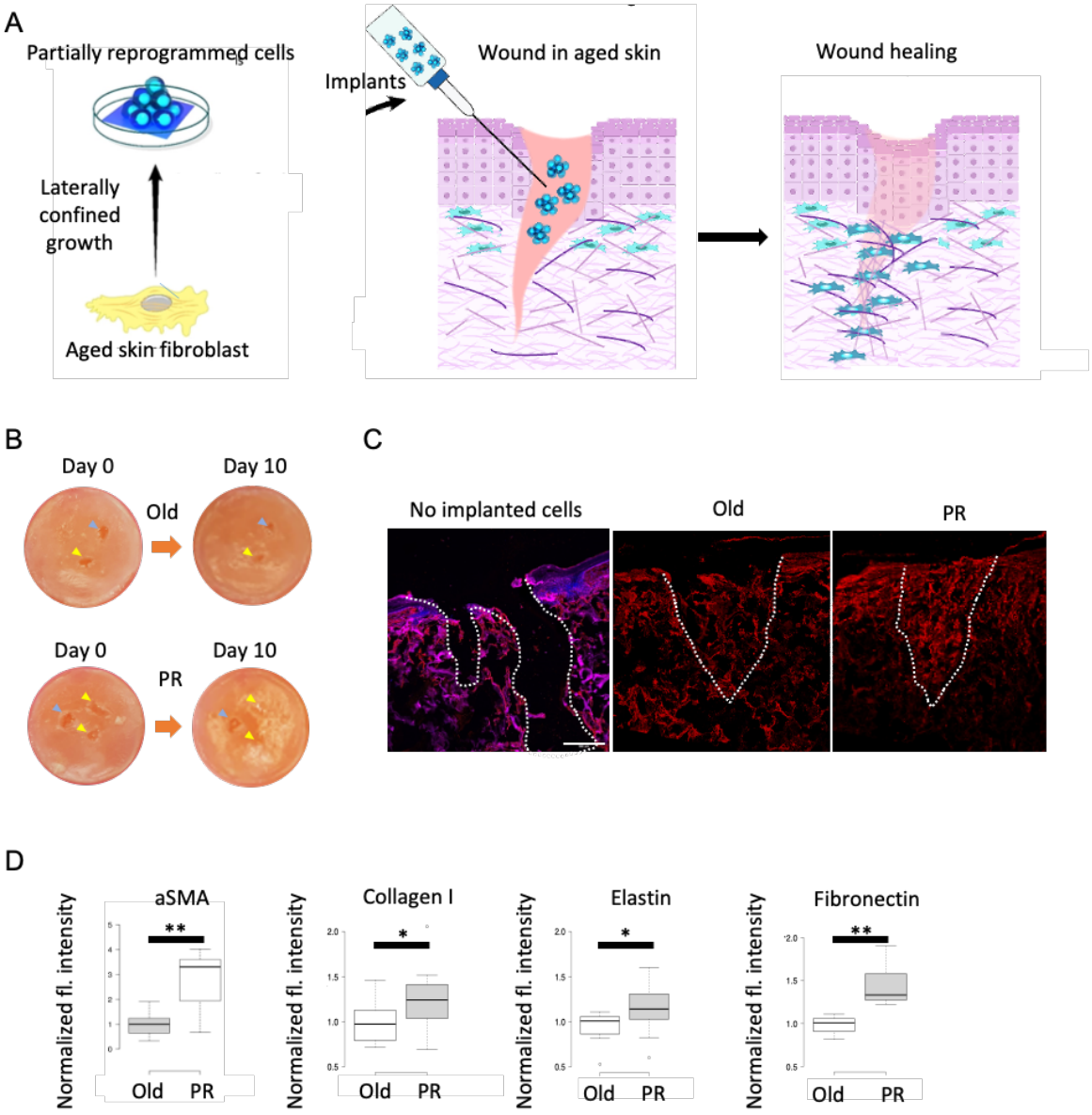

Figure 4-4. (A) Schematic representation of the in vitro aged skin model for wound healing by mechanically reprogrammed cells. (B) Representative top surface view of the wounds on the in vitro aged skin models before and 10 days after the implanted cells. (C) Representative fluorescent images of histological sections of wounds with implanted cells. Matrix stained with collagen I (red). Scale bar: 500μm. (D) Barplots showing the fluorescent intensity of aSMA, Collagen I, Elastin and Fibronectin of implanted Old and PR cells. Raw intensity is normalized to mean value of intensity of the Old condition.

Implanted PRs at wound bed induce enhanced ECM and wound healing gene expression

To gain further insights into the gene expression profiles during the wound healing process, we extracted RNA from the wound bed after 10 days of implantation and conducted global RNA-seq analysis.

sample	total pairs	uniquely mapped	ratio of uniquely mapped
PR_B1	167596636	65699315	0.392009
PR_B2	131081918	74275364	0.566633
CNT_B1	165779715	80992197	0.488553
CNT_B2	127630179	77022710	0.603484

Table 4-1. Descriptive table of RNAseq data for implanted old and PR cells in wound healing model. The table shows the total number of sequences and the mapping rate.

RNA-seq analysis revealed that more than two hundred genes (210 genes) were significantly upregulated (fold change > 2, adjusted p-value < 0.1) and eight genes were downregulated in PRs compared to the old cells (Figure 4-5 A). Remarkably, among the upregulated genes in PRs, three predominant groups emerged: ECM-related genes (GO:0031012), cytoskeleton-related genes (GO:0005856), and wound response genes (GO:0009611) (Figure 4-5 B-D). In addition to the proteins observed in the immunohistological assay, this gene ontology analysis identified other upregulated genes, such as ACAN, COL4A1, LOXL2, MMPs, and TGFB1, which play pivotal roles in ECM biosynthesis and remodelling (Figure 4-5 B). Several cytoskeletal-related genes, including ACTA1/2, CDH2, ERMN, and KRT7, were also upregulated, potentially facilitating matrix contraction during the wound healing process (Figure 4-5 C). Furthermore, various other upregulated genes crucial for the wound healing process were identified (Figure 4-5 D). Functional enrichment analysis of differentially expressed genes further validated the upregulation of ECM biosynthesis and remodeling, cytoskeletal contractility, and cytoskeletal regulation (Figure 4-5 E-G).

Additionally, upregulation of the TGFβ pathway, a well-known regulator of wound healing, was observed in PRs.

To understand the direction taken by implanted PR and old cells in the wound healing model, we incorporated gene expression patterns from publicly available RNA-seq datasets of wound healing processes into our analysis. Principal component analysis (PCA) of RNA-seq data from various stages of in vivo wound healing, obtained from the literature, revealed that our PR-implanted wound model exhibited a similar trend of combined expression changes observed during in vivo wound healing (Figure 4-6). These findings indicate that PR cells, upon implantation into the wound bed, redifferentiate into a fibroblast-like state and exhibit molecular upregulation of ECM, contractility, and wound healing pathways, resulting in faster and more efficient wound healing.

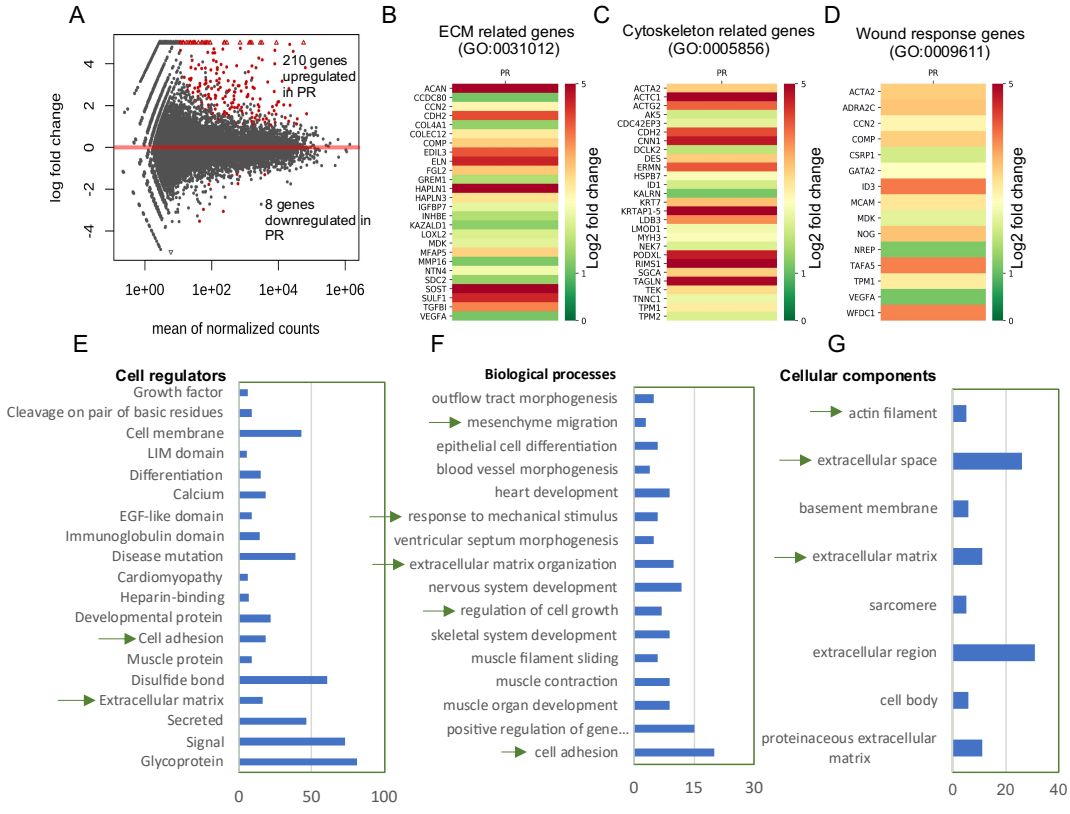

Figure 4-5. RNAseq results showing the differentially expressed genes and differential regulated pathways comparing implanted old and PR cells in the wound healing model. (A) MA-plot for the log2 fold changes shows the differentially expressed genes marked

in red color. These significant differentially expressed genes have adjusted p values < 0.1 (the method of Independent Hypothesis Weighting implemented in DESeq2) and fold change > 2. (B-D) Heatmaps show the log2 fold changes of the upregulated genes in implanted PR cells compared to the implanted old cells in three GO annotated gene lists. GO:0031012 refers to the cellular component extracellular matrix; GO:0005856 refers to the cellular component cytoskeleton; GO:0009611 refers to the biological process response to wounding. (E-G) Barplot shows the number of significant differentially expressed genes annotated by each significant enriched term from the selected categories. For this enrichment analysis, significant enriched terms have the Benjamini p value < 0.1.

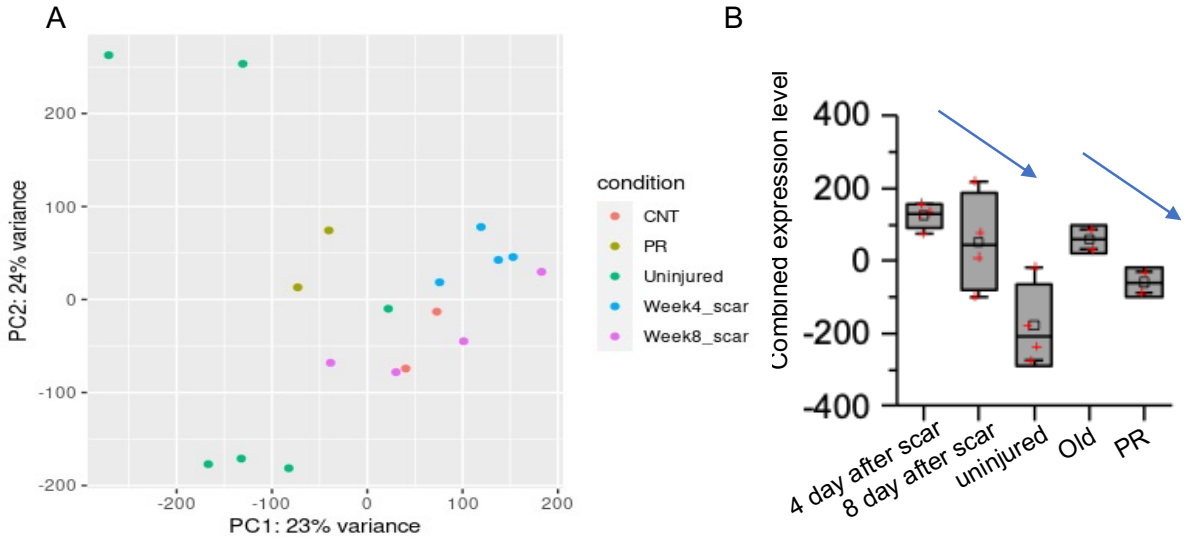

Figure 4-6. Comparison of wound healing response with other publicly available wound healing RNAseq data. (A) The PCA plots of the different data sets (B) Box plot of the combined expression levels (i.e. PC1).

Changes in cell states during wound healing

Similar nucleus feature-based analyses were also conducted on the wound healing model to identify and characterize the implanted cell population throughout this biological process (Figure 4-7A). LDA analysis demonstrated that a linear combination of the four groups of features could effectively differentiate PR cells from old cells with high accuracy (63%~67% for testing) during the wound healing process (Figure 4-7

B). Chromatin textures and the global intensity profile emerged as critical factors in wound healing (Figure 4-7C). Local clusters of injected PR cells exhibited significantly different LDA scores compared to clusters of old cells in the wound healing models (Figure 4-7D). Additionally, angular differences within the local clusters of injected PR cells were smaller than those within old cell clusters in the wound healing model but not observed in the skin rejuvenated model (Figure 4-7E and 4-3E). This suggests that locally aligned injected PR cells may contribute to their enhanced wound healing capabilities.

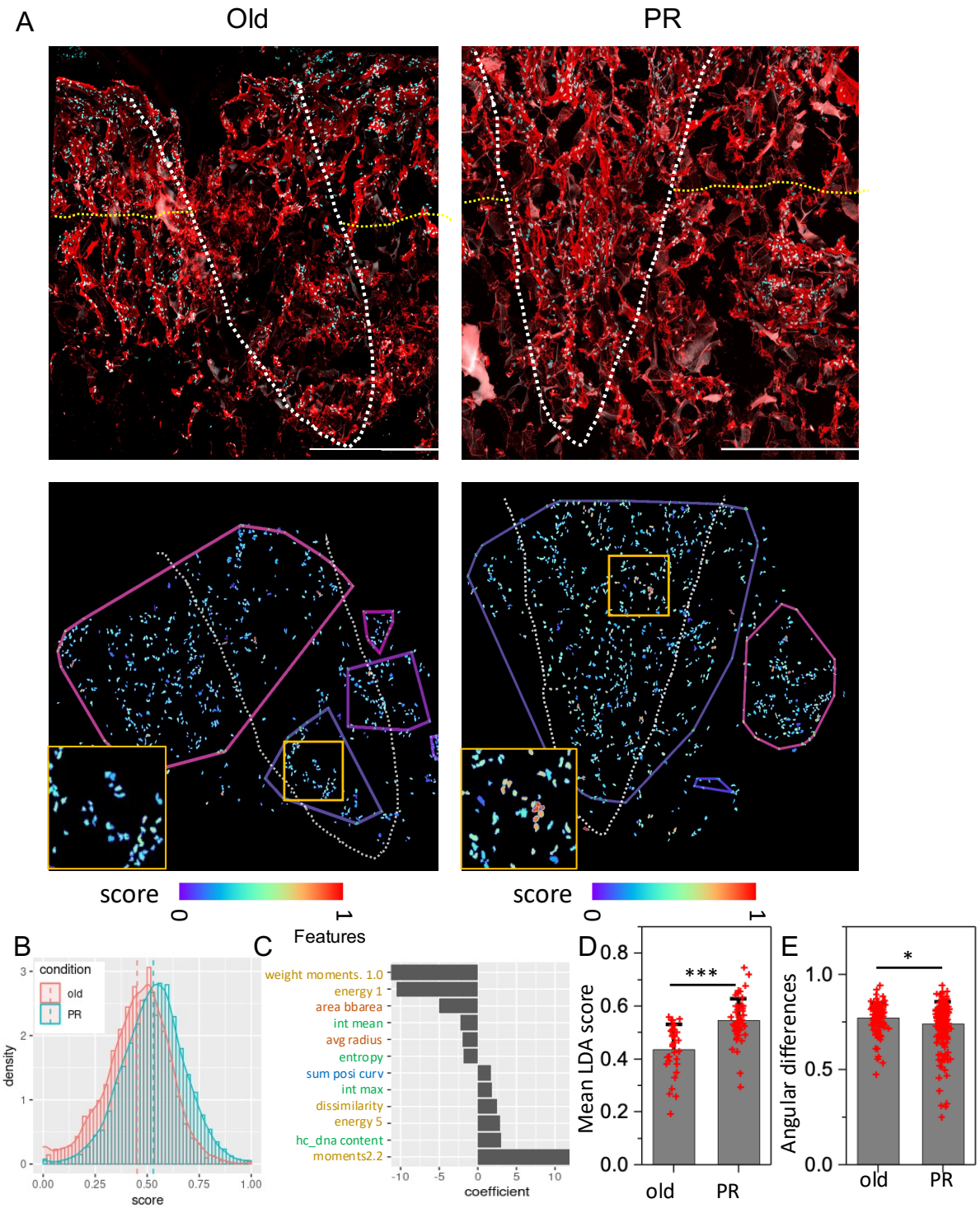

Figure 4-7. Implanted PR cells exhibit specific nuclear and chromatin features from old cells in wound healing model. (A) Representative images of the implanted regions in the wound healing model. Dashed lines indicate approximately the previously created wound regions. (B) Probability density histograms of the normalized LDA score for nuclei from the implanted old (red) or PR (blue) cells. (C) Top nuclear features used in the LDA classifier and the related coefficients. Four groups of nuclear

and chromatin features as top loading features of LDA classifier are chromatin textures (yellow), 2D nuclear morphology features (red), global intensity profile (green), nuclear boundary characteristics (blue). (D) Barplot shows the mean of the LDA scores within the local clusters for the implanted old and PR cells. Each data point refers to one cluster identified by DBSCAN. (E) Barplot shows the mean of the angular difference among any two nuclei within the cluster for the implanted old and PR cells.

Discussion

In summary, our study demonstrates the potential of implanting mechanically reprogrammed aged fibroblasts for tissue regeneration and wound healing. To assess this effect, we utilized an in vitro skin model that closely mimics the physiological characteristics of young and aged skin tissues. As expected, when only aged fibroblasts were implanted, the regeneration and remodelling of the extracellular matrix (ECM) were minimal. However, the implantation of partially reprogrammed cells (PRs) resulted in the differentiation of fibroblasts with a significantly rejuvenated state. These PR-derived cells exhibited enhanced deposition of ECM components, including collagen I, elastin, and fibronectin. Our findings suggest that direct implantation of PRs leads to superior ECM regeneration and remodelling, making it a promising approach for cell therapy models in skin rejuvenation.

Aging is closely associated with the loss of wound healing properties in skin tissue, primarily characterized by a reduced number of fibroblasts in the dermis and impaired ECM regeneration and remodelling properties (Cole et al. 2018; López-Otín et al. 2013; Freitas-Rodríguez, Folgueras, and López-Otín 2017; Gunin et al. 2011; Solé-Boldo et al. 2020; M. Li et al. 2021). In light of this, we investigated whether the implantation of PR-derived aged fibroblasts at a wound site could offer novel cell-based therapies for wound healing. To explore this, we induced sharp wounds in aged skin tissue and implanted either aged fibroblasts or PRs derived from the same fibroblasts. Interestingly, consistent with our previous results, PRs exhibited a substantial increase in the production of ECM proteins at the wound site.

To gain better functional insights into wound healing, we carried out RNA sequencing on cells extracted from the wound site. Differential analysis of gene expression showed the upregulation of ECM genes, cytoskeletal genes, and various signaling pathways related to wound healing for PR cells compared to old cells. In particular, we identified a cluster of 20 growth factors, including VEGFA, TGFBI, IGFBP3, IGFBP6, and IGFBP7, exhibiting a significant RNA expression increase in the injected PR cells when compared with the injected old cells. This underscores the pivotal role of growth factor secretion in the process of tissue rejuvenation. Interestingly, MMP16 displayed marked upregulation in the PR cells in comparison to the old cells, although other MMP genes did not display significant differences under the current experimental protocol. In addition, our gene ontology analysis did not reveal differentially expressed genes linked to extracellular matrix disassembly. Furthermore, cytoskeletal genes such as ACTA1/2, N-cadherin, ERMIN, CTGF, GATA2, ID3, and MIDKINE were differentially regulated in the injected PR cells. Previous studies have shown that these cytoskeletal genes have important roles in wound healing (Momtazi-Borojeni et al. 2018; 2023; Suresh and Diaz 2021; De Wever et al. 2004; M. Wang et al. 2016; Brockschnieder et al. 2006; Rockey, Weymouth, and Shi 2013).

In the context of *in vitro* models, it is essential to acknowledge that while they capture some aspects of aged skin tissue, they lack the full complexity of human skin with other cell types, including immune cells. Nonetheless, our *in vitro* model demonstrates the regenerative capabilities of partially reprogrammed aged fibroblasts when implanted in aged skin tissue. The activation of fibroblasts and the involvement of immune cells play critical roles in *in vivo* skin wound healing to maintain tissue homeostasis (Mishra et al. 2019; Griffin et al. 2021; Park and Barbul 2004). Despite this limitation, our study lays the foundation for understanding the behavior of implanted PR cells and their contribution to tissue regeneration and wound healing.

In conclusion, our results reveal exciting possibilities for personalized cell-based therapies by obtaining patient specific aged cells, reprogramming them *in vitro* and subsequently implanting them back into the same patient for tissue regeneration and wound healing applications.

Chapter 5: Conclusions

This doctoral thesis represents a journey into the fascinating world of mechanical reprogramming and rejuvenation of aged fibroblasts, offering novel insights and promising avenues for regenerative medicine. We embarked on this exploration, connecting the realms of mechanobiology, transcriptional regulation, and regenerative medicine. Each chapter building upon the last to unravel the potential of mechanically induced cell-state transitions.

Mechanical Reprogramming: Lef1's Central Role

Our journey commenced with an investigation into the phenomenon of mechanical reprogramming. It has become increasingly evident that cells are remarkably plastic, with the ability to transition between distinct states based on their microenvironment (Huyghe, Trajkova, and Lavial 2023; Shen and Clairambault 2020). Traditionally, cell-state transitions have been achieved through the introduction of exogenous factors or genetic modifications (Takahashi and Yamanaka 2006; 2016). However, recent discoveries have illuminated the possibility of mechanical cues alone inducing these transitions (Engler et al. 2006; Roy et al. 2018).

In the initial chapter, we unravelled the central role of Lef1, a somatic transcription factor, in orchestrating mechanically induced fibroblast cell-state transitions. This transcription factor, previously implicated in diverse cellular contexts, e.g. stem cell renewal and epithelial mesenchymal transition (Nawshad and Hay 2003; C. Huang and Qin 2010). Through this study, it was identified as a key player in laterally confined growth-induced dedifferentiation. Through a comprehensive network analysis approach called Prize-Collecting Steiner Tree, we identified Lef1 and its potential coactivators, Atf2, and Smad4, as pivotal players. Further experiments and validations solidified Lef1's role in driving these transitions, expanding our understanding of its versatility across different cellular contexts. The complex transcriptional regulatory network also underscores the complexity of mechanotransduction and highlights the importance of multiple pathways converging to activate Lef1 during cell-state transitions induced by mechanical confinement. The interplay of these pathways not

only underscores the multifaceted nature of signalling transduction but also opens up opportunities for further research into the molecular mechanisms governing these cell state transitions.

Cellular rejuvenation through mechanical reprogramming: the role of chromatin reorganization in transcriptional regulation

Moving beyond dedifferentiation, our study introduced the concept of rejuvenation through partial reprogramming, which allows cells to regain youthful characteristics while retaining specialized functions. The traditional approach to cellular rejuvenation often necessitates complete reprogramming, a process laden with limitations, including the risk of genomic mutations and low efficiency (Abad et al. 2013; Shibata et al. 2018; Ohnishi et al. 2014). In our third chapter, we investigated the cellular properties and mechanisms underlying redifferentiation of mechanically induced reprogrammed cells.

We harnessed these partially reprogrammed cells (PRs) and redifferentiated them in the 3D collagen matrix to unveil their rejuvenation potential. The redifferentiated cells are active in extracellular matrix secretion and remodelling. Our investigations into the transcriptional profiles and chromatin structures revealed epigenetic mechanisms governing rejuvenation. A new HiC data analysis approach being developed, aiming at measuring the contact strength between Lamina associated domains (LADs) and non-LADs, provides unique insight into the chromatin organization at nuclear envelope. Combining RNAseq data with measurements of the reorganization of LADs, we identified a small lists of LAD genes associated with young cell state and their corresponding transcriptional regulators. This insight into chromatin reorganization provides a foundation for future research into the epigenetic mechanisms governing rejuvenation.

Practical Applications: Tissue Regeneration and Wound Healing

Furthermore, our research extended to a practical application and we embarked on a journey into the realm of tissue regeneration and wound healing (Atala et al. 2010;

Nourian Dehkordi et al. 2019). We employed an in vitro skin model, designed to closely mimic the physiological characteristics of young and aged skin tissues. The implantation of mechanically reprogrammed aged fibroblasts, which we previously highlighted for their rejuvenation potential, into this model revealed significant promise. This application resulted in the differentiation of fibroblasts into a rejuvenated state, marked by activated cytoskeleton and ECM secretion pathways, enhanced deposition of critical extracellular matrix (ECM) components and uniform spreading into the tissue. These results offer new horizons for tissue regeneration and wound healing, offering insights into personalized cell-based therapies for skin rejuvenation.

Methods investigated in this journey

To support research in this doctoral thesis, multiple approaches were being investigated, implemented or developed to help for the better measurement or giving new insights in the transcriptional regulation, cell state transitions, chromatin organization, etc.. For the imaging approaches, we utilized live cell imaging to measure nucleus dynamics, which reflects global chromatin compaction states and nucleus mechanical states (e.g. nucleus stiffness). High resolution confocal 3D microscope was used to study colocalization of transcription factors, coactivators and RNA polymerases. For the image analysis approaches, 3D nucleus segmentation using Otsu thresholding method and machine learning-based stardist segmentation model were tested in various sample conditions, including 2D cultured fibroblasts, lung tissue slices, 3D cell culture model using collagen gel, etc.. For giving new insights into transcriptional regulation, we extensively explored a new way of using Prize-Collection Steiner tree method on RNAseq dataset and identified several key transcriptional regulators or upstream signaling pathways important in the cell state transition processes, including reprogramming and rejuvenation.

For project specific methods, we tried a new way of measuring chromatin organization at nuclear envelope region combing HiC-seq, RNA-seq and DamID-seq data. Contact among LAD region and non-LAD region provides a unique angle of identifying the role of LAD genes in transcriptional regulation. We also implemented our lab developed nucleus morphometric features to study cellular changes in aging

and rejuvenation processes. This highlights the potential usage of nucleus DAPI image as biomarker of cell states.

Further perspectives

Elucidating Additional Mechanotransduction Pathways: While this research has identified Lef1 as a key transcription factor in mechanically induced reprogramming, there may be other yet-to-be-discovered mechanotransduction pathways. For example, in the constructed transcriptional regulatory network, several transcription factors (e.g. Maf and Mafa) and epigenetic modifiers (e.g. Hdac1) were also identified. Besides, the upstream pathways of Lef1 and other transcriptional regulators in the network have not been investigated. Apart from this, a construction of similar transcriptional regulatory network based on RNAseq data from the reprogrammed human fibroblasts will further advanced our understanding of the mechanically induced reprogramming mechanisms. Future experiments could focus on uncovering additional molecules and signaling pathways involved in this process. This could involve conducting single cell RNAseqs in ten days' lateral confinement growth induced reprogramming of human fibroblasts and utilizing other advanced omics techniques (e.g. HiC-seq) to identify novel players in mechanotransduction.

Enhancing the Efficiency of Fibroblast Rejuvenation: This work highlights the potential for rejuvenating fibroblasts through mechanical reprogramming followed by collagen embedding. To make this approach more practical for regenerative medicine, further experiments could aim to better characterized the differentiated state of the cells and optimize the efficiency of fibroblast reprogramming and rejuvenation. This might involve fine-tuning the mechanical parameters, such as confinement geometry or matrix stiffness.

Epigenetic Profiling and Manipulation: Further experiments could delve deeper into the epigenetic mechanisms underlying cellular rejuvenation. For example, one could explore the detailed changes in chromatin organization at the nuclear envelope and the role of specific histone modifications. Additionally, we can develop strategies for precisely manipulating these epigenetic marks to enhance the rejuvenation process.

This could include using CRISPR-based epigenome editing techniques (Tadić et al. 2019).

Advanced Imaging and Analysis Methods: As the field evolves, integrating advanced imaging and analysis methods will be crucial. This motivates the need for experiments with cutting-edge techniques in microscopy, genomics, and bioinformatics to gain a deeper understanding of cellular processes. For example, single-cell RNA sequencing on mechanically induced reprogramming and rejuvenation processes, super-resolution microscopy on measuring chromatin organization at the nuclear envelope region, and AI-driven image analysis for better nucleus, organelle, cytoskeleton and cell segmentation could provide valuable insights into cell state transitions.

Incorporating these perspectives into future research can propel the field of mechanobiology, transcriptional regulation, and regenerative medicine forward, offering new horizons for clinical applications and advancing our understanding of cellular plasticity.

As we stand at the crossroads of mechanobiology, transcriptional regulation, and regenerative medicine, this work sets the stage for future research and clinical applications, bringing us closer to realizing the full potential of mechanical reprogramming and rejuvenation in the realm of healthcare and longevity. The journey continues, and the possibilities are boundless.

BIBLIOGRAPHY

Abad, María, Lluc Mosteiro, Cristina Pantoja, Marta Cañamero, Teresa Rayon, Inmaculada Ors, Osvaldo Graña, et al. 2013. "Reprogramming in Vivo Produces Teratomas and iPS Cells with Totipotency Features." *Nature* 502 (7471): 340–45. https://doi.org/10.1038/nature12586.

Abdel-Sayed, Philippe, Murielle Michetti, Corinne Scaletta, Marjorie Flahaut, Nathalie Hirt-Burri, Anthony De Buys Roessingh, Wassim Raffoul, and Lee A. Applegate. 2019. "Cell Therapies for Skin Regeneration: An Overview of 40 Years of Experience in Burn Units." *Swiss Medical Weekly* 149 (19–20): 1–7. https://doi.org/10.4414/smw.2019.20079.

Abdennur, Nezar, and Leonid A Mirny. 2020. "Cooler: Scalable Storage for Hi-C Data and Other Genomically Labeled Arrays." Edited by Jonathan Wren. *Bioinformatics* 36 (1): 311–16. https://doi.org/10.1093/bioinformatics/btz540.

Abraham E, et al. 2017. "Platforms for Manufacturing Allogeneic, Autologous and iPSC Cell Therapy Products: An Industry Perspective." In *New Bioprocessing Strategies: Development and Manufacturing of Recombinant Antibodies and Proteins*.

Akkiraju, Hemanth, and Anja Nohe. 2015. "Role of Chondrocytes in Cartilage Formation, Progression of Osteoarthritis and Cartilage Regeneration." *Journal of Developmental Biology* 3 (4): 177–92. https://doi.org/10.3390/jdb3040177.

Suzi A Aleksander, James Balhoff, Seth Carbon, J Michael Cherry, Harold J Drabkin, Dustin Ebert, et al. 2023. "The Gene Ontology Knowledgebase in 2023." *Genetics* 224 (1): 1–14. https://doi.org/10.1093/genetics/iyad031.

Almeida, Filipe V., Gernot Walko, James R. McMillan, John A. McGrath, Gerhard Wiche, Asa H. Barber, and John T. Connelly. 2015. "The Cytolinker Plectin Regulates Nuclear Mechanotransduction in Keratinocytes." *Journal of Cell Science*, January, jcs.173435. https://doi.org/10.1242/jcs.173435.

Aloysius, Ajoy, Ramanuj DasGupta, and Jyotsna Dhawan. 2018. "The Transcription Factor Lef1 Switches Partners from β-Catenin to Smad3 during Muscle Stem Cell Quiescence." *Science Signaling* 11 (540): eaan3000. https://doi.org/10.1126/scisignal.aan3000.

Anders, Simon, Paul Theodor Pyl, and Wolfgang Huber. 2015. "Genome Analysis HTSeq — a Python Framework to Work with High-Throughput Sequencing Data" 31 (2): 166–69. https://doi.org/10.1093/bioinformatics/btu638.

Atala, Anthony, Darrell J. Irvine, Marsha Moses, and Sunil Shaunak. 2010. "Wound Healing Versus Regeneration: Role of the Tissue Environment in Regenerative Medicine." *MRS Bulletin* 35 (8): 597–606. https://doi.org/10.1557/mrs2010.528.

Bannister, Andrew J, and Tony Kouzarides. 2011. “Regulation of Chromatin by Histone Modifications.” *Cell Research* 21 (3): 381–95. https://doi.org/10.1038/cr.2011.22.

Barutcu, A. Rasim, Philipp G. Maass, Jordan P. Lewandowski, Catherine L. Weiner, and John L. Rinn. 2018. “A TAD Boundary Is Preserved upon Deletion of the CTCF-Rich Firre Locus.” *Nature Communications* 9 (1): 1444. https://doi.org/10.1038/s41467-018-03614-0.

Behrens, Jürgen, Jens P. von Kries, Michael Kühl, Laurakay Bruhn, Doris Wedlich, Rudolf Grosschedl, and Walter Birchmeier. 1996. “Functional Interaction of β-Catenin with the Transcription Factor LEF-1.” *Nature* 382 (6592): 638–42. https://doi.org/10.1038/382638a0.

Bershadsky, Alexander D., Nathalie Q. Balaban, and Benjamin Geiger. 2003. “Adhesion-Dependent Cell Mechanosensitivity.” *Annual Review of Cell and Developmental Biology* 19 (1): 677–95. https://doi.org/10.1146/annurev.cellbio.19.111301.153011.

Bitto, Alessandro, Takashi K Ito, Victor V Pineda, Nicolas J LeTexier, Heather Z Huang, Elissa Sutlief, Herman Tung, et al. 2016. “Transient Rapamycin Treatment Can Increase Lifespan and Healthspan in Middle-Aged Mice.” *eLife* 5 (August): e16351. https://doi.org/10.7554/eLife.16351.

Bollati, Valentina, Joel Schwartz, Robert Wright, Augusto Litonjua, Letizia Tarantini, Helen Suh, David Sparrow, Pantel Vokonas, and Andrea Baccarelli. 2009. “Decline in Genomic DNA Methylation through Aging in a Cohort of Elderly Subjects.” *Mechanisms of Ageing and Development* 130 (4): 234–39. https://doi.org/10.1016/j.mad.2008.12.003.

Brasch, Megan E., Giuseppe Passucci, Anushree C. Gulvady, Christopher E. Turner, M. Lisa Manning, and James H. Henderson. 2019. “Nuclear Position Relative to the Golgi Body and Nuclear Orientation Are Differentially Responsive Indicators of Cell Polarized Motility.” Edited by Juan Carlos Del Alamo. *PLOS ONE* 14 (2): e0211408. https://doi.org/10.1371/journal.pone.0211408.

Brockschnieder, Damian, Helena Sabanay, Dieter Riethmacher, and Elior Peles. 2006. “Ermin, a Myelinating Oligodendrocyte-Specific Protein That Regulates Cell Morphology.” *Journal of Neuroscience* 26 (3): 757–62. https://doi.org/10.1523/JNEUROSCI.4317-05.2006.

Brown, R.A., R. Prajapati, D.A. McGrouther, I.V. Yannas, and M. Eastwood. 1998. “Tensional Homeostasis in Dermal Fibroblasts: Mechanical Responses to Mechanical Loading in Three-Dimensional Substrates.” *Journal of Cellular Physiology* 175 (3): 323–32. https://doi.org/10.1002/(SICI)1097-4652(199806)175:3<323::AID-JCP10>3.0.CO;2-6.

Bueno, Franklin Rivera, and Sameer B. Shah. 2008. “Implications of Tensile Loading for the Tissue Engineering of Nerves.” *Tissue Engineering Part B: Reviews* 14 (3): 219–33. https://doi.org/10.1089/ten.teb.2008.0020.

Cai, Xiaomin, Kuei-Chun Wang, and Zhipeng Meng. 2021. “Mechanoregulation of YAP and TAZ in Cellular Homeostasis and Disease Progression.” *Frontiers in Cell and Developmental Biology* 9 (May): 673599. https://doi.org/10.3389/fcell.2021.673599.

Campello, Ricardo J. G. B., Davoud Moulavi, and Joerg Sander. 2013. “Density-Based Clustering Based on Hierarchical Density Estimates.” In *Advances in Knowledge Discovery and Data Mining*, edited by Jian Pei, Vincent S. Tseng, Longbing Cao, Hiroshi Motoda, and Guandong Xu, 7819:160–72. Lecture Notes in Computer Science. Berlin, Heidelberg: Springer Berlin Heidelberg. https://doi.org/10.1007/978-3-642-37456-2_14.

Carbon, Seth, Amelia Ireland, Christopher J Mungall, Shengqiang Shu, Brad Marshall, Suzanna Lewis, Amigo Hub, and Web Presence. 2009. “AmiGO : Online Access to Ontology and Annotation Data” 25 (2): 288–89. https://doi.org/10.1093/bioinformatics/btn615.

Chang, Wakam, Yuexia Wang, G. W. Gant Luxton, Cecilia Östlund, Howard J. Worman, and Gregg G. Gundersen. 2019. “Imbalanced Nucleocytoskeletal Connections Create Common Polarity Defects in Progeria and Physiological Aging.” *Proceedings of the National Academy of Sciences* 116 (9): 3578–83. https://doi.org/10.1073/pnas.1809683116.

Chen, Chia-Yen, Ya-Hui Chi, Rafidah Abdul Mutalif, Matthew F. Starost, Timothy G. Myers, Stasia A. Anderson, Colin L. Stewart, and Kuan-Teh Jeang. 2012. “Accumulation of the Inner Nuclear Envelope Protein Sun1 Is Pathogenic in Progeric and Dystrophic Laminopathies.” *Cell* 149 (3): 565–77. https://doi.org/10.1016/j.cell.2012.01.059.

Chen, Edward Y, Christopher M Tan, Yan Kou, Qiaonan Duan, Zichen Wang, Gabriela Meirelles, Neil R Clark, and Avi Ma’ayan. 2013. “Enrichr: Interactive and Collaborative HTML5 Gene List Enrichment Analysis Tool.” *BMC Bioinformatics* 14 (1): 128. https://doi.org/10.1186/1471-2105-14-128.

Cole, Megan A., Taihao Quan, John J. Voorhees, and Gary J. Fisher. 2018. “Extracellular Matrix Regulation of Fibroblast Function: Redefining Our Perspective on Skin Aging.” *Journal of Cell Communication and Signaling* 12 (1): 35–43. https://doi.org/10.1007/s12079-018-0459-1.

Constantinescu, Dan, Heather L. Gray, Paul J. Sammak, Gerald P. Schatten, and Antonei B. Csoka. 2006. “Lamin A/C Expression Is a Marker of Mouse and Human Embryonic Stem Cell Differentiation.” *Stem Cells* 24 (1): 177–85. https://doi.org/10.1634/stemcells.2004-0159.

Correia-Melo, Clara, Francisco Dm Marques, Rhys Anderson, Graeme Hewitt, Rachael Hewitt, John Cole, Bernadette M Carroll, et al. 2016. “Mitochondria Are Required for Pro-ageing Features of the Senescent Phenotype.” *The EMBO Journal* 35 (7): 724–42. https://doi.org/10.15252/embj.201592862.

Criscione, Steven W., Marco De Cecco, Benjamin Siranosian, Yue Zhang, Jill A. Kreiling, John M. Sedivy, and Nicola Neretti. 2016. “Reorganization of Chromosome Architecture in Replicative Cellular Senescence.” *Science Advances* 2 (2). https://doi.org/10.1126/sciadv.1500882.

Criscione, Steven W., Yee Voan Teo, and Nicola Neretti. 2016. “The Chromatin Landscape of Cellular Senescence.” *Trends in Genetics* 32 (11): 751–61. https://doi.org/10.1016/j.tig.2016.09.005.

Crisp, Melissa, and Brian Burke. 2008. “The Nuclear Envelope as an Integrator of Nuclear and Cytoplasmic Architecture.” *FEBS Letters* 582 (14): 2023–32. https://doi.org/10.1016/j.febslet.2008.05.001.

Crisp, Melissa, Qian Liu, Kyle Roux, J.B. Rattner, Catherine Shanahan, Brian Burke, Phillip D. Stahl, and Didier Hodzic. 2006. “Coupling of the Nucleus and Cytoplasm: Role of the LINC Complex.” *The Journal of Cell Biology* 172 (1): 41–53. https://doi.org/10.1083/jcb.200509124.

Csapo, Robert, Matthias Gumpenberger, and Barbara Wessner. 2020. “Skeletal Muscle Extracellular Matrix – What Do We Know About Its Composition, Regulation, and Physiological Roles? A Narrative Review.” *Frontiers in Physiology* 11 (March): 253. https://doi.org/10.3389/fphys.2020.00253.

Daniel, Cyril, Frank Traub, Saskia Sachsenmaier, Rosa Riester, Moritz Mederake, Christian Konrads, and Marina Danalache. 2023. “An Exploratory Study of Cell Stiffness as a Mechanical Label-Free Biomarker across Multiple Musculoskeletal Sarcoma Cells.” *BMC Cancer* 23 (1): 862. https://doi.org/10.1186/s12885-023-11375-3.

Dasgupta, Ishani, and Dannel McCollum. 2019. “Control of Cellular Responses to Mechanical Cues through YAP/TAZ Regulation.” *Journal of Biological Chemistry* 294 (46): 17693–706. https://doi.org/10.1074/jbc.REV119.007963.

Davidson, Patricia M., and Bruno Cadot. 2021. “Actin on and around the Nucleus.” *Trends in Cell Biology* 31 (3): 211–23. https://doi.org/10.1016/j.tcb.2020.11.009.

Delgado-Olguin, P., and F. Recillas-Targa. 2011. “Chromatin Structure of Pluripotent Stem Cells and Induced Pluripotent Stem Cells.” *Briefings in Functional Genomics* 10 (1): 37–49. https://doi.org/10.1093/bfgp/elq038.

Deng, Xiao-Yue, Hu Wang, Tao Wang, Xian-Tao Fang, Li-Li Zou, Zhi-Ying Li, and Chang-Bai Liu. 2015. “Non-Viral Methods For Generating Integration-Free, Induced Pluripotent Stem Cells.” *Current Stem Cell Research & Therapy* 10 (2): 153–58. https://doi.org/10.2174/1574888X09666140923101914.

Dewey, C. F., S. R. Bussolari, M. A. Gimbrone, and P. F. Davies. 1981. “The Dynamic Response of Vascular Endothelial Cells to Fluid Shear Stress.” *Journal of Biomechanical Engineering* 103 (3): 177–85. https://doi.org/10.1115/1.3138276.

Di, Xingpeng, Xiaoshuai Gao, Liao Peng, Jianzhong Ai, Xi Jin, Shiqian Qi, Hong Li, Kunjie Wang, and Deyi Luo. 2023. “Cellular Mechanotransduction in Health and Diseases: From Molecular Mechanism to Therapeutic Targets.” *Signal Transduction and Targeted Therapy* 8 (1): 282. https://doi.org/10.1038/s41392-023-01501-9.

Díaz, Noelia, Kai Kruse, Tabea Erdmann, Annette M. Staiger, German Ott, Georg Lenz, and Juan M. Vaquerizas. 2018. “Chromatin Conformation Analysis of Primary Patient Tissue Using a Low Input Hi-C Method.” *Nature Communications* 9 (1): 4938. https://doi.org/10.1038/s41467-018-06961-0.

Dimri, G. P., X. Lee, G. Basile, M. Acosta, G. Scott, C. Roskelley, E. E. Medrano, M. Linskens, I. Rubelj, and O. Pereira-Smith. 1995. “A Biomarker That Identifies Senescent Human Cells in Culture and in Aging Skin in Vivo.” *Proceedings of the National Academy of Sciences of the United States of America* 92 (20): 9363–67. https://doi.org/10.1073/pnas.92.20.9363.

Dinella, Jason, Maranke I. Koster, and Peter J. Koch. 2014. “Use of Induced Pluripotent Stem Cells in Dermatological Research.” *The Journal of Investigative Dermatology* 134 (8): 1–5. https://doi.org/10.1038/jid.2014.238.

Dolega, Monika E, Sylvain Monnier, Benjamin Brunel, Jean-François Joanny, Pierre Recho, and Giovanni Cappello. 2021. “Extracellular Matrix in Multicellular Aggregates Acts as a Pressure Sensor Controlling Cell Proliferation and Motility.” *eLife* 10 (March): e63258. https://doi.org/10.7554/eLife.63258.

Downing, Timothy L., Jennifer Soto, Constant Morez, Timothee Houssin, Ashley Fritz, Falei Yuan, Julia Chu, Shyam Patel, David V. Schaffer, and Song Li. 2013. “Biophysical Regulation of Epigenetic State and Cell Reprogramming.” *Nature Materials* 12 (12): 1154–62. https://doi.org/10.1038/nmat3777.

Dupont, Sirio, Leonardo Morsut, Mariaceleste Aragona, Elena Enzo, Stefano Giulitti, Michelangelo Cordenonsi, Francesca Zanconato, et al. 2011. “Role of YAP/TAZ in Mechanotransduction.” *Nature* 474 (7350): 179–83. https://doi.org/10.1038/nature10137.

Eckersley-Maslin, Melanie A., Jan H. Bergmann, Zsolt Lazar, and David L. Spector. 2013. “Lamin A/C Is Expressed in Pluripotent Mouse Embryonic Stem Cells.” *Nucleus* 4 (1): 53–60. https://doi.org/10.4161/nucl.23384.

Engler, Adam J., Shamik Sen, H. Lee Sweeney, and Dennis E. Discher. 2006. “Matrix Elasticity Directs Stem Cell Lineage Specification.” *Cell* 126 (4): 677–89. https://doi.org/10.1016/j.cell.2006.06.044.

Even-Ram, Sharona, Vira Artym, and Kenneth M. Yamada. 2006. “Matrix Control of Stem Cell Fate.” *Cell* 126 (4): 645–47. https://doi.org/10.1016/j.cell.2006.08.008.

Fang, Shuo, Ming Liu, Lei Li, Fei-Fei Zhang, Yun Li, Qian Yan, Yu-Zhu Cui, Ying-Hui Zhu, Yun-Fei Yuan, and Xin-Yuan Guan. 2019. “Lymphoid Enhancer-Binding Factor-1 Promotes Stemness and Poor Differentiation of Hepatocellular Carcinoma by Directly Activating the NOTCH Pathway.” *Oncogene* 38 (21): 4061–74. https://doi.org/10.1038/s41388-019-0704-y.

Frantz, Christian, Kathleen M. Stewart, and Valerie M. Weaver. 2010. “The Extracellular Matrix at a Glance.” *Journal of Cell Science* 123 (24): 4195–4200. https://doi.org/10.1242/jcs.023820.

Franze, Kristian, Paul A. Janmey, and Jochen Guck. 2013. “Mechanics in Neuronal Development and Repair.” *Annual Review of Biomedical Engineering* 15 (1): 227–51. https://doi.org/10.1146/annurev-bioeng-071811-150045.

Freitas-Rodríguez, Sandra, Alicia R. Folgueras, and Carlos López-Otín. 2017. “The Role of Matrix Metalloproteinases in Aging: Tissue Remodeling and Beyond.” *Biochimica et Biophysica Acta - Molecular Cell Research* 1864 (11): 2015–25. https://doi.org/10.1016/j.bbamcr.2017.05.007.

Gaspar-Maia, Alexandre, Adi Alajem, Eran Meshorer, and Miguel Ramalho-Santos. 2011. “Open Chromatin in Pluripotency and Reprogramming.” *Nature Reviews. Molecular Cell Biology* 12 (1): 36–47. https://doi.org/10.1038/nrm3036.

Ghosh, Zhumur, Mei Huang, Shijun Hu, Kitchener D. Wilson, Devaveena Dey, and Joseph C. Wu. 2011. “Dissecting the Oncogenic and Tumorigenic Potential of Differentiated Human Induced Pluripotent Stem Cells and Human Embryonic Stem Cells.” *Cancer Research* 71 (14): 5030–39. https://doi.org/10.1158/0008-5472.CAN-10-4402.

Giese, K., J. Cox, and R. Grosschedl. 1992. “The HMG Domain of Lymphoid Enhancer Factor 1 Bends DNA and Facilitates Assembly of Functional Nucleoprotein Structures.” *Cell* 69 (1): 185–95. https://doi.org/10.1016/0092-8674(92)90129-z.

Gordon, Emma, Lilian Schimmel, and Maike Frye. 2020. “The Importance of Mechanical Forces for in Vitro Endothelial Cell Biology.” *Frontiers in Physiology* 11 (June): 684. https://doi.org/10.3389/fphys.2020.00684.

Gracia, Mélanie, Sophie Theis, Amsha Proag, Guillaume Gay, Corinne Benassayag, and Magali Suzanne. 2019. “Mechanical Impact of Epithelial−mesenchymal Transition on Epithelial

Morphogenesis in Drosophila." *Nature Communications* 10 (1): 2951. https://doi.org/10.1038/s41467-019-10720-0.

Grether-Beck, Susanne, Alessandra Marini, Thomas Jaenicke, Petra Goessens-Rück, Kevin John McElwee, Rolf Hoffmann, and Jean Krutmann. 2020. "Autologous Cell Therapy for Aged Human Skin: A Randomized, Placebo-Controlled, Phase-I Study." *Skin Pharmacology and Physiology* 33 (1): 9–16. https://doi.org/10.1159/000502240.

Griffin, Donald R., Maani M. Archang, Chen Hsiang Kuan, Westbrook M. Weaver, Jason S. Weinstein, An Chieh Feng, Amber Ruccia, et al. 2021. "Activating an Adaptive Immune Response from a Hydrogel Scaffold Imparts Regenerative Wound Healing." *Nature Materials* 20 (4): 560–69. https://doi.org/10.1038/s41563-020-00844-w.

Grumolato, Luca, Guizhong Liu, Tomomi Haremaki, Sathish Kumar Mungamuri, Phyllus Mong, Gal Akiri, Pablo Lopez-Bergami, et al. 2013. "β-Catenin-Independent Activation of TCF1/LEF1 in Human Hematopoietic Tumor Cells through Interaction with ATF2 Transcription Factors." *PLoS Genetics* 9 (8): e1003603. https://doi.org/10.1371/journal.pgen.1003603.

Guelen, Lars, Ludo Pagie, Emilie Brasset, Wouter Meuleman, Marius B. Faza, Wendy Talhout, Bert H. Eussen, et al. 2008. "Domain Organization of Human Chromosomes Revealed by Mapping of Nuclear Lamina Interactions." *Nature* 453 (7197): 948–51. https://doi.org/10.1038/nature06947.

Guenou, Hind, Xavier Nissan, Fernando Larcher, Jessica Feteira, Gilles Lemaitre, Manoubia Saidani, Marcela Del Rio, et al. 2009. "Human Embryonic Stem-Cell Derivatives for Full Reconstruction of the Pluristratified Epidermis: A Preclinical Study." *The Lancet* 374 (9703): 1745–53. https://doi.org/10.1016/S0140-6736(09)61496-3.

Gunin, G., N. K. Kornilova, V. V. Petrov, and O. V. Vasilyeva. 2011. "Age Changes in the Number and Proliferation of Fibroblasts in the Human Skin." *Advances in Gerontology* 1 (4): 299–303. https://doi.org/10.1134/S2079057011040059.

Guo, S., and L.A. DiPietro. 2010. "Factors Affecting Wound Healing." *Journal of Dental Research* 89 (3): 219–29. https://doi.org/10.1177/0022034509359125.

Gurdon, J. B. 1962. "Adult Frogs Derived from the Nuclei of Single Somatic Cells." *Developmental Biology* 4 (April): 256–73. https://doi.org/10.1016/0012-1606(62)90043-x.

Hall, Alan. 1998. "Rho GTPases and the Actin Cytoskeleton." *Science* 279 (5350): 509–14. https://doi.org/10.1126/science.279.5350.509.

Hardman, Katie, Adrian Goldman, and Christos Pliotas. 2023. "Membrane Force Reception: Mechanosensation in G Protein-Coupled Receptors and Tools to Address It." *Current Opinion in Physiology* 35 (October): 100689. https://doi.org/10.1016/j.cophys.2023.100689.

Harn, Hans I-Chen, Rei Ogawa, Chao-Kai Hsu, Michael W. Hughes, Ming-Jer Tang, and Cheng-Ming Chuong. 2019. “The Tension Biology of Wound Healing.” *Experimental Dermatology* 28 (4): 464–71. https://doi.org/10.1111/exd.13460.

Hickey, Ryan, and Andrew E. Pelling. 2017. “The Rotation of Mouse Myoblast Nuclei Is Dependent on Substrate Elasticity: HICKEY and PELLING.” *Cytoskeleton* 74 (4): 184–94. https://doi.org/10.1002/cm.21357.

Hill, Caroline S., Judy Wynne, and Richard Treisman. 1995. “The Rho Family GTPases RhoA, Racl , and CDC42Hsregulate Transcriptional Activation by SRF.” *Cell* 81 (7): 1159–70. https://doi.org/10.1016/S0092-8674(05)80020-0.

Ho, Ritchie, Bernadett Papp, Jackson A. Hoffman, Bradley J. Merrill, and Kathrin Plath. 2013. “Stage-Specific Regulation of Reprogramming to Induced Pluripotent Stem Cells by Wnt Signaling and T Cell Factor Proteins.” *Cell Reports* 3 (6): 2113–26. https://doi.org/10.1016/j.celrep.2013.05.015.

Hou, P., Y. Li, X. Zhang, C. Liu, J. Guan, H. Li, T. Zhao, et al. 2013. “Pluripotent Stem Cells Induced from Mouse Somatic Cells by Small-Molecule Compounds.” *Science* 341 (6146): 651–54. https://doi.org/10.1126/science.1239278.

Howard, Sara, Tom Deroo, Yasuyuki Fujita, and Nobue Itasaki. 2011. “A Positive Role of Cadherin in Wnt/β-Catenin Signalling during Epithelial-Mesenchymal Transition.” Edited by Carl-Philipp Heisenberg. *PLoS ONE* 6 (8): e23899. https://doi.org/10.1371/journal.pone.0023899.

Hsu, S. C., J. Galceran, and R. Grosschedl. 1998. “Modulation of Transcriptional Regulation by LEF-1 in Response to Wnt-1 Signaling and Association with Beta-Catenin.” *Molecular and Cellular Biology* 18 (8): 4807–18. https://doi.org/10.1128/MCB.18.8.4807.

Huang, Chen, and Dajiang Qin. 2010. “Role of Lef1 in Sustaining Self-Renewal in Mouse Embryonic Stem Cells.” *Journal of Genetics and Genomics* 37 (7): 441–49. https://doi.org/10.1016/S1673-8527(09)60063-1.

Huang, Da Wei, Brad T Sherman, and Richard A Lempicki. 2008. “Systematic and Integrative Analysis of Large Gene Lists Using DAVID Bioinformatics Resources.” *Nature Protocols* 4 (1): 44–57. https://doi.org/10.1038/nprot.2008.211.

Huang, S.-s. C., and E. Fraenkel. 2009. “Integrating Proteomic, Transcriptional, and Interactome Data Reveals Hidden Components of Signaling and Regulatory Networks.” *Science Signaling* 2 (81): ra40–ra40. https://doi.org/10.1126/scisignal.2000350.

Huyghe, Aurélia, Aneta Trajkova, and Fabrice Lavial. 2023. “Cellular Plasticity in Reprogramming, Rejuvenation and Tumorigenesis: A Pioneer TF Perspective.” *Trends in Cell Biology*, August, S0962892423001575. https://doi.org/10.1016/j.tcb.2023.07.013.

Ibañez-Solé, Olga, Alex M Ascensión, Marcos J Araúzo-Bravo, and Ander Izeta. 2022. “Lack of Evidence for Increased Transcriptional Noise in Aged Tissues.” *eLife* 11 (December): e80380. https://doi.org/10.7554/eLife.80380.

Jaalouk, Diana E., and Jan Lammerding. 2009. “Mechanotransduction Gone Awry.” *Nature Reviews Molecular Cell Biology* 10 (1): 63–73. https://doi.org/10.1038/nrm2597.

Jain, N., K. V. Iyer, A. Kumar, and G. V. Shivashankar. 2013. “Cell Geometric Constraints Induce Modular Gene-Expression Patterns via Redistribution of HDAC3 Regulated by Actomyosin Contractility.” *Proceedings of the National Academy of Sciences* 110 (28): 11349–54. https://doi.org/10.1073/pnas.1300801110.

Jiang, Kuan, Su Bin Lim, Jingwei Xiao, Doorgesh Sharma Jokhun, Menglin Shang, Xiao Song, Pan Zhang, et al. 2023. “Deleterious Mechanical Deformation Selects Mechanoresilient Cancer Cells with Enhanced Proliferation and Chemoresistance.” *Advanced Science* 10 (22): 2201663. https://doi.org/10.1002/advs.202201663.

Jing, Junjun, Zhuoxuan Wu, Jiahe Wang, Guowen Luo, Hengyi Lin, Yi Fan, and Chenchen Zhou. 2023. “Hedgehog Signaling in Tissue Homeostasis, Cancers, and Targeted Therapies.” *Signal Transduction and Targeted Therapy* 8 (1): 315. https://doi.org/10.1038/s41392-023-01559-5.

Joshi, Onkar, Shuang-Yin Wang, Tatyana Kuznetsova, Yaser Atlasi, Tianran Peng, Pierre J. Fabre, Ehsan Habibi, et al. 2015. “Dynamic Reorganization of Extremely Long-Range Promoter-Promoter Interactions between Two States of Pluripotency.” *Cell Stem Cell* 17 (6): 748–57. https://doi.org/10.1016/j.stem.2015.11.010.

Kang, Yibin, Chang-Rung Chen, and Joan Massagué. 2003. “A Self-Enabling TGFβ Response Coupled to Stress Signaling.” *Molecular Cell* 11 (4): 915–26. https://doi.org/10.1016/S1097-2765(03)00109-6.

Karolchik, D. 2004. “The UCSC Table Browser Data Retrieval Tool.” *Nucleic Acids Research* 32 (90001): 493D – 496. https://doi.org/10.1093/nar/gkh103.

Kim, Chang Gun, Il-Yup Chung, Yoongho Lim, Young Han Lee, and Soon Young Shin. 2011. “A Tcf/Lef Element within the Enhancer Region of the Human NANOG Gene Plays a Role in Promoter Activation.” *Biochemical and Biophysical Research Communications* 410 (3): 637–42. https://doi.org/10.1016/j.bbrc.2011.06.044.

Kim, Daehwan, Joseph M. Paggi, Chanhee Park, Christopher Bennett, and Steven L. Salzberg. 2019. “Graph-Based Genome Alignment and Genotyping with HISAT2 and HISAT-Genotype.” *Nature Biotechnology* 37 (8): 907–15. https://doi.org/10.1038/s41587-019-0201-4.

Kim, Daehwan, Geo Pertea, Cole Trapnell, Harold Pimentel, Ryan Kelley, and Steven L Salzberg. 2013. "TopHat2: Accurate Alignment of Transcriptomes in the Presence of Insertions, Deletions and Gene Fusions." *Genome Biology* 14 (4): R36. https://doi.org/10.1186/gb-2013-14-4-r36.

Kim, Do Hyung, Tiaosi Xing, Zhibin Yang, Ronald Dudek, Qun Lu, and Yan-Hua Chen. 2017. "Epithelial Mesenchymal Transition in Embryonic Development, Tissue Repair and Cancer: A Comprehensive Overview." *Journal of Clinical Medicine* 7 (1): 1. https://doi.org/10.3390/jcm7010001.

Kim, Dong-Hwee, and Denis Wirtz. 2015. "Cytoskeletal Tension Induces the Polarized Architecture of the Nucleus." *Biomaterials* 48 (April): 161–72. https://doi.org/10.1016/j.biomaterials.2015.01.023.

Kimbrel, Erin A., and Robert Lanza. 2015. "Current Status of Pluripotent Stem Cells: Moving the First Therapies to the Clinic." *Nature Reviews. Drug Discovery* 14 (10): 681–92. https://doi.org/10.1038/nrd4738.

Ladiges, Warren, Holly Van Remmen, Randy Strong, Yuji Ikeno, Piper Treuting, Peter Rabinovitch, and Arlan Richardson. 2009. "Lifespan Extension in Genetically Modified Mice." *Aging Cell* 8 (4): 346–52. https://doi.org/10.1111/j.1474-9726.2009.00491.x.

Langevin, Helene M., Kirsten N. Storch, Robert R. Snapp, Nicole A. Bouffard, Gary J. Badger, Alan K. Howe, and Douglas J. Taatjes. 2010. "Tissue Stretch Induces Nuclear Remodeling in Connective Tissue Fibroblasts." *Histochemistry and Cell Biology* 133 (4): 405–15. https://doi.org/10.1007/s00418-010-0680-3.

Laufer, M., C. Ashkenazi, D. Katz, and M. Wolman. 1974. "Orientation of Collagen in Wound Healing." *British Journal of Experimental Pathology* 55 (3): 233–36.

Lee, Han-Woong, Maria A. Blasco, Geoffrey J. Gottlieb, James W. Horner, Carol W. Greider, and Ronald A. DePinho. 1998. "Essential Role of Mouse Telomerase in Highly Proliferative Organs." *Nature* 392 (6676): 569–74. https://doi.org/10.1038/33345.

Lee, Yaelim, and G. V. Shivashankar. 2020. "Analysis of Transcriptional Modules during Human Fibroblast Ageing." *Scientific Reports* 10 (1): 19086. https://doi.org/10.1038/s41598-020-76117-y.

Lemke, Sandra B., and Frank Schnorrer. 2017. "Mechanical Forces during Muscle Development." *Mechanisms of Development* 144 (April): 92–101. https://doi.org/10.1016/j.mod.2016.11.003.

Li, Heng, and Richard Durbin. 2009. "Fast and Accurate Short Read Alignment with Burrows–Wheeler Transform." *Bioinformatics* 25 (14): 1754–60. https://doi.org/10.1093/bioinformatics/btp324.

Li, Honghu, Qian Luo, Wei Shan, Shuyang Cai, Ruxiu Tie, Yulin Xu, Yu Lin, Pengxu Qian, and He Huang. 2021. “Biomechanical Cues as Master Regulators of Hematopoietic Stem Cell Fate.” *Cellular and Molecular Life Sciences* 78 (16): 5881–5902. https://doi.org/10.1007/s00018-021-03882-y.

Li, Mansheng, Xiao Li, Binghui Liu, Luye Lv, Wenjuan Wang, Dunqin Gao, Qiyu Zhang, et al. 2021. “Time-Resolved Extracellular Matrix Atlas of the Developing Human Skin Dermis.” *Frontiers in Cell and Developmental Biology* 9 (November): 1–12. https://doi.org/10.3389/fcell.2021.783456.

Li, Xuefei, Rajesh Balagam, Ting-Fang He, Peter P. Lee, Oleg A. Igoshin, and Herbert Levine. 2017. “On the Mechanism of Long-Range Orientational Order of Fibroblasts.” *Proceedings of the National Academy of Sciences* 114 (34): 8974–79. https://doi.org/10.1073/pnas.1707210114.

Lim, S. Kyun, and F. Michael Hoffmann. 2006. “Smad4 Cooperates with Lymphoid Enhancer-Binding Factor 1/T Cell-Specific Factor to Increase c-Myc Expression in the Absence of TGF-Beta Signaling.” *Proceedings of the National Academy of Sciences of the United States of America* 103 (49): 18580–85. https://doi.org/10.1073/pnas.0604773103.

Liu, Jiaqi, Qing Xiao, Jiani Xiao, Chenxi Niu, Yuanyuan Li, Xiaojun Zhang, Zhengwei Zhou, Guang Shu, and Gang Yin. 2022. “Wnt/β-Catenin Signalling: Function, Biological Mechanisms, and Therapeutic Opportunities.” *Signal Transduction and Targeted Therapy* 7 (1): 3. https://doi.org/10.1038/s41392-021-00762-6.

Lombardi, Maria Lucia, and Jan Lammerding. 2010. “Altered Mechanical Properties of the Nucleus in Disease.” In *Methods in Cell Biology*, 98:121–41. Elsevier. https://doi.org/10.1016/S0091-679X(10)98006-0.

López-Otín, Carlos, Maria A. Blasco, Linda Partridge, Manuel Serrano, and Guido Kroemer. 2013. “The Hallmarks of Aging.” *Cell* 153 (6). https://doi.org/10.1016/j.cell.2013.05.039.

———. 2023. “Hallmarks of Aging: An Expanding Universe.” *Cell* 186 (2): 243–78. https://doi.org/10.1016/j.cell.2022.11.001.

Love, Michael I., Wolfgang Huber, and Simon Anders. 2014. “Moderated Estimation of Fold Change and Dispersion for RNA-Seq Data with DESeq2.” *Genome Biology* 15 (12): 1–21. https://doi.org/10.1186/s13059-014-0550-8.

Lüke, Yvonne, Hafida Zaim, Iakowos Karakesisoglou, Verena M. Jaeger, Lorenz Sellin, Wenshu Lu, Maria Schneider, et al. 2008. “Nesprin-2 Giant (NUANCE) Maintains Nuclear Envelope Architecture and Composition in Skin.” *Journal of Cell Science* 121 (11): 1887–98. https://doi.org/10.1242/jcs.019075.

Makhija, Ekta, K Iyer, Shefali Talwar, and G Shivashankar. 2014. “Probing Chromatin Structure and Dynamics Using Fluorescence Anisotropy Imaging.” In *Handbook of Imaging in Biological Mechanics*, edited by Corey Neu and Guy Genin, 391–400. CRC Press. https://doi.org/10.1201/b17566-42.

Maninová, Miloslava, Zuzana Klímová, J. Thomas Parsons, Michael J. Weber, Marcin P. Iwanicki, and Tomáš Vomastek. 2013. “The Reorientation of Cell Nucleus Promotes the Establishment of Front–Rear Polarity in Migrating Fibroblasts.” *Journal of Molecular Biology* 425 (11): 2039–55. https://doi.org/10.1016/j.jmb.2013.02.034.

Martin, Fergal J, M Ridwan Amode, Alisha Aneja, Olanrewaju Austine-Orimoloye, Andrey G Azov, If Barnes, Arne Becker, et al. 2023. “Ensembl 2023.” *Nucleic Acids Research* 51 (D1): D933–41. https://doi.org/10.1093/nar/gkac958.

McInnes, Leland, John Healy, and Steve Astels. 2017. “Hdbscan: Hierarchical Density Based Clustering.” *The Journal of Open Source Software* 2 (11): 205. https://doi.org/10.21105/joss.00205.

Meinke, Peter, Elisabetta Mattioli, Farhana Haque, Susumu Antoku, Marta Columbaro, Kees R. Straatman, Howard J. Worman, et al. 2014. “Muscular Dystrophy-Associated SUN1 and SUN2 Variants Disrupt Nuclear-Cytoskeletal Connections and Myonuclear Organization.” Edited by Gregory A. Cox. *PLoS Genetics* 10 (9): e1004605. https://doi.org/10.1371/journal.pgen.1004605.

Meiss, Richard A. 2000. “Mechanics of Smooth Muscle.” In *Advances in Organ Biology*, 8:1–48. Elsevier. https://doi.org/10.1016/S1569-2590(00)08002-2.

Meng, Guofeng, Hong Xu, Dong Lu, Shensuo Li, Zhenzhen Zhao, Haohao Li, and Weidong Zhang. 2023. “Three-Dimensional Chromatin Architecture Datasets for Aging and Alzheimer’s Disease.” *Scientific Data* 10 (1): 51. https://doi.org/10.1038/s41597-023-01948-z.

Mi, Huaiyu, Anushya Muruganujan, Xiaosong Huang, Dustin Ebert, Caitlin Mills, Xinyu Guo, and Paul D. Thomas. 2019. “Protocol Update for Large-Scale Genome and Gene Function Analysis with the PANTHER Classification System (v.14.0).” *Nature Protocols* 14 (3): 703–21. https://doi.org/10.1038/s41596-019-0128-8.

Miard, Stéphanie, Luce Dombrowski, Sophie Carter, Louise Boivin, and Frédéric Picard. 2009. “Aging Alters PPARgamma in Rodent and Human Adipose Tissue by Modulating the Balance in Steroid Receptor Coactivator-1.” *Aging Cell* 8 (4): 449–59. https://doi.org/10.1111/j.1474-9726.2009.00490.x.

Miralles, Francesc, Guido Posern, Alexia-Ileana Zaromytidou, and Richard Treisman. 2003. “Actin Dynamics Control SRF Activity by Regulation of Its Coactivator MAL.” *Cell* 113 (3): 329–42. https://doi.org/10.1016/S0092-8674(03)00278-2.

Mishra, Pankaj K., Mark Palma, Bonnie Buechel, Jeffrey Moore, Viralkumar Davra, Niansheng Chu, Ariel Millman, et al. 2019. “Sterile Particle-Induced Inflammation Is Mediated by Macrophages Releasing IL-33 through a Bruton’s Tyrosine Kinase-Dependent Pathway.” *Nature Materials* 18 (3): 289–97. https://doi.org/10.1038/s41563-018-0271-6.

Mitra, Aninda, Saradha Venkatachalapathy, Prasuna Ratna, Yejun Wang, Doorgesh Sharma Jokhun, and G. V. Shivashankar. 2017. “Cell Geometry Dictates TNFα-Induced Genome Response.” *Proceedings of the National Academy of Sciences of the United States of America* 114 (20): E3882–91. https://doi.org/10.1073/pnas.1618007114.

Momtazi-Borojeni, Amir Abbas, Faezeh Ghasemi, Amirreza Hesari, Muhammed Majeed, Michele Caraglia, and Amirhossein Sahebkar. 2018. “Gene Ontology: Tool for the Unification of Biology.” *Nature Genetics* 24 (19): 2121–28. https://doi.org/10.2174/1381612824666180522105202.

Morita, Tsuyoshi, and Ken’ichiro Hayashi. 2013. “G-Actin Sequestering Protein Thymosin-B4 Regulates the Activity of Myocardin-Related Transcription Factor.” *Biochemical and Biophysical Research Communications* 437 (3): 331–35. https://doi.org/10.1016/j.bbrc.2013.06.069.

Mroß, Carmen, Marija Marko, Martina Munck, Gernot Glöckner, Susanne Motameny, Janine Altmüller, Angelika A. Noegel, Ludwig Eichinger, Vivek S. Peche, and Sascha Neumann. 2018. “Depletion of Nesprin-2 Is Associated with an Embryonic Lethal Phenotype in Mice.” *Nucleus* 9 (1): 503–15. https://doi.org/10.1080/19491034.2018.1523664.

Nakazawa, Naotaka, and Mineko Kengaku. 2020. “Mechanical Regulation of Nuclear Translocation in Migratory Neurons.” *Frontiers in Cell and Developmental Biology* 8 (March): 150. https://doi.org/10.3389/fcell.2020.00150.

Nava, Michele M., Yekaterina A. Miroshnikova, Leah C. Biggs, Daniel B. Whitefield, Franziska Metge, Jorge Boucas, Helena Vihinen, et al. 2020. “Heterochromatin-Driven Nuclear Softening Protects the Genome against Mechanical Stress-Induced Damage.” *Cell* 181 (4): 800-817.e22. https://doi.org/10.1016/j.cell.2020.03.052.

Nawshad, Ali, and Elizabeth D. Hay. 2003. “TGFbeta3 Signaling Activates Transcription of the LEF1 Gene to Induce Epithelial Mesenchymal Transformation during Mouse Palate Development.” *The Journal of Cell Biology* 163 (6): 1291–1301. https://doi.org/10.1083/jcb.200306024.

Németh, Zoltán H., Edwin A. Deitch, Marson T. Davidson, Csaba Szabó, E. Sylvester Vizi, and György Haskó. 2004. “Disruption of the Actin Cytoskeleton Results in Nuclear factor-κB Activation and Inflammatory Mediator Production in Cultured Human Intestinal Epithelial Cells.” *Journal of Cellular Physiology* 200 (1): 71–81. https://doi.org/10.1002/jcp.10477.

Nourian Dehkordi, Azar, Fatemeh Mirahmadi Babaheydari, Mohammad Chehelgerdi, and Shiva Raeisi Dehkordi. 2019. “Skin Tissue Engineering: Wound Healing Based on Stem-Cell-Based Therapeutic Strategies.” *Stem Cell Research & Therapy* 10 (1): 111. https://doi.org/10.1186/s13287-019-1212-2.

Ocampo, Alejandro, Pradeep Reddy, Paloma Martinez-Redondo, Aida Platero-Luengo, Fumiyuki Hatanaka, Tomoaki Hishida, Mo Li, et al. 2016. “In Vivo Amelioration of Age-Associated Hallmarks by Partial Reprogramming.” *Cell* 167 (7): 1719-1733.e12. https://doi.org/10.1016/j.cell.2016.11.052.

Ohnishi, Kotaro, Katsunori Semi, Takuya Yamamoto, Masahito Shimizu, Akito Tanaka, Kanae Mitsunaga, Keisuke Okita, et al. 2014. “Premature Termination of Reprogramming in Vivo Leads to Cancer Development through Altered Epigenetic Regulation.” *Cell* 156 (4): 663–77. https://doi.org/10.1016/j.cell.2014.01.005.

Park, Julie E., and Adrian Barbul. 2004. “Understanding the Role of Immune Regulation in Wound Healing.” *American Journal of Surgery* 187 (5 SUPPL. 1): S11–16. https://doi.org/10.1016/S0002-9610(03)00296-4.

Patteson, Alison E., Amir Vahabikashi, Katarzyna Pogoda, Stephen A. Adam, Kalpana Mandal, Mark Kittisopikul, Suganya Sivagurunathan, Anne Goldman, Robert D. Goldman, and Paul A. Janmey. 2019. “Vimentin Protects Cells against Nuclear Rupture and DNA Damage during Migration.” *Journal of Cell Biology* 218 (12): 4079–92. https://doi.org/10.1083/jcb.201902046.

Pei, Duanqing, Xiaodong Shu, Ama Gassama-Diagne, and Jean Paul Thiery. 2019. “Mesenchymal–Epithelial Transition in Development and Reprogramming.” *Nature Cell Biology* 21 (1): 44–53. https://doi.org/10.1038/s41556-018-0195-z.

Phan, Quan M, Gracelyn M Fine, Lucia Salz, Gerardo G Herrera, Ben Wildman, Iwona M Driskell, and Ryan R Driskell. 2020. “Lef1 Expression in Fibroblasts Maintains Developmental Potential in Adult Skin to Regenerate Wounds.” *eLife* 9 (September): e60066. https://doi.org/10.7554/eLife.60066.

Phillip, Jude M., Ivie Aifuwa, Jeremy Walston, and Denis Wirtz. 2015. “The Mechanobiology of Aging.” *Annual Review of Biomedical Engineering* 17: 113–41. https://doi.org/10.1146/annurev-bioeng-071114-040829.

Prasad, Ashok, and Elaheh Alizadeh. 2019. “Cell Form and Function: Interpreting and Controlling the Shape of Adherent Cells.” *Trends in Biotechnology* 37 (4): 347–57. https://doi.org/10.1016/j.tibtech.2018.09.007.

Przybyla, Laralynne, Jonathon M. Muncie, and Valerie M. Weaver. 2016. “Mechanical Control of Epithelial-to-Mesenchymal Transitions in Development and Cancer.” *Annual Review of Cell and Developmental Biology* 32 (1): 527–54. https://doi.org/10.1146/annurev-cellbio-111315-125150.

Puckelwartz, Megan J., Eric J. Kessler, Gene Kim, Megan M. DeWitt, Yuan Zhang, Judy U. Earley, Frederic F.S. Depreux, et al. 2010. “Nesprin-1 Mutations in Human and Murine Cardiomyopathy.” *Journal of Molecular and Cellular Cardiology* 48 (4): 600–608. https://doi.org/10.1016/j.yjmcc.2009.11.006.

Rice, A J, E Cortes, D Lachowski, B C H Cheung, S A Karim, J P Morton, and A Del Río Hernández. 2017. “Matrix Stiffness Induces Epithelial–Mesenchymal Transition and Promotes Chemoresistance in Pancreatic Cancer Cells.” *Oncogenesis* 6 (7): e352–e352. https://doi.org/10.1038/oncsis.2017.54.

Richardson, William J., and Jeffrey W. Holmes. 2016. “Emergence of Collagen Orientation Heterogeneity in Healing Infarcts and an Agent-Based Model.” *Biophysical Journal* 110 (10): 2266–77. https://doi.org/10.1016/j.bpj.2016.04.014.

Robin, Jérôme D., and Frédérique Magdinier. 2016. “Physiological and Pathological Aging Affects Chromatin Dynamics, Structure and Function at the Nuclear Edge.” *Frontiers in Genetics* 7 (August). https://doi.org/10.3389/fgene.2016.00153.

Rockey, Don C., Nate Weymouth, and Zengdun Shi. 2013. “Smooth Muscle α Actin (Acta2) and Myofibroblast Function during Hepatic Wound Healing.” *PloS One* 8 (10). https://doi.org/10.1371/journal.pone.0077166.

Rodríguez Cruz, Pedro M., Judith Cossins, David Beeson, and Angela Vincent. 2020. “The Neuromuscular Junction in Health and Disease: Molecular Mechanisms Governing Synaptic Formation and Homeostasis.” *Frontiers in Molecular Neuroscience* 13 (December): 610964. https://doi.org/10.3389/fnmol.2020.610964.

Rossi, Derrick J., David Bryder, Jun Seita, Andre Nussenzweig, Jan Hoeijmakers, and Irving L. Weissman. 2007. “Deficiencies in DNA Damage Repair Limit the Function of Haematopoietic Stem Cells with Age.” *Nature* 447 (7145): 725–29. https://doi.org/10.1038/nature05862.

Rouillard, Andrew D., Gregory W. Gundersen, Nicolas F. Fernandez, Zichen Wang, Caroline D. Monteiro, Michael G. McDermott, and Avi Ma’ayan. 2016. “The Harmonizome: A Collection

of Processed Datasets Gathered to Serve and Mine Knowledge about Genes and Proteins." *Database* 2016: baw100. https://doi.org/10.1093/database/baw100.

Rowat, A.C., J. Lammerding, and J.H. Ipsen. 2006. "Mechanical Properties of the Cell Nucleus and the Effect of Emerin Deficiency." *Biophysical Journal* 91 (12): 4649–64. https://doi.org/10.1529/biophysj.106.086454.

Roy, Bibhas, Saradha Venkatachalapathy, Prasuna Ratna, Yejun Wang, Doorgesh Sharma Jokhun, Mallika Nagarajan, and G. V. Shivashankar. 2018. "Laterally Confined Growth of Cells Induces Nuclear Reprogramming in the Absence of Exogenous Biochemical Factors." *Proceedings of the National Academy of Sciences* 115 (21): E4741–50. https://doi.org/10.1073/pnas.1714770115.

Roy, Bibhas, Luezhen Yuan, Yaelim Lee, Aradhana Bharti, Aninda Mitra, and G. V. Shivashankar. 2020. "Fibroblast Rejuvenation by Mechanical Reprogramming and Redifferentiation." *Proceedings of the National Academy of Sciences of the United States of America* 117 (19): 10131–41. https://doi.org/10.1073/pnas.1911497117.

Salazar, Valerie S., Laura W. Gamer, and Vicki Rosen. 2016. "BMP Signalling in Skeletal Development, Disease and Repair." *Nature Reviews Endocrinology* 12 (4): 203–21. https://doi.org/10.1038/nrendo.2016.12.

Schakenraad, Koen, Jeremy Ernst, Wim Pomp, Erik H. J. Danen, Roeland M. H. Merks, Thomas Schmidt, and Luca Giomi. 2020. "Mechanical Interplay between Cell Shape and Actin Cytoskeleton Organization." *Soft Matter* 16 (27): 6328–43. https://doi.org/10.1039/D0SM00492H.

Schiebinger, Geoffrey, Jian Shu, Marcin Tabaka, Brian Cleary, Vidya Subramanian, Aryeh Solomon, Joshua Gould, et al. 2019. "Optimal-Transport Analysis of Single-Cell Gene Expression Identifies Developmental Trajectories in Reprogramming." *Cell* 176 (4): 928-943.e22. https://doi.org/10.1016/j.cell.2019.01.006.

Schiffhauer, Eric S., and Douglas N. Robinson. 2017. "Mechanochemical Signaling Directs Cell-Shape Change." *Biophysical Journal* 112 (2): 207–14. https://doi.org/10.1016/j.bpj.2016.12.015.

Schlesinger, Sharon, and Eran Meshorer. 2019. "Open Chromatin, Epigenetic Plasticity, and Nuclear Organization in Pluripotency." *Developmental Cell* 48 (2): 135–50. https://doi.org/10.1016/j.devcel.2019.01.003.

Schmitz, Carola, Ekaterina Potekhina, Teresa Irianto, Vsevolod V. Belousov, and Antonina Lavrentieva. 2021. "Hypoxia Onset in Mesenchymal Stem Cell Spheroids: Monitoring With Hypoxia Reporter Cells." *Frontiers in Bioengineering and Biotechnology* 9 (February): 611837. https://doi.org/10.3389/fbioe.2021.611837.

Schulze, Christian, Franziska Wetzel, Thomas Kueper, Anke Malsen, Gesa Muhr, Soeren Jaspers, Thomas Blatt, Klaus-Peter Wittern, Horst Wenck, and Josef A. Käs. 2010. "Stiffening of Human Skin Fibroblasts with Age." *Biophysical Journal* 99 (8): 2434–42. https://doi.org/10.1016/j.bpj.2010.08.026.

Senoo, H., and R. Hata. 1994. "Extracellular Matrix Regulates Cell Morphology, Proliferation, and Tissue Formation." *Kaibogaku Zasshi. Journal of Anatomy* 69 (6): 719–33.

Shen, Shensi, and Jean Clairambault. 2020. "Cell Plasticity in Cancer Cell Populations." *F1000Research* 9 (June): 635. https://doi.org/10.12688/f1000research.24803.1.

Sherman, Brad T, Ming Hao, Ju Qiu, Xiaoli Jiao, Michael W Baseler, H Clifford Lane, Tomozumi Imamichi, and Weizhong Chang. 2022. "DAVID: A Web Server for Functional Enrichment Analysis and Functional Annotation of Gene Lists (2021 Update)." *Nucleic Acids Research* 50 (W1): W216–21. https://doi.org/10.1093/nar/gkac194.

Shibata, Hirofumi, Shingo Komura, Yosuke Yamada, Nao Sankoda, Akito Tanaka, Tomoyo Ukai, Mio Kabata, et al. 2018. "In Vivo Reprogramming Drives Kras-Induced Cancer Development." *Nature Communications* 9 (1): 2081. https://doi.org/10.1038/s41467-018-04449-5.

Shivashankar, G. V. 2011. "Mechanosignaling to the Cell Nucleus and Gene Regulation." *Annual Review of Biophysics* 40 (1): 361–78. https://doi.org/10.1146/annurev-biophys-042910-155319.

Shivashankar, G.V. 2019. "Mechanical Regulation of Genome Architecture and Cell-Fate Decisions." *Current Opinion in Cell Biology* 56 (February): 115–21. https://doi.org/10.1016/j.ceb.2018.12.001.

Shokrollahi, Mitra, and Karim Mekhail. 2021. "Interphase Microtubules in Nuclear Organization and Genome Maintenance." *Trends in Cell Biology* 31 (9): 721–31. https://doi.org/10.1016/j.tcb.2021.03.014.

Sokolov, Igor, Swaminathan Iyer, and Craig D. Woodworth. 2006. "Recovery of Elasticity of Aged Human Epithelial Cells in Vitro." *Nanomedicine: Nanotechnology, Biology and Medicine* 2 (1): 31–36. https://doi.org/10.1016/j.nano.2005.12.002.

Solé-Boldo, Llorenç, Günter Raddatz, Sabrina Schütz, Jan Philipp Mallm, Karsten Rippe, Anke S. Lonsdorf, Manuel Rodríguez-Paredes, and Frank Lyko. 2020. "Single-Cell Transcriptomes of the Human Skin Reveal Age-Related Loss of Fibroblast Priming." *Communications Biology* 3 (1): 1–12. https://doi.org/10.1038/s42003-020-0922-4.

Sprinzak, David, and Stephen C. Blacklow. 2021. "Biophysics of Notch Signaling." *Annual Review of Biophysics* 50 (1): 157–89. https://doi.org/10.1146/annurev-biophys-101920-082204.

Stadhouders, Ralph, Enrique Vidal, François Serra, Bruno Di Stefano, François Le Dily, Javier Quilez, Antonio Gomez, et al. 2018. “Transcription Factors Orchestrate Dynamic Interplay between Genome Topology and Gene Regulation during Cell Reprogramming.” *Nature Genetics* 50 (2): 238–49. https://doi.org/10.1038/s41588-017-0030-7.

Sukharev, Sergei, and Frederick Sachs. 2012. “Molecular Force Transduction by Ion Channels – Diversity and Unifying Principles.” *Journal of Cell Science*, January, jcs.092353. https://doi.org/10.1242/jcs.092353.

Sun, Bryan K., Zurab Siprashvili, and Paul A. Khavari. 2014. “Advances in Skin Grafting and Treatment of Cutaneous Wounds.” *Science* 346 (6212): 941–45. https://doi.org/10.1126/science.1253836.

Sun, Jinglucy, and William I. Weis. 2011. “Biochemical and Structural Characterization of β-Catenin Interactions with Nonphosphorylated and CK2-Phosphorylated Lef-1.” *Journal of Molecular Biology* 405 (2): 519–30. https://doi.org/10.1016/j.jmb.2010.11.010.

Sun, Zhiqi, Shengzhen S. Guo, and Reinhard Fässler. 2016. “Integrin-Mediated Mechanotransduction.” *Journal of Cell Biology* 215 (4): 445–56. https://doi.org/10.1083/jcb.201609037.

Suresh, Rahul, and Roberto J. Diaz. 2021. “The Remodelling of Actin Composition as a Hallmark of Cancer.” *Translational Oncology* 14 (6): 101051. https://doi.org/10.1016/j.tranon.2021.101051.

Szklarczyk, Damian, Andrea Franceschini, Stefan Wyder, Kristoffer Forslund, Davide Heller, Jaime Huerta-Cepas, Milan Simonovic, et al. 2015. “STRING V10: Protein–Protein Interaction Networks, Integrated over the Tree of Life.” *Nucleic Acids Research* 43 (D1): D447–52. https://doi.org/10.1093/nar/gku1003.

Tadić, Vanja, Goran Josipović, Vlatka Zoldoš, and Aleksandar Vojta. 2019. “CRISPR/Cas9-Based Epigenome Editing: An Overview of dCas9-Based Tools with Special Emphasis on off-Target Activity.” *Methods* 164–165 (July): 109–19. https://doi.org/10.1016/j.ymeth.2019.05.003.

Takahashi, Kazutoshi, and Shinya Yamanaka. 2006. “Induction of Pluripotent Stem Cells from Mouse Embryonic and Adult Fibroblast Cultures by Defined Factors.” *Cell* 126 (4): 663–76. https://doi.org/10.1016/j.cell.2006.07.024.

———. 2016. “A Decade of Transcription Factor-Mediated Reprogramming to Pluripotency.” *Nature Reviews Molecular Cell Biology* 17 (3): 183–93. https://doi.org/10.1038/nrm.2016.8.

Talwar, Shefali, Nikhil Jain, and G.V. Shivashankar. 2014. “The Regulation of Gene Expression during Onset of Differentiation by Nuclear Mechanical Heterogeneity.” *Biomaterials* 35 (8): 2411–19. https://doi.org/10.1016/j.biomaterials.2013.12.010.

Theunissen, Thorold W., and Rudolf Jaenisch. 2014. “Molecular Control of Induced Pluripotency.” *Cell Stem Cell* 14 (6): 720–34. https://doi.org/10.1016/j.stem.2014.05.002.

Thiery, Jean Paul, Hervé Acloque, Ruby Y.J. Huang, and M. Angela Nieto. 2009. “Epithelial-Mesenchymal Transitions in Development and Disease.” *Cell* 139 (5): 871–90. https://doi.org/10.1016/j.cell.2009.11.007.

Trapnell, Cole, David G Hendrickson, Martin Sauvageau, Loyal Goff, John L Rinn, and Lior Pachter. 2013. “Differential Analysis of Gene Regulation at Transcript Resolution with RNA-Seq.” *Nature Biotechnology* 31 (1): 46–53. https://doi.org/10.1038/nbt.2450.

Trapnell, Cole, Brian A Williams, Geo Pertea, Ali Mortazavi, Gordon Kwan, Marijke J van Baren, Steven L Salzberg, Barbara J Wold, and Lior Pachter. 2010. “Transcript Assembly and Quantification by RNA-Seq Reveals Unannotated Transcripts and Isoform Switching during Cell Differentiation.” *Nature Biotechnology* 28 (5): 511–15. https://doi.org/10.1038/nbt.1621.

Tseng, Yiider, Jerry S. H. Lee, Thomas P. Kole, Ingjye Jiang, and Denis Wirtz. 2004. “Micro-Organization and Visco-Elasticity of the Interphase Nucleus Revealed by Particle Nanotracking.” *Journal of Cell Science* 117 (10): 2159–67. https://doi.org/10.1242/jcs.01073.

Tzur, Yonatan B., Katherine L. Wilson, and Yosef Gruenbaum. 2006. “SUN-Domain Proteins: ‘Velcro’ That Links the Nucleoskeleton to the Cytoskeleton.” *Nature Reviews Molecular Cell Biology* 7 (10): 782–88. https://doi.org/10.1038/nrm2003.

Uchida, T, H Ohashi, E Aoki, Y Nakahara, T Hotta, T Murate, H Saito, and T Kinoshita. 2000. “Bio-Technical Methods Section (Bts).” *Leukemia* 14 (1): 207–12.

Uhler, Caroline, and G. V. Shivashankar. 2017. “Regulation of Genome Organization and Gene Expression by Nuclear Mechanotransduction.” *Nature Reviews Molecular Cell Biology* 18 (12): 717–27. https://doi.org/10.1038/nrm.2017.101.

Vahabikashi, Amir, Suganya Sivagurunathan, Fiona Ann Sadsad Nicdao, Yu Long Han, Chan Young Park, Mark Kittisopikul, Xianrong Wong, et al. 2022. “Nuclear Lamin Isoforms Differentially Contribute to LINC Complex-Dependent Nucleocytoskeletal Coupling and Whole-Cell Mechanics.” *Proceedings of the National Academy of Sciences* 119 (17): e2121816119. https://doi.org/10.1073/pnas.2121816119.

Valencia, Alfredo M., and Cigall Kadoch. 2019. “Chromatin Regulatory Mechanisms and Therapeutic Opportunities in Cancer.” *Nature Cell Biology* 21 (2): 152–61. https://doi.org/10.1038/s41556-018-0258-1.

Van Ingen, Maria J. A., and Tyler J. Kirby. 2021. “LINCing Nuclear Mechanobiology With Skeletal Muscle Mass and Function.” *Frontiers in Cell and Developmental Biology* 9 (July): 690577. https://doi.org/10.3389/fcell.2021.690577.

Venkatachalapathy, Saradha, Doorgesh Sharma Jokhun, and G. V. Shivashankar. 2020. “Multivariate Analysis Reveals Activation-Primed Fibroblast Geometric States in Engineered 3D Tumor Microenvironments.” Edited by Alex Dunn. *Molecular Biology of the Cell* 31 (8): 803–12. https://doi.org/10.1091/mbc.E19-08-0420.

Venkatachalapathy, Saradha, Dyuthi Sreekumar, Prasuna Ratna, and G. V. Shivashankar. 2022. “Actomyosin Contractility as a Mechanical Checkpoint for Cell State Transitions.” *Scientific Reports* 12 (1): 16063. https://doi.org/10.1038/s41598-022-20089-8.

Walcher, Lia, Ann-Kathrin Kistenmacher, Huizhen Suo, Reni Kitte, Sarah Dluczek, Alexander Strauß, André-René Blaudszun, Tetyana Yevsa, Stephan Fricke, and Uta Kossatz-Boehlert. 2020. “Cancer Stem Cells—Origins and Biomarkers: Perspectives for Targeted Personalized Therapies.” *Frontiers in Immunology* 11 (August): 1280. https://doi.org/10.3389/fimmu.2020.01280.

Walma, David A. Cruz, and Kenneth M. Yamada. 2020. “The Extracellular Matrix in Development.” *Development* 147 (10): dev175596. https://doi.org/10.1242/dev.175596.

Wang, Audrey S., and Oliver Dreesen. 2018. “Biomarkers of Cellular Senescence and Skin Aging.” *Frontiers in Genetics* 9: 247. https://doi.org/10.3389/fgene.2018.00247.

Wang, Min, Dong Ren, Wei Guo, Shuai Huang, Zeyu Wang, Qiji Li, Hong Du, Libing Song, and Xinsheng Peng. 2016. “N-Cadherin Promotes Epithelial-Mesenchymal Transition and Cancer Stem Cell-like Traits via ErbB Signaling in Prostate Cancer Cells.” *International Journal of Oncology* 48 (2): 595–606. https://doi.org/10.3892/ijo.2015.3270.

Wang, Xian, Haijiao Liu, Min Zhu, Changhong Cao, Zhensong Xu, Yonit Tsatskis, Kimberly Lau, et al. 2018. “Mechanical Stability of the Cell Nucleus: Roles Played by the Cytoskeleton in Nuclear Deformation and Strain Recovery.” *Journal of Cell Science*, January, jcs.209627. https://doi.org/10.1242/jcs.209627.

Wang, Yejun, Mallika Nagarajan, Caroline Uhler, and G. V. Shivashankar. 2017. “Orientation and Repositioning of Chromosomes Correlate with Cell Geometry–Dependent Gene Expression.” Edited by Alex Dunn. *Molecular Biology of the Cell* 28 (14): 1997–2009. https://doi.org/10.1091/mbc.E16-12-0825.

Wever, Olivier De, Wendy Westbroek, An Verloes, Nele Bloemen, Marc Bracke, Christian Gespach, Erik Bruyneel, and Marc Mareel. 2004. “Critical Role of N-Cadherin in Myofibroblast Invasion

and Migration in Vitro Stimulated by Colon-Cancer-Cell-Derived TGF-β or Wounding." *Journal of Cell Science* 117 (20): 4691–4703. https://doi.org/10.1242/jcs.01322.

Wilde, Caroline, Jakob Mitgau, Tomáš Suchý, Torsten Schöneberg, and Ines Liebscher. 2022. "Translating the Force—Mechano-Sensing GPCRs." *American Journal of Physiology-Cell Physiology* 322 (6): C1047–60. https://doi.org/10.1152/ajpcell.00465.2021.

Wilson, Meredith H., and Erika L. F. Holzbaur. 2012. "Opposing Microtubule Motors Drive Robust Nuclear Dynamics in Developing Muscle Cells." *Journal of Cell Science*, January, jcs.108688. https://doi.org/10.1242/jcs.108688.

Wlaschek, Meinhard, Pallab Maity, Evgenia Makrantonaki, and Karin Scharffetter-Kochanek. 2021. "Connective Tissue and Fibroblast Senescence in Skin Aging." *Journal of Investigative Dermatology* 141 (4): 985–92. https://doi.org/10.1016/j.jid.2020.11.010.

Worman, Howard J., and Gregg G. Gundersen. 2006. "Here Come the SUNs: A Nucleocytoskeletal Missing Link." *Trends in Cell Biology* 16 (2): 67–69. https://doi.org/10.1016/j.tcb.2005.12.006.

Xia, Peng, Daniel Gütl, Vanessa Zheden, and Carl-Philipp Heisenberg. 2019. "Lateral Inhibition in Cell Specification Mediated by Mechanical Signals Modulating TAZ Activity." *Cell* 176 (6): 1379-1392.e14. https://doi.org/10.1016/j.cell.2019.01.019.

Xie, Yangli, Nan Su, Jing Yang, Qiaoyan Tan, Shuo Huang, Min Jin, Zhenhong Ni, et al. 2020. "FGF/FGFR Signaling in Health and Disease." *Signal Transduction and Targeted Therapy* 5 (1): 181. https://doi.org/10.1038/s41392-020-00222-7.

Xie, Zhuorui, Allison Bailey, Maxim V. Kuleshov, Daniel J. B. Clarke, John E. Evangelista, Sherry L. Jenkins, Alexander Lachmann, et al. 2021. "Gene Set Knowledge Discovery with Enrichr." *Current Protocols* 1 (3): e90. https://doi.org/10.1002/cpz1.90.

Xu, Wenwei, Roman Mezencev, Byungkyu Kim, Lijuan Wang, John McDonald, and Todd Sulchek. 2012. "Cell Stiffness Is a Biomarker of the Metastatic Potential of Ovarian Cancer Cells." Edited by Surinder K. Batra. *PLoS ONE* 7 (10): e46609. https://doi.org/10.1371/journal.pone.0046609.

Xu, Xin, Liwei Zheng, Quan Yuan, Gehua Zhen, Janet L. Crane, Xuedong Zhou, and Xu Cao. 2018. "Transforming Growth Factor-β in Stem Cells and Tissue Homeostasis." *Bone Research* 6 (1): 2. https://doi.org/10.1038/s41413-017-0005-4.

Yan, Jian, Shi-An A. Chen, Andrea Local, Tristin Liu, Yunjiang Qiu, Kristel M. Dorighi, Sebastian Preissl, et al. 2018. "Histone H3 Lysine 4 Monomethylation Modulates Long-Range Chromatin Interactions at Enhancers." *Cell Research* 28 (2): 204–20. https://doi.org/10.1038/cr.2018.1.

Yang, Benjamin A., Jacqueline A. Larouche, Kaitlyn M. Sabin, Paula M. Fraczek, Stephen C. J. Parker, and Carlos A. Aguilar. 2023. “Three-dimensional Chromatin Re-organization during Muscle Stem Cell Aging.” *Aging Cell* 22 (4): e13789. https://doi.org/10.1111/acel.13789.

Yap, Alpha S., Kinga Duszyc, and Virgile Viasnoff. 2018. “Mechanosensing and Mechanotransduction at Cell–Cell Junctions.” *Cold Spring Harbor Perspectives in Biology* 10 (8): a028761. https://doi.org/10.1101/cshperspect.a028761.

Yu, Hongshuang, Yuanyuan Tian, Ying Wang, Shin Mineishi, and Yi Zhang. 2019. “Dendritic Cell Regulation of Graft Vs.-Host Disease: Immunostimulation and Tolerance Immunostimulation.” *Frontiers in Immunology* 10 (FEB): 14–17. https://doi.org/10.3389/fimmu.2019.00093.

Yun, Kangsun, Yoo Duk Choi, Jong Hee Nam, Zeeyoung Park, and Sin-Hyeog Im. 2007. “NF-κB Regulates Lef1 Gene Expression in Chondrocytes.” *Biochemical and Biophysical Research Communications* 357 (3): 589–95. https://doi.org/10.1016/j.bbrc.2007.03.170.

Zerbino, Daniel R, Premanand Achuthan, Wasiu Akanni, M Ridwan Amode, Daniel Barrell, Jyothish Bhai, Konstantinos Billis, et al. 2018. “Ensembl 2018.” *Nucleic Acids Research* 46 (D1): D754–61. https://doi.org/10.1093/nar/gkx1098.

Zhang, Qiong, Wei Liu, Hong-Mei Zhang, Gui-Yan Xie, Ya-Ru Miao, Mengxuan Xia, and An-Yuan Guo. 2020. “hTFtarget: A Comprehensive Database for Regulations of Human Transcription Factors and Their Targets.” *Genomics, Proteomics & Bioinformatics* 18 (2): 120–28. https://doi.org/10.1016/j.gpb.2019.09.006.

Zhang, Xiaochang, Kai Lei, Xiaobing Yuan, Xiaohui Wu, Yuan Zhuang, Tian Xu, Rener Xu, and Min Han. 2009. “SUN1/2 and Syne/Nesprin-1/2 Complexes Connect Centrosome to the Nucleus during Neurogenesis and Neuronal Migration in Mice.” *Neuron* 64 (2): 173–87. https://doi.org/10.1016/j.neuron.2009.08.018.

Zhang, Yu, Yunlong Xiang, Qiangzong Yin, Zhenhai Du, Xu Peng, Qiujun Wang, Miguel Fidalgo, et al. 2018. “Dynamic Epigenomic Landscapes during Early Lineage Specification in Mouse Embryos.” *Nature Genetics* 50 (1): 96–105. https://doi.org/10.1038/s41588-017-0003-x.

Zhao, Yue, Ji Zhu, Bowen Shi, Xinyu Wang, Qijue Lu, Chunguang Li, and Hezhong Chen. 2019. “The Transcription Factor LEF1 Promotes Tumorigenicity and Activates the TGF-β Signaling Pathway in Esophageal Squamous Cell Carcinoma.” *Journal of Experimental & Clinical Cancer Research: CR* 38 (1): 304. https://doi.org/10.1186/s13046-019-1296-7.